Université de Liège

Faculté des Sciences
Département de Physique
Group for Research and Applications in Statistical Physics

Bouncing droplets, the role of deformations

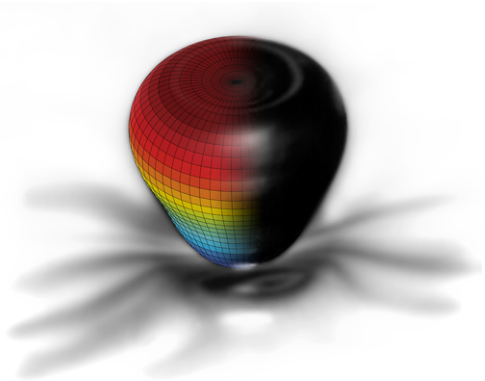

Dissertation présentée par

Denis TERWAGNE

en vue de l'obtention du titre de
Docteur en Sciences
Année académique 2011-2012

Je tiens avant tout à remercier les Professeurs John Bush, Yves Couder et Thierry Bastin et le Docteur Philippe Brunet d'avoir accepté de faire partie de mon jury de thèse.

J'aimerais ensuite adresser un merci tout particulier à mes promoteurs, le Docteur Stéphane Dorbolo et le Professeur Nicolas Vandewalle qui m'ont suivi et formé tout le long de ce travail de thèse. Ils m'ont offert l'opportunité de faire partie de la dynamique équipe du GRASP.

Stéphane a été pour moi le promoteur idéal. Il est disponible, patient, efficace, modeste, encourageant et à l'écoute. Son imagination, ses conseils avisés et le recul qu'il peut prendre devant divers problèmes physiques m'ont toujours impressionné. Il a pris son rôle de formateur à coeur et a toujours agi dans mon intérêt. Stéphane, merci pour tout!

Le Professeur Nicolas Vandewalle mène son équipe de façon efficace. Durant mes années d'études, il a fait naître en moi une passion pour la physique expérimentale qui continue d'exister. Il a toujours su mettre les moyens à la disposition de ses chercheurs pour les former au mieux. Merci pour vos conseils, vos encouragements et la liberté que vous m'avez accordée durant toutes ces années de thèse.

Au GRASP, j'ai pu goûter au travail d'équipe et j'en suis sorti grandi. J'ai apprécié les discussions entre collègues, la façon dont nous unifions nos efforts et nos expertises pour mener nos recherches. Un merci particulier à Tristan avec qui j'ai travaillé sur les gouttes. Il maîtrise les équations comme personne et a directement donné du rythme au début de ma thèse. Je remercie également François, l'as des simulations numériques. Dans notre bureau, les simulations se sont succédées au rythme de Rammstein. Kev, le jeune Padawan récemment arrivé, est toujours là pour mettre l'ambiance. Je sais qu'il se réjouit de s'installer à ma place près de la fenêtre! Merci à Geoffroy pour les bons moments passés au "minus one", à Giles pour ses idées tant scientifiques que culturelles et pour ses blagues "à deux balles". Merci à Hervé, pour son humanité et ses qualités de pédagogue qui sont pour moi un modèle à suivre. Merci à Eric, la force tranquille, avec qui j'ai partagé de bons moments depuis nos tout premiers instants à l'Université. Merci aux nouveaux venus, Damien et Florian, les Français qui seront bientôt considérés comme de vrais Belges. Je remercie

bien Damien pour les images de PIV. Je remercie également le reste de la bande, Bob, Malika, Ariane, Marjo et Laurent Dreesen. Je n'oublie pas les techniciens qui sont évidemment essentiels dans la réalisation de ce travail. Nous avons la chance de travailler avec des techniciens d'une qualité exceptionnelle. Merci à Jean-Claude, l'as des as, à Chouaib, le réparateur hors pair, à Médéric dont les yeux brillent quand il parle d'électronique et à Sébastien sur qui on peut toujours compter. Je voudrais également remercier Frédéric Lebeau, Professeur à Gembloux Agro-Bio Tech (ULg), de m'avoir initié au dispenseur à gouttes qui s'est révélé extrêmement utile pour finaliser cette thèse.

J'aimerais profiter de l'occasion pour remercier le Professeur Yves Couder de l'Université Paris Diderot-Paris 7 d'avoir accepté de m'accueillir au sein de son groupe pour un séjour d'un mois. Yves est un expérimentateur impressionnant, il a toujours de petits trucs et astuces à partager. Plusieurs de ses montages ont été utilisés et réutilisés tout au long de cette thèse, certains ont même fait le voyage jusqu'à Boston. De plus son humilité et sa maîtrise des phénomènes physiques sont pour moi exemplaires. Je remercie également, son étudiant, Antonin Eddi, pour nos nombreuses discussions enrichissantes.

I gratefully acknowledge Professor John Bush from the Massachusetts Institute of Technology in Boston (USA). He gave me the opportunity to work during three months in his lab. John leads his research energetically with a really inspiring enthusiasm. He is persistent and makes people give the best of themselves. He encourages his group to work really hard on the projects and it is worth the effort. I also thank Jim Bales, of MIT's Edgerton Center and Barbara Hughey for their technical help during my stay at the MIT. Finally, I thank Professor Pedro Reis to host me next year as a post-doc at the MIT.

Je remercie mes parents pour leur soutien depuis toutes ces années. Avec deux parents physiciens, il n'est pas étonnant de me voir arrivé là où je suis. Je remercie mon frère, mes soeurs et ma belle-soeur pour tout ce qu'ils m'apportent au cours de ma vie. Je n'oublie pas mes beaux-parents qui sont une aide précieuse. Je remercie tout particulièrement mon beau-père pour ses nombreuses relectures et ses conseils linguistiques avisés. Sa rigueur et sa patience m'ont toujours impressionné. Je remercie également mes amis et le reste de ma famille simplement pour la vie telle qu'elle est.

Merci infiniment à mon épouse, Stéphanie, physicienne comme moi, qui m'accompagne et me soutient depuis mes tout premiers instants à l'Université. Nous partageons tout, jusqu'à la rédaction de nos thèses que nous défendrons "presque" ensemble (on n'est pas complètement fous). Stef, tu m'es indispensable et je te dédie cette thèse.

Villers-aux-Tours, Denis Terwagne

Contents

Publications

The work that I present in this manuscript has been published in a number of publications which are listed below.

1. D. Terwagne, T. Gilet, N. Vandewalle and S. Dorbolo,
   From a bouncing compound drop to a double emulsion,
   Langmuir **26**, 11680 (2011).

2. T. Gilet, D. Terwagne, N. Vandewalle and S. Dorbolo,
   Drop and Bubble Interfaces Vol. 2, in Progress in Colloid and Interface Science,
   Chapter entitled *Manipulation of droplets onto a planar interface,*
   (Brill Publ., Leiden, 2010).

3. D. Terwagne, T. Gilet, N. Vandewalle and S. Dorbolo,
   Double emulsion in a compound droplet,
   Coll. Surf. A : Physicochem. Eng. Aspect **365**, 178-180 (2011).

4. N. Vandewalle, D. Terwagne, T. Gilet, H. Caps and S. Dorbolo,
   Antibubbles, liquid onions and bouncing droplets,
   Coll. Surf. A : Physicochem. Eng. Aspect **344**, 42-47 (2011).

5. D. Terwagne, N. Mack, S. Dorbolo, T. Gilet and N. Vandewalle,
   The mayonnaise droplet,
   Chaos **18**, 041104 (2009).

6. D. Terwagne, T. Gilet, N. Vandewalle and S. Dorbolo,
   Metastable bouncing droplets,
   Phys. Fluids **21**, 054103 (2009).

7. S. Dorbolo, D. Terwagne, N. Vandewalle and T. Gilet,
   Resonant and rolling droplets,
   New J. Phys. **10**, 113021 (2008).

8. D. Terwagne, T. Gilet, N. Vandewalle and S. Dorbolo,
   From bouncing to boxing,
   Chaos **18**, 041104 (2008).

9. D. Terwagne, T. Gilet, N. Vandewalle and S. Dorbolo,
   A drop of spectroscopy,
   Physicalia Magazine **30**, 161 (2008).

10. T. Gilet, D. Terwagne, N. Vandewalle and S. Dorbolo,
    Dynamics of a bouncing droplet onto a vertically vibrated interface,
    Phys. Rev. Lett. **100**, 167802 (2008).

11. D. Terwagne, N. Vandewalle and S. Dorbolo,
    Lifetime of a bouncing droplet,
    Phys. Rev. E **76**, 056311 (2007).

12. N. Vandewalle, D. Terwagne, K. Mulleners, T. Gilet and S. Dorbolo,
    Dancing droplets onto liquid surfaces,
    Phys. Fluids **18**, 091106 (2006).

I have also been involved in several research works. The related publications are listed below.

13. S. Dorbolo, M. Brandenbourger, F. Damanet, H. Dister, F. Ludewig, D. Terwagne, G. Lumay, and N. Vandewalle,
Granular gas in a periodic lattice,
Eur. J. Phys., to be published (2011).

14. D. Terwagne and J.W.M. Bush,
The Tibetan singing bowl,
Nonlinearity **24**, R51-R66 (2011).

15. N. Vandewalle, M. Noirhomme, J. Schockmel, E. Mersch, G. Lumay, D. Terwagne and S. Dorbolo,
Hysteretic behaviour in three-dimensional soap film rearrangements,
Phys. Rev. E **83**, 021403 (2011).

16. J. Zawala, S. Dorbolo, D. Terwagne, N. Vandewalle and K. Malysa,
Bouncing bubble on a liquid/gas interface resting or vibrating,
Soft Matter **7**, 6719-6726 (2011).

17. G. Delon, D. Terwagne, N. Adami, A. Bronfort, N. Vandewalle, S. Dorbolo and H. Caps,
Faraday instability on a network,
Chaos **20**, 041103 (2010).

18. S. Dorbolo, D. Terwagne, R. Delhalle, J. Dujardin, N. Huet, N. Vandewalle and N. Denkov,
Antibubble lifetime : Influence of the bulk viscosity and of the surface modulus of the mixture,
Coll. Surf. A : Physicochem. Eng. Aspect **365,**, 43-45 (2010).

19. T. Gilet, D. Terwagne and N. Vandewalle,
Droplet sliding on fibres,
Eur. Phys. J. E **31**, 253-262 (2010).

20. T. Gilet, D. Terwagne and N. Vandewalle,
Digital microfluidics on a wire,
Appl. Phys. Lett. **95**, 014106 (2009).

21. A. Eddi, D. Terwagne, E. Fort and Y.Couder,
Wave propelled ratchets and drifting rafts,
Europhys. Lett. **82**, 44001 (2008).

Summary

Nowadays, innovative applications such as "lab-on-a-chip", micro-reactors or biological chips are developed for industry, biology or medicine. Capillary issues are encountered which are not yet fully understood. It is therefore essential to open up ways to manipulate tiny amounts of liquid in order to mix them, encapsulate them or to create emulsions. The bouncing droplets on an oscillating liquid interface allow their manipulation. Indeed, under certain conditions, droplets can bounce indefinitely on a bath surface as long as the squeezed air film which separates the drop from the bath is renewed at each bounce. We chose to study deformable droplets on a non-deformable bath. The droplets are deformable because they are large or made of a low viscous oil, the liquid of the bath being highly viscous silicone oil. We investigated how the deformations, the stability and the trajectories of the droplets depends on the forcing parameters such as the frequency and the amplitude of the oscillation. We also studied the possibility of mixing and emulsifying droplets on the bath. Finally, we showed the effect of the deformation of the bath on these bouncing droplets and studied the trajectories of walking droplets [1] which are used as a model for quantum-like particles [2–5]. In this manuscript, we reported an exploration of the droplets behavior as a function of the ability of the bath and/or the droplet to deform.

Depending on the forcing frequency, specific deformation modes are excited on the bouncing droplets. We used these modes to rationalize their bouncing stability and to create double emulsions in a compound droplet. Then, we determined numerically the complex bifurcation diagrams of the trajectories of a bouncing droplet thanks to a model based on a spring. On a low viscous bath, we evidenced the importance of its deformation. We showed that a walker exists as soon as the droplet experiences, once every two oscillation periods, a

jump high enough to trigger a Faraday wave. As a consequence, we have to take the bouncing droplets into account when looking for an alternative way to manipulate them or as a model of quantum-like particles. The bouncing droplets still exhibit lots of intriguing behaviors which have yet to be explained. They can therefore remain the focus of future works.

Résumé

Depuis peu, de nouvelles applications telles que des laboratoires miniaturisés, des microréacteurs ou des puces biologiques voient le jour. Elles sont utilisées par l'industrie, la biologie ou encore la médecine. Des problèmes de capillarité sont régulièrement rencontrés et ne sont pas encore complètement compris. C'est pourquoi, il est essentiel d'ouvrir de nouvelles voies pour la manipulation de petites quantités de fluides dans le but de créer des mélanges, des encapsulations ou des émulsions. Les gouttes rebondissantes sur une surface liquide oscillante permettent leur manipulation sans contamination. En effet, dans certaines conditions, des gouttes peuvent rebondir indéfiniment car le film d'air qui sépare la goutte du bain est comprimé et renouvelé à chaque rebond. Dans ce travail, nous avons choisi d'étudier la déformation des gouttes sur un bain très visqueux et en conséquence très peu déformable. Quant aux gouttes, elles sont déformables car elles sont de tailles importantes ou formées d'un liquide peu visqueux. Nous avons étudié les déformations, la stabilité ainsi que les trajectoires des gouttes rebondissantes en fonction des différents paramètres de forçage tels que la fréquence d'oscillation du bain et son amplitude. Nous avons également étudié la possibilité d'effectuer un mélange ou une émulsion à l'intérieur d'une seule goutte rebondissante. Finalement, nous avons montré l'effet de la déformation du bain sur le rebond des gouttes et analysé les trajectoires d'une goutte dite marcheuse [1]. Celle-ci est utilisée comme modèle de particule pseudo-quantique [2–5]. En résumé, dans ce manuscrit, nous développons une exploration du comportement de la goutte rebondissante en fonction de ses capacités de déformation en tenant compte de la rigidité du bain.

Selon la fréquence de forçage, certains modes de déformation spécifiques de la goutte rebondissante sont excités. Ces modes sont utilisés pour expliquer la stabilité des gouttes sur le bain et aussi pour initier des doubles émulsions dans

des gouttes bi-composées. Grâce à un modèle de ressort, nous avons retrouvé numériquement les diagrammes de bifurcations observés. Pour un bain peu visqueux, nous avons mis en évidence sa déformation. Nous avons démontré qu'un marcheur peut exister aussitôt que la goutte émet un rebond qui se produit toutes les deux périodes de l'oscillation du bain et qui est d'amplitude suffisante pour déclencher des ondes de Faraday. Au vu de nos résultats, nous pouvons affirmer que les gouttes rebondissantes peuvent être envisagées comme une alternative pour la manipulation de petites quantités de liquide et aussi comme des modèles de pseudo-particules quantiques. Les gouttes rebondissantes présentent de nombreux comportements intéressants qui peuvent encore faire l'objet de nombreuses recherches.

Introduction

Little drops of water, little grains of sand,
Make the mighty ocean and the pleasant land.
Julia A. Fletcher Carney (1824-1908).

A droplet is defined as the tiniest quantity of liquid that one can observe. It is short-lived, it may spread when placed in contact with a solid or merge with another miscible liquid. Everyday, we interact with these extremely small objects. The rain for example, really common in our country (Belgium), is made of a myriad of minuscule droplets. During their fall, they keep a spherical shape when their diameter is smaller than a millimeter. If it is larger, they take the amazing shape of a parachute before splitting themselves. When we make coffee, the water percolates into the ground grains and falls, drop by drop, in a tank. If we pay attention to these falling drops, we observe that they surf on the freshly brewed coffee before coalescing (merging) with it. Farmers spraying their fields with phytosanitary liquids have to face the hydrophobic properties of certain plants. Supercooling water droplets instantly freeze when impacting the blades of a wind turbine or the wings of an airplane weighing them down. Nowadays, innovative applications using micro-scale flows and tiny fluid objects are developed for industry, biology or medicine. Due to the very small scale, some physical problems are encountered. These everyday examples involve series of questions on the droplets. How can they levitate on the freshly brewed coffee? How can the farmers compel them to completely spread on the leaves of the plants? How can one prevent droplets from freezing and inducing the collapse of engineering structures? How can we handle undersized quantities of fluid?

Answers to these questions entail the understanding of the physics of tiny

amounts of fluid. Relevant processes are the displacement division, fusion or mixing of droplets but also encapsulation and emulsions. In the present work, we studied an original way to manipulate droplets without touching or contaminating them. We worked with a model liquid which is silicone oil, the molecular interactions within which are of the Van der waals type. The general principle consists of making a droplet bounce on an oscillating liquid surface. Under specific conditions, the air film which separates the droplet from the bath is squeezed and resists the weight of the droplet. Given that the bath is oscillating, it enables the droplet to bounce and consequently to regenerate the air film. Moreover, these bouncing droplets can emit waves on the liquid surface, and by interacting with them, create a quantum-like system, called a "walker", that exhibits some intriguing behaviors. The association of a wave and a droplet is the main topic of ongoing researches on macroscopic experiments reproducing quantum behaviors. These bouncing droplets and walkers are studied extensively since 2005 [1] and are not yet fully understood.

In the writing of this manuscript, we chose to focus on the influence of the deformations (bath and/or droplet) on the bouncing dynamics. We thus had to leave some interesting works on the side such as some publications initiated during internships abroad [7,8]. The reader is most welcome to consider them in Appendix E. In 2007, we had the momentous occasion to spend a month within the "Laboratoire Matière et Systèmes Complexes" in the team of Yves Couder, at the Université Paris Diderot-Paris 7 (France). There, we worked on the ratchet behavior of droplets that are interacting through the wave fields that they emit on the bath [7]. This behavior has been rationalized thanks to our observation of a single bouncing droplet, this is presented in Chapter 4. We also have been invited in 2011, for a three months internship, in John Bush's group at the MIT - Massachusetts Institute of Technology (USA) to explain the mystery of droplets ejection in the fluid-filled Tibetan singing bowl [8]. This bowl is a type of bell originating from the Himalayan region which throws droplets over the edge when stroked. Thanks to our understanding of the Faraday waves and the bouncing droplets, we investigated these ejected droplets and generated bouncing droplets within the confines of the vessel.

The purpose of this thesis is the fundamental study of the influence of the deformations on the bouncing droplets phenomenon. We shall demonstrate that

these droplets can move, interact, merge or emulsify. First of all, we rigidified the oscillating liquid interface and studied the droplet deformations and the role of the latter on the bounce. Then, choosing a specific deformation mode, we studied the possibility of performing double emulsions in a bouncing compound drop. Afterwards, we limited our investigation to small deformations and proposed a model that was simulated numerically to explain our observations. Finally, we extended our investigation to slightly deformable droplets bouncing on a deformable bath in order to explain the role played by its deformations. In the continuity of our investigation, we then analyzed the behavior of the walker.

Following this strategy, our manuscript is a compilation of different works, already or not yet published, that we conducted on the bouncing droplets. We focussed on the role of the deformations of the droplet and/or of the bath in the bouncing droplet phenomenon. This study is placed in its context in Chapter 1. At the end of this chapter, relevant questions are raised and our work strategy is proposed. Following this plan of action, in Chapter 2, we developed the droplet deformations on a rigid bath. Then, in Chapter 3, we modeled our observations of the trajectories of small droplets bouncing on a rigid bath. Finally, in Chapter 4, we reported the observations made on a deformable bath and we proposed a generalization of the walker behavior. After our conclusion, we propose some perspectives.

Chapter 1

Research context

Contents

1.1 When surface effects dominate volume effects

Liquid and gas motions are mathematically described by the Navier-Stokes equations [9], which is the application of the second Newton's law to a fluid particle. In these equations, interfaces, between two fluids or between a fluid and a solid,

have to be considered through boundary conditions. The boundaries are crucial for small quantities of fluid. When, two hundred years ago, Laplace and Young initiated researches on capillarity, their venerable works developed the basic idea that creating a surface S between two fluids has an energetic cost E. Systems presenting such an interface tend to minimize their surface energy. As a consequence, a force can be derived from this potential surface energy, which acts on the interface to minimize it. The surface tension σ is given by the ratio E/S. For an air/water interface, σ is equal to $72\,10^{-3}\,\mathrm{N/m}$ and for mercury, $\sigma = 485.5\,10^{-3}\,\mathrm{N/m}$ at 25 °C. Under given conditions, surface effects compete with volume effects, such as gravity. On a solid surface, the shape of a sitting droplet, of mass M and radius R, depends on the relative importance of these effects. This can be quantified by the dimensionless Bond number $Bo = Mg/4\pi\sigma R$, where g is the gravitational acceleration. When this ratio is larger than unity, the gravity effect surpasses the surface tension effects, consequently the droplet looks like a puddle. Equivalently, this criteria corresponds to droplet sizes larger than a characteristic length, the capillary length, defined as $\kappa^{-1} = \sqrt{\sigma/\rho g}$, with ρ being the density of the liquid.

1.2 Delay of coalescence

A drop laid on a liquid surface may float, bounce or splash depending on the impact velocity. At a low velocity, Reynolds [10] observed, in 1881, that a drop impacting a liquid floats on the surface for several seconds before coalescing (merging with the bath). He noticed that the cleaner the liquid surface is, the longer is the delay before coalescence. Under some conditions, the droplet partially coalesces leaving a daughter droplet floating on the surface, then the process starts again [11, 12]. With a soapy water droplet, a cascade up to six partial coalescences can be observed.

In 1886, Reynolds developed the lubrication theory [13] in which he explained the delay of coalescence. The cause is found in the air film that is squeezed between the droplet and the liquid surface under the action of the droplet weight. The drainage is not instantaneous, consequently the air film "resists" the squeezing (cf. Fig. 1.1). When the thickness of the air film reaches a critical point, it breaks due to the attractive Van der waals forces between the fluid phases.

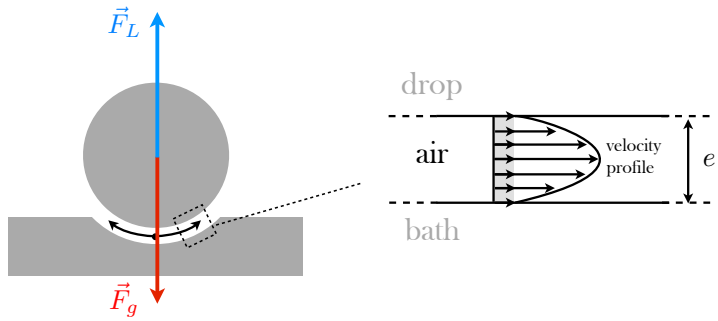

Figure 1.1: The air film between a floating droplet and a liquid bath is squeezed and drains out. In reaction, the air film of decreasing thickness e generates a lubrication force F_L that balances the droplet weight F_g. The airflow dynamics is a Poiseuille flow with a speed limit at boundaries which can be non negligible and change its shape.

The lubrication equation emanates from the solving of the Navier-Stokes equations for an air film bounded by two plates in relative motion. Let us consider two disks of radius R, parallel, separated by a distance e ($e \ll R$) and approaching each other with a relative velocity $\dot{e}$. As $e \ll R$, the pressure is constant throughout the thickness and the flow is a Poiseuille flow. The overpressure gives rise to a lubrication force F_L given by

$$F_L \sim \frac{\mu_a R^4 \dot{e}}{e^3}. \tag{1.1}$$

$\mu_a = 18\,10^{-6}$ Pa.s being the dynamic viscosity of air [13].

The thinning speed $\dot{e}$ of a film between a floating droplet and the bath surface diminishes drastically with the thickness e. The drainage time should therefore be infinite. However, when two free surfaces are close enough from each other (approximately 100 nm), attractive Van der waals forces between the two fluids are no longer negligible and the intervening air film breaks. Once the contact is made, surface tension minimizes the surface energy and coalescence occurs. The lifetime t_L of the droplet scales thus as

$$t_L \sim \frac{\mu_a R^4}{M g e_c^2}, \tag{1.2}$$

e_c being the critical thickness of the air film when it breaks [13]. For a water droplet with a diameter of 1 mm coalescing when the critical thickness is about $1\,\mu$m, this lifetime is estimated to 200 ms.

However, as the boundaries are liquid, the fluid speed at boundaries can be non negligible. The consequence is a modification of the shape of the Poiseuille flow (cf. Fig. 1.1). The drainage rate is affected as well as the lubrication force.

1.3 Inhibition of coalescence

Some physical effects can delay and even eliminate the coalescence of a droplet. To be comprehensive, we can cite some relevant works. Dell'Aversana *et al.* [14] have observed that a possible cause could be a thermal convective flow that is induced when the liquid drop and the liquid surface are at different temperatures. Amarouchene *et al.* [15] have studied the surfactant effect on drop coalescence. Coalescence with the bath can be completely prevented by using oppositely charged drop and bath [16]. Droplets may levitate on an air cushion [17] or due to an acoustic pressure node [18]. A hydraulic jump formed by a liquid film moving horizontally can maintain a droplet in rotation on the liquid surface (cf. Fig. 1.2a) [19]. Leidenfrost [20] deposited droplets onto a solid surface heated at a temperature above the liquid boiling temperature, an effect recently revisited by Biance *et al.* [21]. This way the drop does not touch the surface and levitates on its own vapor (Fig. 1.2b-c).

Preventing droplet coalescence or deposition allows us to manipulate it. Each way of preserving the droplet shape has its advantages and its drawbacks. We will focus on an original manner based on vibration which is described hereafter.

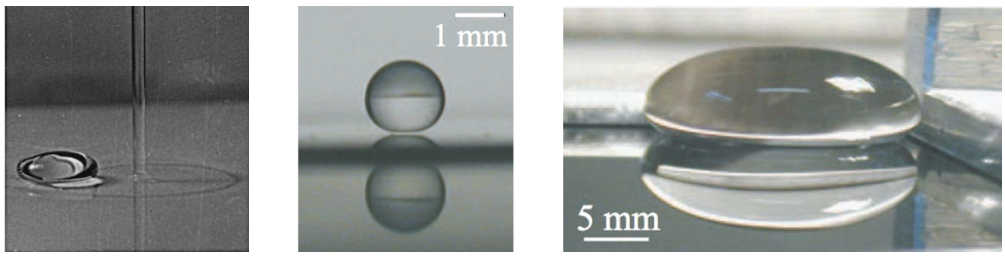

Figure 1.2: a) A water droplet of diameter 1.6 cm levitating due to a hydraulic jump (from [19]). b-c) Water drops deposited on a solid silicon surface maintained at a temperature of 200° C (from [21]).

1.3.1 Bouncing droplets

When a droplet is laid on a liquid bath that oscillates vertically, under given conditions we can see that it bounces (the core of this thesis) (cf. Fig. 1.3). The air film between the drop and the liquid surface is squeezed and regenerated at each successive bounce, its sustenance precluding coalescence and enabling the droplet bouncing. This bouncing occurs when the forcing amplitude exceeds a threshold which depends on various parameters such as the size of the droplet and the forcing frequency. On Fig. 1.3, a small drop takes off each time the acceleration of the surface is approximately equal to g. A small drop can be maintained in this state for a long time. In 1978, Walker [22] related a way to observe bouncing droplets on a liquid surface thanks to a vibration originating from a loudspeaker. This has been revisited since 2005 by a french team led by Couder [1] and the droplets have shown some really intriguing behaviors that we will detail hereafter.

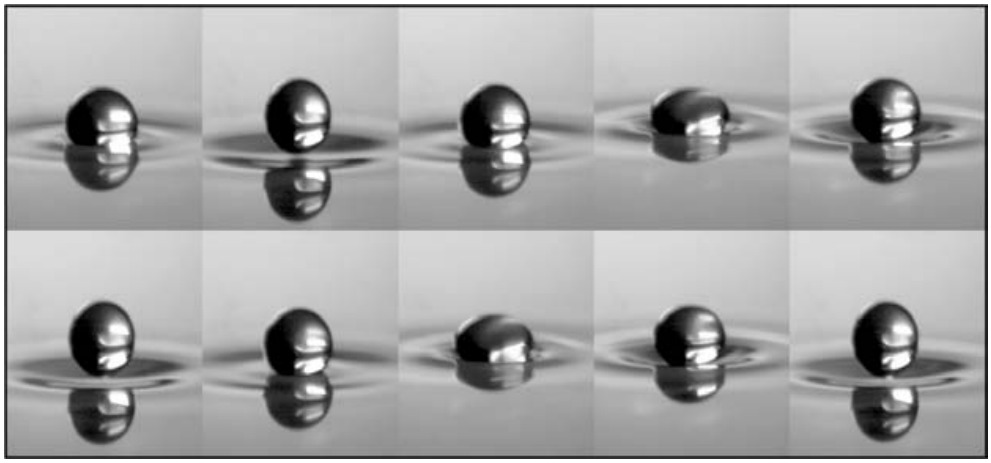

Figure 1.3: A drop of about 1 mm of diameter bounces on a liquid surface oscillating at 80 Hz together with an amplitude sufficient for the bouncing to occur. Drop and bath are made of silicone oil of viscosity 50 cSt.

1.3.2 Bouncing threshold

Droplets are laid on a liquid bath that oscillates vertically at a frequency f, the equation of motion of this bath is $A\sin\omega t$ where A is the amplitude and

$\omega = 2\pi f$. The plate acceleration is thus $\gamma = -A\omega^2 \sin \omega t$ and the maximal acceleration is defined by $\gamma_m = A\omega^2$. We observe that the droplet can bounce when γ_m is larger than a critical value γ_b. Couder *et al.* [23] have demonstrated that, with a silicone oil of kinematic viscosity $\nu = 500$ cSt, this critical acceleration γ_b increases as the square of the frequency. These results are presented on Figure 1.4. The dimensionless threshold acceleration $\Gamma_b = \gamma_b/g$ is plotted as a function of the forcing frequency f for various droplet diameters. The minimal threshold is observed, at low frequency, at $1g$ for the smallest droplets ($R \ll \kappa^{-1}$). We note a similarity with the inelastic bouncing ball model since small drops deform the bath weakly. The threshold γ_b increases more rapidly with larger drops. This is due to the fact that larger drops absorb a part of the energy in deformations, larger accelerations are needed for these drops to take off. Let us emphasize that deformations play a fundamental role in the expression of the acceleration threshold.

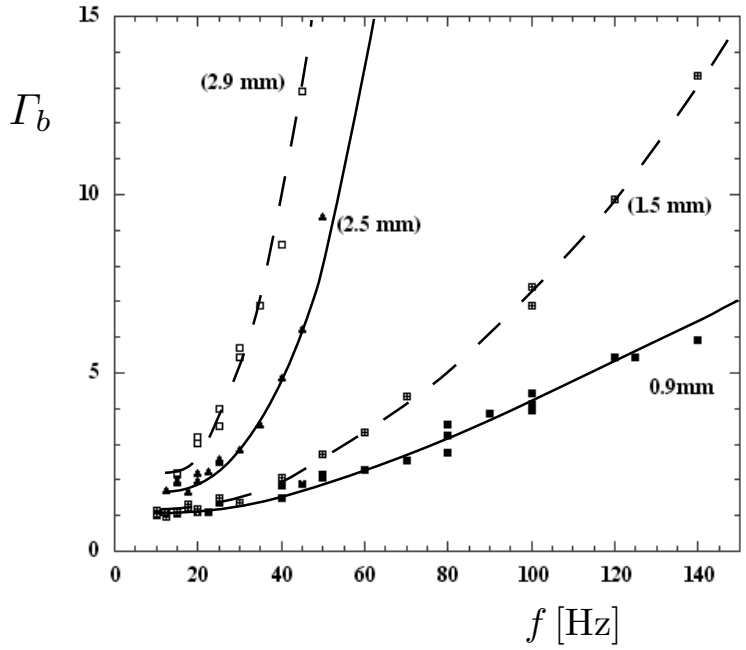

Figure 1.4: The bouncing acceleration threshold Γ_b increases as the square of the frequency (from [23]). The threshold increases more rapidly when the droplet diameter is large.

Couder [23] gives the following explanation to the bouncing threshold. We observed that the droplet lands and lifts off while the bath goes upwards. Firstly, the drop lands when the plate moves up and the acceleration vector of the plate $\vec{\gamma}$ is pointing upwards as indicated on Fig. 1.5b. During this phase, the air film thins. In the moving frame of the bath, the lubrication force F_L given in Eq. 1.1 is resisting to the apparent weight of the droplet $M(g+\gamma)$. Secondly, the droplet lifts off when the plate moves upward but the acceleration vector of the bath points downwards as indicated on Fig. 1.5c. During lift-off, the thickness of the air film increases. The lubrication force F_L resists to the lift-off of the droplet. In order to allow lift-off, the acceleration of the plate γ has to be sufficiently negative (smaller than the acceleration of the droplet). The condition for bouncing is therefore written as

$$|\gamma| > \frac{|F_g + F_L|}{M}. \tag{1.3}$$

The lubrication force F_L appears when the droplet lands on the bath. The air film decreases rapidly to a characteristic thickness e_0 when viscous forces in the air film become larger than inertia. It occurs in a finite time of the order of f. The lubrication force is important when the Reynolds number, Re, which is the ratio between the inertia and the viscosity, is smaller than a critical number

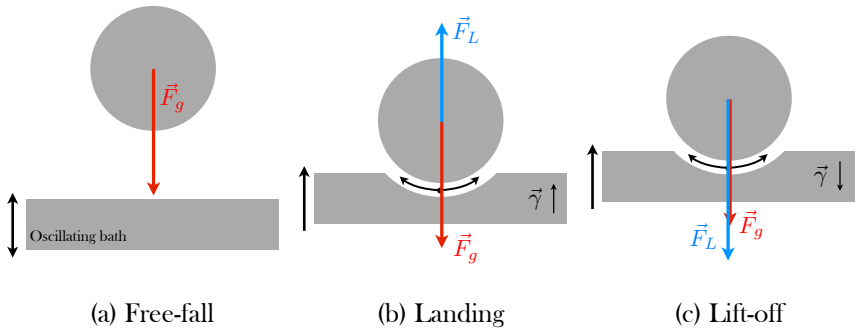

Figure 1.5: A droplet bouncing periodically on an oscillating liquid bath regenerates the air film at each bounce. The free-falling droplet (a) is landing on the bath (b). The lubrication force F_L prevents the droplet, subjected to its weight F_g, to coalesce with the bath. When the droplet lifts off the bath (c), the lubrication force F_L points downwards as the air film thickens. The droplet lifts off when the norm of the plate acceleration $|\gamma|$ is larger than the norm of the droplet acceleration.

Re_c given by

$$Re_c = \rho_a h_0^2 f/\mu_a \tag{1.4}$$

where ρ_a is the air density. The droplet viscosity μ is supposed to be much larger than the air viscosity μ_a, the dynamics of the air film can be supposed to be a Poiseuille like flow. The magnitude of the lubrication force is then evaluated by

$$F_L \sim \mu_a r_F^4 f/h_0^2, \tag{1.5}$$

where r_F is the radius of the air film which is related to the area of the droplet in apparent contact with the liquid bath. This length is proportional to the droplet radius R and is calculated from the shape of a floating droplet at rest on a bath made of the same liquid. The bouncing condition given by Eq. 1.3 is rewritten as

$$|\gamma_m| > g + \frac{1}{Re_c}\frac{\rho_a}{\rho}\frac{r_F^4}{R^3}f^2 \tag{1.6}$$

This expression is consistent with the experimental results presented in Fig. 1.4 and plotted, in dashed and solid lines, for four sizes of droplets.

Note that, using the acceleration threshold for bouncing, Gilet *et al.* [24] explained that when droplets are too big, one observes a cascade of partial coalescences which stops when a daughter droplet becomes small enough to start bouncing. This process can be compared to a droplet size filter.

1.3.3 Bouncing periodicity

Beyond the threshold, a droplet bounces and this may be compared to a bouncing ball problem. On a bath, oscillating at about 80 Hz just above the threshold, droplets bounce at the same frequency as the bath. We have shot a movie, at 1000 fps, of the bouncing of a droplet. Then, for each image, we have taken a vertical slice passing through the droplet centerline and finally we have juxtaposed all these images. This way, we have been able to reconstruct a space-time image illustrating the dynamics of the droplet (cf. Fig. 1.6a). Note that the time elapses from left to right and that the drop's reflection on the bath is apparent. When the forcing acceleration is increased, droplets experience different bouncing modes, e.g. period doubling or chaotic behavior. On Fig. 1.6b, during two oscillations of the plate, the droplet undergoes two bounces of different heights and the bouncing period is twice the bath oscillation. Protière *et*

al. [25] explored the bouncing mode phase diagram of droplets of 50 cSt silicone oil bouncing on a bath of the same liquid. On Fig. 1.7, these observations are reported as a function of the droplet diameter D and of the bath maximal acceleration $\Gamma = \gamma_m/g$. We will give more explanation about that in Chapter 4. In the case of a droplet bouncing on a vibrating soap film, the bouncing periodicity is very rich. This system has been investigated experimentally and has been rationalized theoretically [26]. We have demonstrated that these modes of bouncing also occur in a Tibetan singing bowl [8]. A bowl deformation mode is excited by rubbing the rim with a leather mallet. The bound liquid in the vessel is perturbed by the horizontal oscillation of the rim leading to a surface motion suitable for droplets to bounce.

Several droplets may interact through the capillary waves they emit leading to a self-organization on the bath, more likely in a triangular lattice [25, 27, 28]. Recently, Eddi *et al.* [29] reproduced droplet rafts with a crystalline structure related to the Archimedean tilings of the plane by fine tuning the bouncing modes. Then, when tuning the forcing acceleration, they evidenced some vibration modes that arise in hexagonal and square lattices [30].

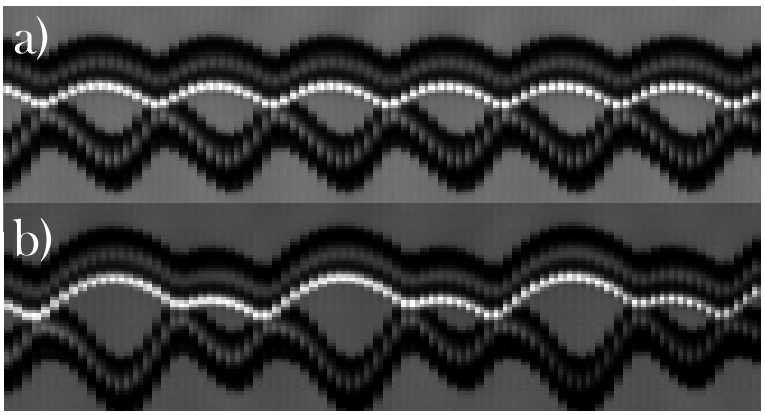

Figure 1.6: Spatio-temporal diagrams indicating the vertical trajectory of a droplet of diameter $D = 820\,\mu$m bouncing on an oscillating bath at a frequency $f = 80$ Hz. Both droplet and bath are made of 20 cSt silicone oil. The periodicity of the droplet bounces is the same as the oscillating bath period when the maximal acceleration of the bath is a) $\gamma_m = 1.7g$; and doubled when b) $\gamma_m = 2g$. Time elapses from left to right and the drop's reflection is apparent.

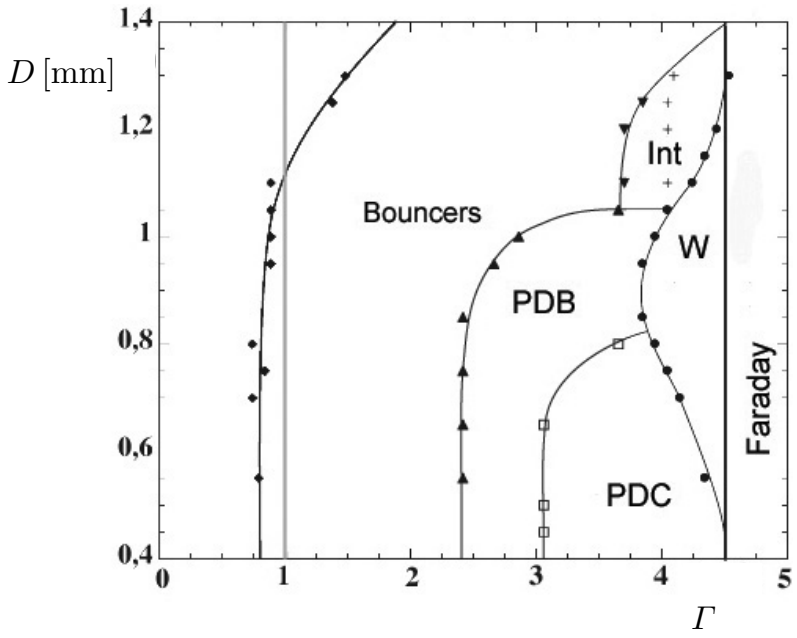

Figure 1.7: Bouncing droplets, on a 50 Hz oscillating bath, experience different bouncing modes which depend on their diameter D and the bath acceleration Γ. The liquid used for droplets and the bath is 50 cSt silicone oil. Region "Bouncers" corresponds to simple droplet bouncing, "PDB" to period doubling bouncing, "PDC" to a transition to chaos, "Int" to an intermittent behavior and "W" is the walker region, situated just below the Faraday instability region (from [25]).

1.3.4 Faraday instability

When the forcing acceleration is too large, the bouncing is limited by the Faraday instability. Indeed, when a liquid bath is vibrating vertically, Faraday has demonstrated, in 1831, that its interface remains flat until a critical acceleration is exceeded [31]. Above this threshold, a field of waves appears at the interface, parametric standing waves oscillating with half the forcing frequency [32–37]. The form of such Faraday waves depends on the container geometry. However, boundary effects can be minimized when using a large container. The Faraday waves have a wavelength prescribed by the relative importance of the surface tension and the gravity, being respectively capillary and gravity waves in the short and long wavelength limits. In Fig. 1.8, Faraday waves are created on the surface of a 20 cSt square silicone oil bath (11x11 cm^2), oscillating at 80 Hz at

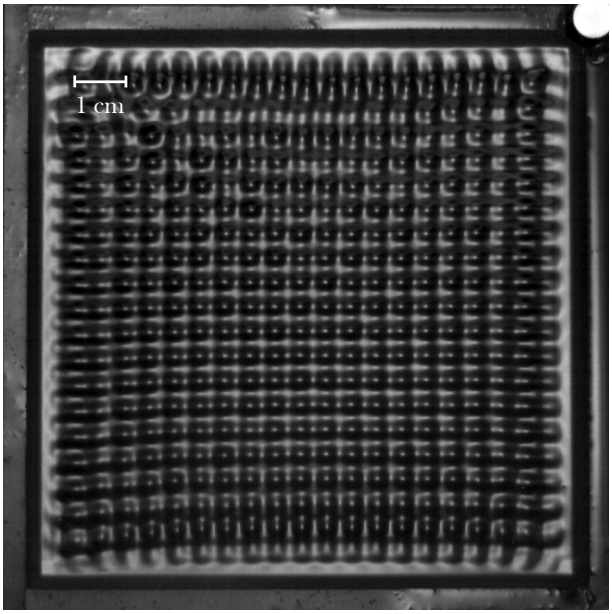

Figure 1.8: Stationary Faraday waves oscillates at half the of forcing frequency $f_0/2$. They are excited on a 20 cSt Silicone oil surface.

an acceleration just above the Faraday threshold. As the forcing acceleration is increased, more complex wave patterns arise progressively, and the interfacial dynamics become chaotic [36–38]. Ultimately, large amplitude forcing leads to the surface fracture and the ejection of droplets from the fluid bath [39, 40].

Assuming capillary waves ($Bo \ll 1$) in an unbounded and infinite depth liquid, a Faraday wavelength can be infered :

$$\lambda_F = (2\pi)^{1/3}(\sigma/\rho)^{1/3}(f_0/2)^{-2/3}. \tag{1.7}$$

and the critical acceleration needed to induce parametric instability is given by [36, 41]

$$\Gamma_F \propto \frac{1}{g}(\rho/\sigma)^{1/3}\nu f_0^{5/3}, \tag{1.8}$$

where ν is the kinematic viscosity of the fluid. The origin of these equations is also detailed in [8].

1.3.5 Wave propelled ratchets and drifting rafts

Near the Faraday instability threshold, the bouncing of the droplet can become sub-harmonic (cf. Fig. 1.6b) and the drop can become the source of a local Faraday wave packet. Motionless bouncing droplets, when isolated, can be assembled and form a bound states that spontaneously moves on the surface (cf. inset in Fig. 1.9a). The bound state has to be made of uneven droplets in order to induce a symmetry breaking in the waves emitted outwards (cf. Fig. 1.9a). In reaction, the bound state moves on the surface at a speed of the order of 3 mm/s. Such a means of propulsion, by reaction to the emission of surface waves, was one of the mechanisms proposed to explain the motion of water striders [42], even if more recent works [43] have shown that in this case the emission of vortices is the dominant effect. In this experiment, as the reaction depends on the frequency and the amplitude of the waves, bound states of uneven size droplets present reversals in their motions when one of the drops undergoes sub-harmonic period doubling (cf. Fig. 1.9b). Aggregates of uneven size droplets can also be formed, the asymmetry leading to spontaneous translation or rotation (cf. Fig. 1.9c). The publication related to this study is presented in Appendix E

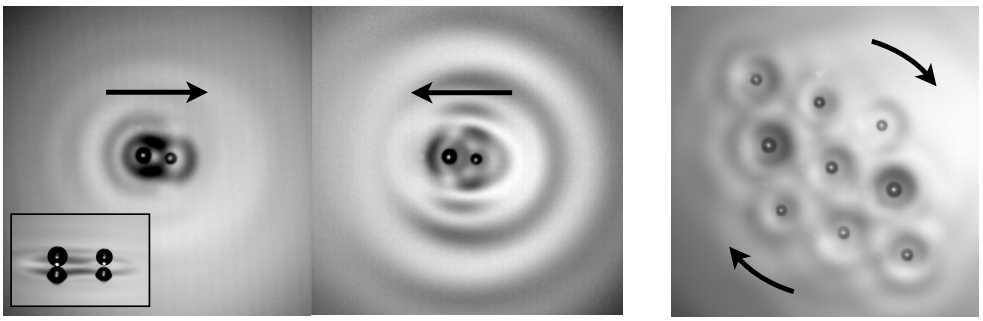

(a) (b) (c)

Figure 1.9: In the inset, a photograph of self-assembled bouncers forming self-propelled bound states. The two droplets are 20 cSt silicone oil of diameters of 0.73 mm and 0.89 mm. The 20 cSt silicone oil bath oscillates at 80 Hz. (a) Viewed from the top. The two droplets are simple bouncers and the ratchet is pushed by the largest droplet since it emits a wave of larger amplitude. Thus the bound state propagates to the right. (b) The smaller droplet has undergone a period doubling and emits a Faraday wave of larger amplitude : the bound state propagates to the left. (c) An asymmetric crystalline aggregate made of simple bouncers rotating around itself. [7]

1.3.6 Walker droplets

Couder *et al.* [1] have shown a particular state for bouncing droplets. In the vicinity of the Faraday instability, the droplets generate an extended wave field on the bath. Moreover, through the waves that are occurring, some droplets are able to "walk" horizontally across the liquid surface. Several factors are needed to sustain a so-called "walker" [4]. Firstly, the drop has to bounce at half the forcing frequency, so that it resonates with the resulting Faraday wave field. Secondly, the bath is to be close to the Faraday instability threshold so that Faraday waves of large amplitude and spatial extent can be excited subcritically by the drop impacts. The droplet bounces on the slope of the wave emitted at the previous bounce and so receives an impulsive force in a specific direction, along which it walks with a constant speed. These walkers are located in the "W" region of Fig. 1.7. Such walkers have both wave and particle components and have been shown to exhibit quantum-like dynamical behavior previously thought to be peculiar to the microscopic realm [2,3,5,6].

The analogy is even stronger, interactions in between these walkers - orbital motion, repulsion - have been studied in detail [25,44]. Consequently, we can associate to this walker a system composed of a wave field interacting with a particle. Couder *et al.* demonstrated that this system obeys a diffraction law when passing trough a submarine slit [2]. More precisely, after interaction, the walker follows the same spatial distribution statistics as a photon or an electron diffracting through a slit. Interference patterns have even been observed during a double slit experiment.

The following step was the examination of a "tunnel effect" for the walkers. When a walker collides with a submarine barrier, a part of the waves produced by the walker is transmitted and the other part is reflected. The consequence is that the walker either reflects off the barrier or passes through it. Depending on the height of this barrier, the passing probability has been measured as a function of this potential barrier [3]. The tunneling probability is shown to decrease when the width or the height of the barrier increases. Conversely, it increases when approaching the Faraday instability.

One of the latest papers by Couder and his co-workers [5] reports the observation of walkers on a rotating bath. The walker, being subject to Coriolis and centripetal forces, orbit in the frame moving with the bath. These orbits

can be quantified as being very close to the Faraday instability threshold. By identifying the de Broglie wavelength as the Faraday wavelength, once again an analogy can be made with quantum mechanics. Indeed, charged particles moving in magnetic fields are equivalently subject to a force perpendicular to the direction of motion and can only occupy discrete orbits with discrete energy values, called Landau levels.

The quantization of droplets orbits evidence a memorization of the path followed by the walker. Successive bounces of the walker are stored in the Faraday waves and the closer to the Faraday instability the more effective is the quantization and the *path memory*. The latter is being investigated experimentally, numerically and theoretically by Eddi *et al.* [4]. When interacting with obstacles, walkers exhibit different dynamics depending on the importance of this *path memory*. A careful analogy is made in this paper between the dynamics of these walkers with quantum particles. That reminds of the pilot wave theory initiated by de Broglie [45] in 1926. However, a difference is that the storage of information in the wave field piloting the droplet - a particle - seems to be a necessary condition to observe the quantum-like behavior in experiments.

1.3.7 Quantum behaviors

Diffraction through a slit, wave interferences and tunnel effect are well known in the microscopic world where they are explained by quantum mechanics. The latter is based on a probabilistic theory while our macroscopic world is governed by deterministic theories, this is paradoxal. Bush has written a interesting paper [6] pointing out similarities between the macroscopic experiments and the microscopic effects. Couder's microscopic-like experiments are all founded on the interaction of a particle and the emitted guiding wave. A walker is an association of a droplet and a wave, the one cannot exist without the other. This could reawaken the pilot wave theory, a microscopic theory that has been overtaken by the Copenhagen interpretation. The former theory, first introduced by de Broglie [45], has been revisited by Bohm [46]. For the first time, this theory has a macroscopic analogy.

1.4 Relevant questions

The state of the art demonstrates that the bouncing droplet problem has huge consequences ranging from the fundamental understanding of physics to the industrial manipulation of droplets. These researches are at their beginning. As long as discoveries are made in this domain, more intriguing questions and ideas of experiments arise.

Couder rationalized the observation of the acceleration threshold for the bouncing of highly viscosity droplets on a highly viscous bath, which is observed to start at $\Gamma_b = 1$ and to increase as f^2 [23]. However, low viscous droplets have a threshold Γ_b lower than 1 with several minima at different frequencies [47,48]. Does it mean that deformations and flows induced in the droplet are affecting the drainage flow? Besides, we demonstrated that above the acceleration threshold, the droplet periodically bounces without aging. Below the threshold, we observed that the bouncing droplet coalesces after a finite time. Is this a consequence of the particularity of the lubrication force acting from the air film on the droplet? Depending on the frequency and the size of the droplet, particular deformation modes are excited. Can we model our observations? Taking advantage of certain deformations can we achieve some microfluidic processes, e.g. droplet displacement, merging or emulsification?

A bouncing droplet follows complex trajectories which can be periodic. The dependence on the initial conditions plays a key role. For the same set of parameters, different trajectories are observed. Trajectories of a droplet bouncing on a soap film or of a bouncing ball on a vibrated plate have been investigated theoretically [26, 49]. Can we develop such a theoretical or a numerical model on the droplet bouncing on a vibrating bath? Can we extend this model to a deformable bath and explain the interesting behavior of the walkers?

1.5 Strategy

1.5.1 Dimensionless analysis

Let us strive to have a global view of the problem. A liquid droplet of diameter D bounces on a liquid interface oscillating sinusoidally at a frequency f and an amplitude A. The bath and the drop liquids are characterized by kinematic

viscosities ν_b and ν_d, densities ρ_b and ρ_d, and surface tensions σ_b and σ_d , respectively. The whole is submitted to the gravitational acceleration g. This system can be described in terms of 9 controlled physical variables leading to 6 independent dimensionless groups, which we choose to be ρ_d/ρ_b, D/A, $\Gamma = 4\pi^2 A f^2/g$, $f\sqrt{\rho_d D^3/\sigma_d}$, and two Ohnesorge numbers, one for the droplet $Oh_d = \nu_d\sqrt{\rho_d/\sigma_d D}$ and the other for the bath $Oh_b = \nu_b\sqrt{\rho_b/\sigma_b D}$, which indicate the relative magnitudes of the viscosity forces and the surface tension forces. Note that we should also consider the physical parameters related to the surrounding gas, the air. This has not been done because, all over the experiments the surrounding gas, will be air at ambient temperature and pressure which are supposed to remain constant.

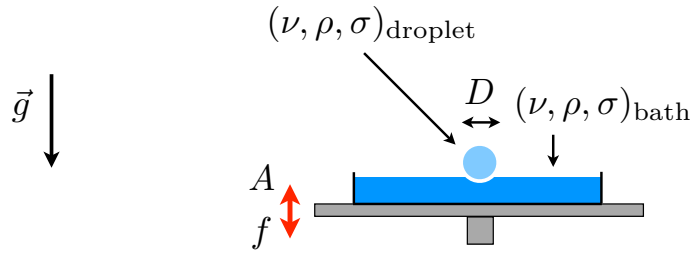

Figure 1.10: Schematic illustration of a droplet bouncing on a vibrating liquid bath. Relevant parameters are the gravity acceleration g, the droplet diameter D, the viscosity ν, the density ρ and the surface tension σ for the bath and the droplet, the amplitude A and the frequency f of the oscillating plate.

1.5.2 Ohnesorge numbers phase diagram

The angle from which we choose to attack the problem is the bouncing droplet question related to the deformability of either the bath or the droplet or both or none. Ohnesorge numbers of the bath and of the droplet indicate how oscillations are damped by viscosity. These parameters can be used to characterize the different behaviors of the bouncing droplet. On Fig. 1.11a, we have plotted a selection of bouncing droplet studies on a map depending on the Ohnesorge numbers Oh_d and Oh_b. We adjusted the plotted areas for a better visualiza-

tion. Obviously, these two parameters are not sufficient to describe unequivocally the behaviors of the droplets. Parameters such as the Reynolds number $Re = \gamma D/\omega\nu$ could also be used to evaluate the size of the crater. The map on Fig. 1.11a is a projection of the phase diagram on a 2D map defined by Oh_d and Oh_b. The first model for the threshold has been developed by Couder *et al.* [23] for highly viscous droplets on a highly viscous bath, it is located at the top right corner of the map. Protière *et al.* investigated the interactions of droplets through the capillary waves they emitted and initiated fundamental studies on the walker's mechanism [1,25,44,50,51]. Using oil of viscosity 50 cSt, this series of experiments were based on small droplets emitting waves on the liquid surface, they are located on the left upper part of the map. Eddi *et al.* performed quantum-like experiments with 20 cSt silicone oil. They are also based on the interaction of small droplets (walkers) with their emitted waves [3, 4]. Experiments on ratchet motion, drifting rafts, Archimedean lattices and oscillations in crystal of droplets were performed with the same set of experimental conditions [7, 29, 30]. All these experiments are located near the 50 cSt region of the map. Fort *et al.* changed the viscosity of the droplet and the bath in order to change the length of the Faraday waves emitted by the walkers [5], these experiments on the Landau levels are located in grey around the two previous described regions.

1.5.3 Exploration of the map

On Fig. 1.12a, we summarized the Fig. 1.11 in four extreme regions of the map where oscillations of the droplet or on the bath are relatively damped by the viscosity. Sketches illustrated the general behavior of the droplets: high or low deformable droplets on a highly or low deformable bath. We positioned our strategy on Fig. 1.12a and completed the diagram of Fig. 1.11 with our works and publications on Fig. 1.12b[1]. Note that we used two possibilities to vary the Ohnesorge number of the bath and the drop, i.e. the droplet size and the liquid viscosity.

[1]Even if we did not developed in this manuscript the small droplets that we observed to bounce in Tibetan singing bowls [8], the lifetime measurements of 50 cSt droplets on a bath of the same viscosity [52] and the wave propelled ratchet [7], we represented these works on Fig. 1.12b.

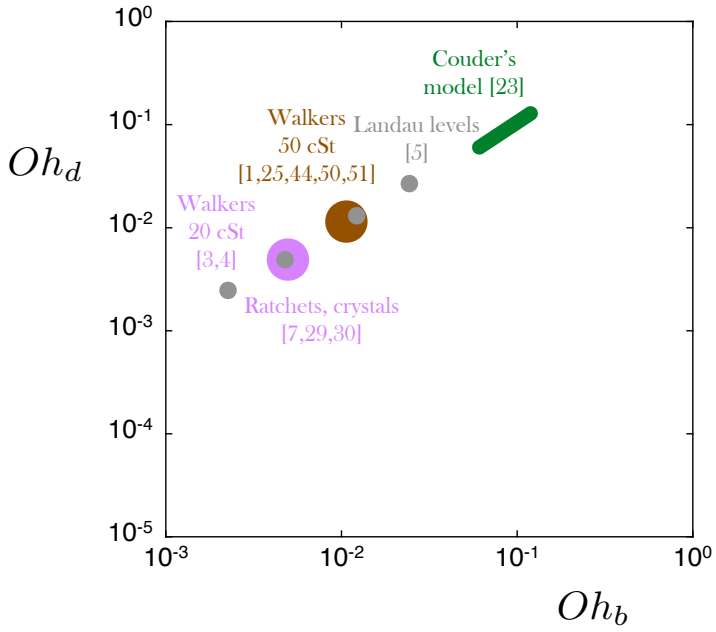

Figure 1.11: A selection of relevant works on bouncing droplets are plotted as a function of both Ohnesorge parameters Oh_d and Oh_b of the experiments. These represent the relative damping of the oscillations on the droplet and on the bath.

In this manuscript, we started by isolating the droplet deformation effects of the bouncing from the bath deformation in Chapter 2. We used large droplets of low viscosity silicone oil on a highly viscosity bath (cf. map on Fig. 1.12a). In Section 2.1 of this chapter, we described the resonant mode that can be excited on a droplet ([47] on Fig. 1.12b). In Section 2.2, we measured the bouncing acceleration threshold as a function of several controlled parameters. Above this threshold, bouncing is periodic and a droplet bounces sustainably. Below this acceleration threshold, a finite bouncing lifetime, originating from an evolution of the air film leading to the death of the droplet, is observed ([53] on Fig. 1.12b). Due to the peculiarity of the lubrication force acting on the bouncing droplet, we observed major differences compared with the bouncing ball, its solid counterpart. We then developed a bouncing droplet model in Section 2.3 to rationalize the bouncing threshold and the finite lifetime of the droplet below the bouncing threshold ([48,53] on Fig. 1.12b). Taking advantage of a particular mode of deformation, we performed a double emulsion in a compound droplet

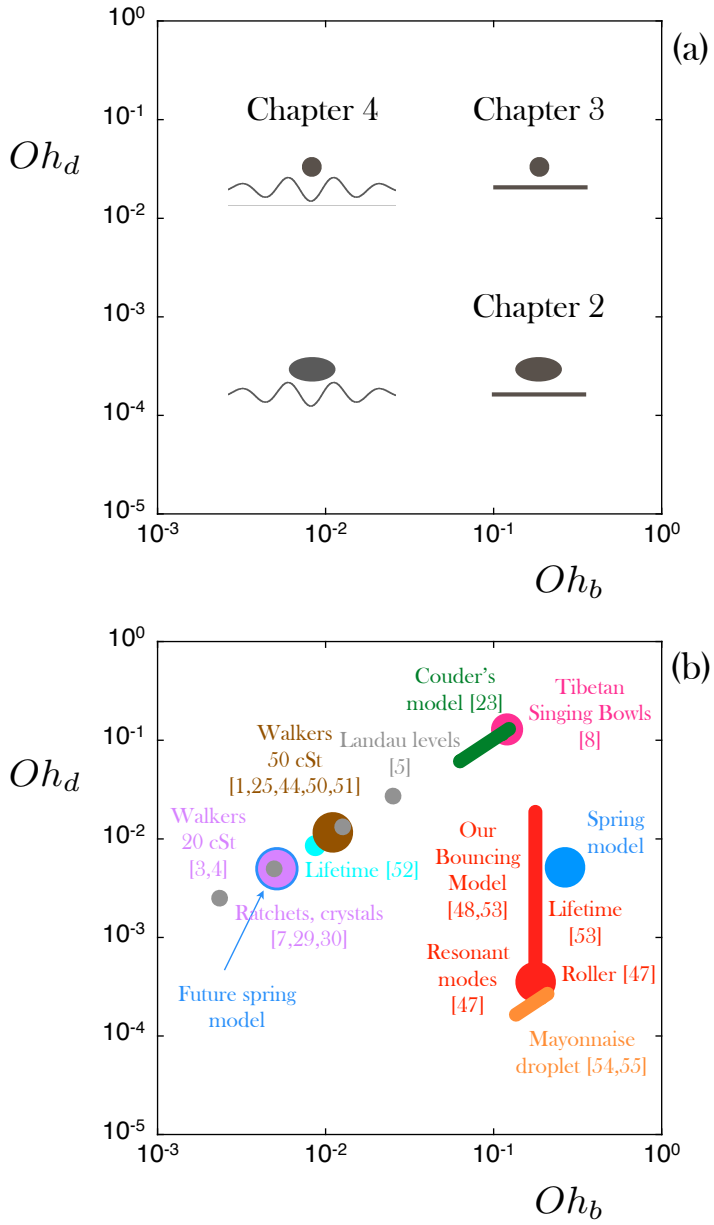

Figure 1.12: (a) Four extreme cases are spotted on Fig. 1.11, when oscillations are damped or not on the bath and on the droplet, i.e. Oh of the bath and of the droplet is large or small, respectively. Three extreme regions were visited in Chapter 2, 3 and 4 which are illustrated on the map. (b) We added to Fig. 1.11 all the works and the publications that are developed in this manuscript (except [7, 8, 52]).

made of two immiscible fluids. We observed an emulsion threshold that we show in Section 2.4 ([54,55] on Fig. 1.12b).

In Chapter 3, to simplify, we considered small bouncing droplets, which slightly deforms, on a highly viscous bath. We started, in Section 3.1, by investigating the deformation and the restitution coefficient of droplets bouncing on the bath when the bath is static. Section 3.1 is the basis of Section 3.2, where we studied the bouncing trajectories of these small droplets on the highly viscous bath when it was oscillating (cf. map on Fig. 1.12a). When the forcing acceleration or the frequency is tuned, droplets take various trajectories. We highlighted several periodic bouncing modes in Section 3.3, with a spring bouncing on a solid plate (blue disk on Fig. 1.12b). The spring parameters were adjusted from the study of the droplets falling on the static highly viscous bath. A non-instantaneous impact and a trajectory varying with the frequency are the reasons why it was necessary to develop such a model contrasting with the classical bouncing ball model.

We have naturally extended our study of these small droplets to a highly deformable bath in Chapter 4 (cf. map on Fig. 1.12a). In Section 4.1, we have observed small droplets falling on a static low viscous bath (20 cSt Silicone oil). We then constructed, in Section 4.3, a bouncing phase diagram that we discussed based on the observations made on the highly viscous bath in Chapter 3. After that, we presented a bifurcation diagram of a droplet that is able to walk on the surface. We discussed this diagram with measurements of the bouncing trajectories and gave an explanation of the speed of these walkers. To close the chapter, we proposed an extension of the model, developed in Chapter 3, taking the deformation of the bath into account. This study joined the previous works that are located in the "Walker 20 cSt" region on Fig. 1.12b.

Chapter 2

Only the droplet can be deformed

Contents

As stated in the strategy section, we start by studying the relevance of droplet deformations in the bouncing problem, while choosing to inhibit any deformations of the liquid bath. In Section 2.1, we present the deformation modes of droplets bouncing on a highly viscous bath that oscillates. The bouncing acceleration threshold Γ_b is observed versus the forcing frequency f according to the deformation mode. Beyond it, the bouncing is stable whereas below it is characterized by a lifetime. In Section 2.2, we present threshold and lifetime measurements as a function of the forcing parameters. In Section 2.3, we then build a model which is valid for the first bouncing mode in order to rationalize previous observations. This is the reason why some fits are plotted on experimental measurements and are explained later. Finally, in Section 2.4, we develop a method to make double emulsion in compound drops taking advantage of the droplet deformations.

2.1 Droplet deformation modes

In this section, according to the forcing frequency, specific vibrational modes of the droplet are excited which are attributed to spherical harmonics similar to those introduced by Rayleigh [56]. Then, we evidence their effect on the bouncing threshold. Eventually, taking advantage of an asymmetric mode of deformation, we uncover a mode of self-propulsion. The droplet, called a roller, translates horizontally on the surface of the bath.

How to obtain a non deformable bouncing surface

As we want to study the bouncing of a droplet on a rigid surface, we tried different approaches in order to obtain such a surface. A simplistic way could have been using a solid plane. Unfortunately, a droplet cannot start bouncing without inevitably entering in contact with the solid plane surface because the air film collapses immediately due to the roughness of the surface [57]. To delay this rapid collapse, a perfectly smooth liquid could be spread out on the surface of the solid plane to take advantage of both the rigidity of this plane and the smooth interface of the liquid. However, the thickness of this layer is not finely controllable.

That is for these reasons that we opted for the following system. We focussed on a highly viscous silicone oil bath, of viscosity $\nu = 1000$ cSt of about 1 cm depth. With such a bath, the capillary waves are fully damped as the Ohnesorge number $Oh = \nu\sqrt{\rho/\sigma D}$ is about 7, when taking the droplet diameter $D \sim$ 1 mm as the typical crater size. The Reynolds number $Re = \Gamma g D/\omega\nu$ is small, typically about 0.01, which ensures that the bath can be considered as a flat and rigid surface. The bottom of the container does not influence the bouncing droplets since the bath depth is larger than the penetration depth $\sqrt{\nu/f}$ which is about 6 mm for a droplet bouncing at 25 Hz. Note that we did not observed Faraday waves on the 1000 cSt bath as Faraday threshold Γ_F is higher than the accelerations we investigated. More precisely, the threshold Γ_F is 20 times higher than on a 50 cSt silicone oil bath, as predicted by Eq. 1.8.

Deformable droplets

Droplets of silicone oil were produced using a syringe and needles of different sections. The droplets diameter was $D = 1.53$ mm of silicone oil of viscosities ranging between 1.5 and 100 cSt. Their Ohnesorge numbers Oh were 0.01, 0.06 and 0.56 for droplets of viscosity 1.5, 10 and 100 cSt respectively. The damping of the droplet oscillations thus becomes much more efficient when the viscosity is increased.

Experimental considerations

A container, typically a cylindrical Petri box of diameter 10 cm and height 1 cm, is made to vibrate vertically via an electromagnetic shaker GW-V55 or GW-V20 according to a sinusoidal motion $A\sin(2\pi ft)$ (cf. Fig. 1.10). An accelerometer (PCB-Piezotronics, 352C65), which delivers a tension proportional to the acceleration with a factor of 101.2 mV/g, is glued on the vibrating plate. With the latter linked to an oscilloscope, we measured the maximal dimensionless acceleration of the plate $\Gamma = 4\pi^2 Af^2/g$, where g is the acceleration of the gravity. All the acceleration values in this manuscript are given with an error of 2 %. In appendix A, B and C, the reader will find information on silicone oils, experimental techniques for generating droplets and appropriate lighting used for images analysis.

2.1.1 Seeking the acceleration threshold for bouncing

Periodic bouncing only occurs when Γ is higher than a threshold value Γ_b. We created a droplet bouncing on the bath at a frequency f and an acceleration $\Gamma > \Gamma_b$. The forcing amplitude was then slowly decreased. At each decrement, the droplet was left bouncing on the bath for several minutes, if coalescence occurred during that time, Γ_b was reached. Since the droplet and the bath were made from different liquids, when coalescence occurs the bath is contaminated locally. To carry on our experiments, it was thus necessary to lay the droplets at different locations on the bath.

In Fig. 2.1, the threshold acceleration Γ_b is represented as a function of f, for droplets of diameter $D = 1.53$ mm with viscosities $\nu = 1.5$, 10 and 100 cSt. Here are our observations:

- The threshold acceleration for the 100 cSt droplet increases monotonically with the frequency and is always higher than 1 as demonstrated by Couder [23]. However, when the droplet viscosity is lower than the one used by Couder, the threshold does not increase following a power 2 law of the frequency f. The exponent is higher, closer to 3.5.

- We observed two minima on the 10 cSt curve. We could not initially explain why the first minimum was lower than 1 as reported in the Couder's bouncing mechanism [23].

- Three regularly spaced local minima are present on the 1.5 cSt curve at 50, 150 and 275 Hz. It suggests a resonance of the system: a minimal energy supply is required to sustain the periodic bouncing motion. The first minimum, at $f = 50$ Hz, occurs for $\Gamma_b = 0.25$, a value significantly less than the 1 g minimal threshold required by inelastic bouncing objects on a vibrating plate [49].

2.1.2 Uncovering the resonant states

We examined the behavior of droplets at the minima of the 1.5 cSt curve represented in Fig. 2.1. Using a high speed video camera, we recorded movies of droplets bouncing just above the acceleration threshold for each minimum. We observed modes of deformation which are analogous to the natural modes of

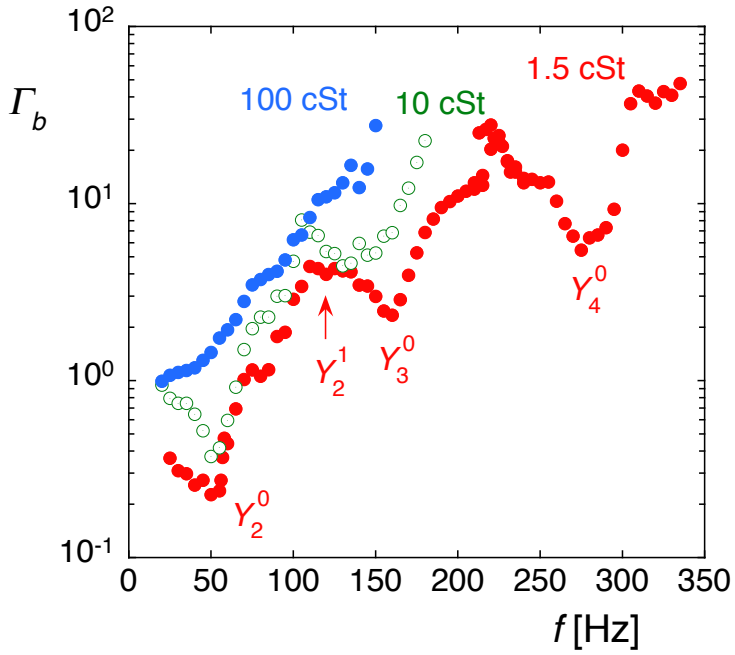

Figure 2.1: Evolution of the bouncing threshold acceleration Γ_b with respect to the forcing frequency. The red bullets (•), green circles (⊙) and blue bullets (•) correspond to droplets with viscosity ν =1.5, 10 and 100 cSt respectively, for a constant diameter $D = 1.53$ mm. Depending on the forcing frequency, various modes are observed that are related to spherical harmonics Y_ℓ^m.

deformation introduced by Rayleigh [56] and are expressed in terms of spherical harmonics Y_ℓ^m. We denoted by Y_ℓ^m the vibrational mode with m nodal meridians and $(\ell - m)$ nodal parallels. The fundamental mode for bouncing is the mode Y_2^0. On Fig. 2.2, movie snapshots of the observed deformation modes Y_ℓ^m are represented, on each line, with $m = 0$ and ℓ equals 2, 3 and 4, respectively. They are observed, at the acceleration threshold Γ_b, for forcing frequencies corresponding to the different minima in the threshold acceleration curve: Y_2^0, Y_3^0 and Y_4^0 modes occur at a frequency of 50, 160 and 275 Hz, respectively. The higher the frequency, the higher the order of the excited mode, and the higher the corresponding acceleration threshold. The first column shows the droplet shape during the landing phase while the second column shows the free fall. Each image was constructed from an experimental snapshot of the droplet (the right hand side) and the calculated 3D spherical harmonic (the left hand side in

color). The third column was obtained by subtracting the image of the columns A from the image of the column B. This evidences the nodal parallels, highlighted by orange points, which are the intersection of the nodal parallels with the vertical projection of the drop.

At the maximum, we also noted (we will be coming back to this later) that an asymmetric mode Y_2^1 is present at a local maximum of the threshold curve. We observed that these droplets roll horizontally on the liquid surface. As the bath deformations are not necessary, this mode of self-propulsion contrasts drastically with the bouncing walker mode described by Protière *et al.* [44]. Indeed to obtain these walkers, the liquid bath has to oscillate at an acceleration close to the Faraday instability threshold.

In 1879, Lord Rayleigh [56] described the natural oscillations of an inviscid droplet. Since these oscillations are due to the surface tension, the natural frequencies scale as the capillary frequency $f_c = \sqrt{\sigma/M}$, where $M = \pi\rho D^3/6$ is the droplet mass. More exactly, the dispersion relation brings out the natural "Rayleigh" frequency f_R related to a ℓ-mode:

$$\left(\frac{f_R(\ell)}{f_c}\right)^2 = F(\ell) = \frac{1}{3\pi}\ell(\ell-1)(\ell+2) \tag{2.1}$$

The function $F(\ell)$ may vary (frequencies are shifted by a multiplicative factor), depending on the way the droplet is excited [58, 59]. For free oscillations, this Eq. 2.1 is degenerated according to the m parameter. In Fig. 2.3, threshold data obtained for various droplet sizes collapse on a single curve by using the Rayleigh scaling. At the bouncing threshold, the vertical force resulting from the coupling between the deformation and the lubrication force in the air film balances the gravity. One may define a characteristic length $L_c = g/f_c^2$ corresponding to the free fall distance during the capillary time $1/f_c$. As shown in Fig. 2.3, the threshold amplitude $A_b = \Gamma_b g/(4\pi^2 f^2)$ scales as the length L_c, regardless of the droplet size. The minimum value of $A_b f_c^2/g$ does not vary significantly with the mode index ℓ. The natural frequencies defined in Eq. 2.1 neither correspond to the threshold minima nor maxima. However, these frequencies multiplied by 1.20 give the maxima positions, at $f/f_c = 1.20, 2.19$ and 3.39 for ℓ =2, 3 and 4 respectively. By analogy to previous works, this numerical factor is thought to depend on the geometry of the excitation mode (bouncing in this case) : e.g. another factor of about 0.74 is obtained when the droplet is stuck on a vibrating

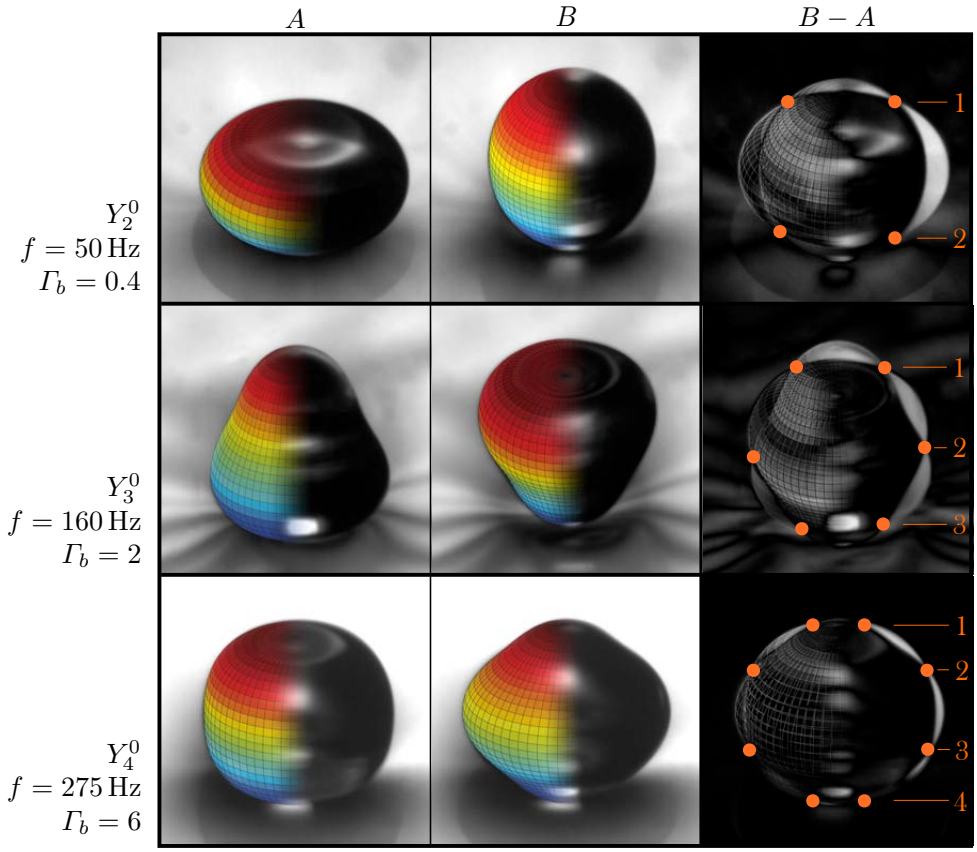

Figure 2.2: Axisymmetric deformation modes of a bouncing droplet of diameter $D = 1.53$ mm corresponding to the three minima of the acceleration threshold curve represented in Fig. 2.1 for ν=1.5 cSt. The two first columns represent snapshots taken at different phases of the oscillation, i.e. during landing and flying. The spherical harmonic solutions (in color on the left) are superposed to the experimental pictures (in grey on the right). Subtraction of the two first columns are presented in the third column. Nodal parallels are highlighted in orange.

solid surface [58,59]. Rigorously, this factor depends slightly on ℓ. On Fig. 2.4, we plotted the dimensionless frequency as a function of ℓ for the theoretical case of a levitating droplet given by Eq. 2.1, the sitting droplet experiments [58], and our measurements in the case of a bouncing drop. All data points are fitted by Eq. 2.1 with an adjustable prefactor which is 0.74 for the sitting droplet as predicted by [58] and 1.20 in our case.

2.1.3 Analysis of the bouncing mechanism

The bouncing droplet may be considered as an oscillating system analogous to the damped driven harmonic oscillator in which the surface tension is the restoring force and the viscosity the damping process. The dimensionless ratio between both phenomena is the Ohnesorge number. When $Oh \ll 1$, the viscous damping is negligible and the resonance is acute. Damping increases as Oh gets closer to 1. As seen in Fig. 2.1, the bouncing droplet responds to an increased damping in the same way as the harmonic oscillator : (i) the resonance frequency slightly decreases, shifting the whole threshold curve to the left, (ii) the required input Γ_b increases and (iii) extrema tend to disappear. At 100 cSt ($Oh = 0.775$), the damping is fully active, the threshold curve increases monotonically with the frequency and no more resonance is observed. This high-viscosity behavior has already been observed by Couder *et al* [23] for 500 cSt droplets bouncing on a 500 cSt bath. Those authors proposed to model the threshold curve by Eq. 1.6 detailed in Section 1.3.2. This equation is obtained by considering only the motion of the mass center of the droplet and the squeezing of the air film between a deformed droplet and bath under higher apparent gravity. This theory is not applicable in our case because we observe a minimum in the threshold curve $\Gamma_b(f)$ combined with a Γ_b value much lower than 1 for the first minimum. In our case, deformations are large. The deformation dynamics is more likely influencing the air drainage dynamics. That is the reason why, in Section 2.3, we developed a bouncing model in which droplet deformation dynamics are taken into account in the lubrication force to rationalize our observations. According to this model, minima in Γ_b curves correspond to a resonance phenomenon of the system droplet-air film.

So far, we can propose an intuitive mechanism to explain the extrema: the bouncing ability of the droplets results from the combination of (i) the droplet

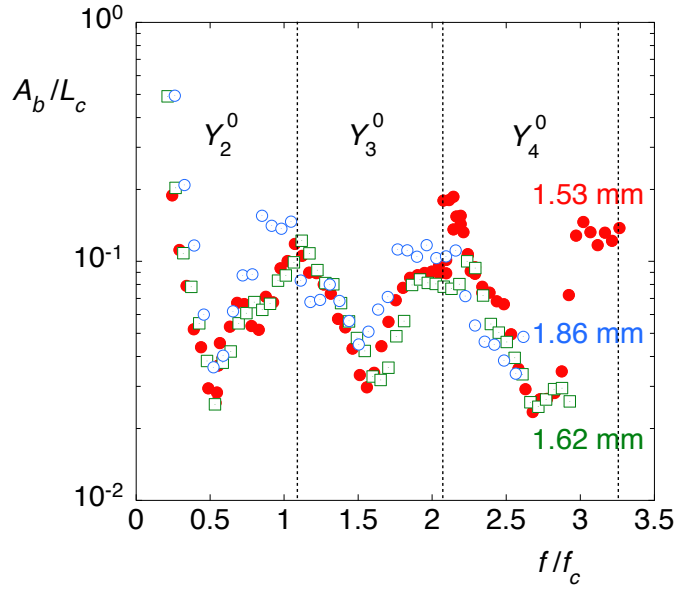

Figure 2.3: Dimensionless amplitude A_b/L_c as a function of the reduced forcing frequency f/f_c. Red bullets (•), green squares (⊡) and blue circles (⊙) symbols correspond to droplets of viscosity $\nu = 1.5$ cSt and diameter $D = 1.53$ mm, 1.62 mm and 1.86 mm respectively. Note that red bullets (•) are the same measurements as those presented on Fig. 2.1. Modes Y_2^0, Y_3^0 and Y_4^0 in between dashed lines. Maxima in the threshold curves correspond to frequencies that are obtained by multiplying the Rayleigh natural frequencies Eq. 2.1 by a factor 1.20.

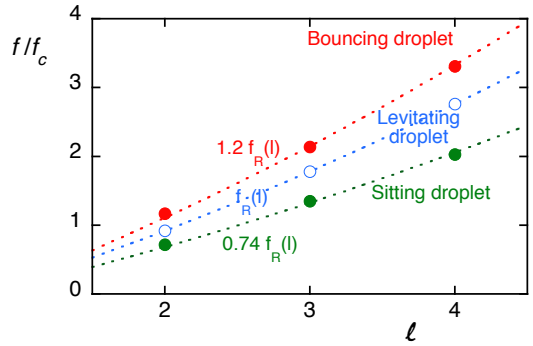

Figure 2.4: Dimensionless resonant frequencies of a droplet that deforms following the deformation mode Y_ℓ^0 as a function of ℓ. In blue, we plotted, for $\ell = 2$, 3 and 4, the theoretical natural frequencies of a levitating inviscid droplet prescribed by Eq. 2.1 [56]. In green, we plotted the measurements of the resonance of a sitting droplet on a solid plate that is vibrating [58]. In red, we plotted our measurements of the resonance of a bouncing droplet. Dashed lines are plots of Eq. 2.1 with an adjustable prefactor which is indicated on the graph. These are guides for the eyes.

deformation that stores potential energy and (ii) the vertical force that results from the squeezing of the intervening air layer between the droplet and the bath. The injection of energy by the bath is distributed between (i) translational energy of the droplet (the droplet bounce), (ii) internal kinetic energy due to the internal liquid motions in the droplet, (iii) the work consumed by the lubrication force and (iv) surface energy due to the deformation. Minima (maxima) in the threshold curve correspond to a maximum (minimum) of the ratio of energy converted to translational energy. Note that the maxima in threshold correspond to boundaries between modes. At those points, corresponding to a forcing frequency of $1.20\, f_R$, the most energy is spent in internal motions : the droplet resonates and absorbs energy.

In order to validate the mechanism that we propose, we started some experiments on the visualization of the internal flows in a bouncing drop. We used an optical method called Particle Image Velocimetry (PIV). Some fluorescent microspheres of diameter $15\,\mu m$ were dispersed in a 5 cSt silicone oil droplet of diameter 1.5 mm. This droplet was laid on an oscillating 1000 cSt silicone oil bath. The droplet was lit by the side with a vertical laser layer (green laser ND:YAG emitting at 535 nm). The microspheres fluoresce in orange and emit light at 580 nm. The microspheres motion were recorded from the side and perpendicularly to the laser beam, using a high speed camera Phantom v9.1 from Vision Research with a filter. Some snapshots of a bouncing droplet are displayed on Fig. 2.5. Using PIV, we observed that a flow is induced at the impact. Indeed, the bottom of the droplet receives a kick when the droplet lands, capillary waves are emitted and the top of the droplet flattens in turn. When the droplets take off, the microspheres are observed to nearly come back to their initial positions. Tracking the microspheres on the snapshots taken at each period where the droplet is at a maximum of its trajectory, we revealed a slow internal recirculation of frequency of about 0.5 Hz, far below the excitation frequency. This flow is suggested on Fig. 2.5 by white arrows. We are now investigating the characteristics of this recirculation as a function of the forcing acceleration Γ and frequency f. We observed that the frequency of the recirculation increases with Γ. We could also evidence the flow in each of the deformation modes. It would also be interesting to observe the flow in a walking droplet [1]. Is the walker droplet rotating?

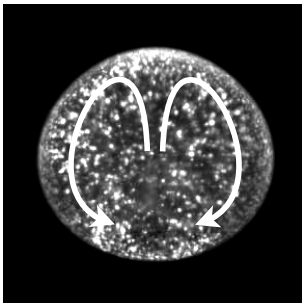

Figure 2.5: A snapshot of a bounce (at a maximum of trajectory) of a 5 cSt silicone oil droplet on a high viscous bath that oscillates at 50 Hz and at an acceleration $\Gamma = 2.5$. The internal flows are revealed by fluorescent microspheres.

2.1.4 A self-propelled mode

In the vicinity of the first maximum in the threshold curve, at 115 Hz, the droplet moves along a linear trajectory in a manner analogous to the walkers observed in [1, 25]. In the latter study, 50 cSt droplets with a diameter of 1 mm were produced on a 50 cSt silicon oil bath. The mechanism causing the walking motion is the interaction between the droplet and the bath surface wave generated by the bouncing. Such a mechanism does not work in the case of a 1000 cSt silicon oil bath. Indeed, the generated waves are rapidly damped and cannot be responsible for the motion of the droplet. A movie of this droplet was recorded using a high speed camera (Fig. 2.6a). Two first images A and B are separated by half of a period of the forcing oscillation and the third one is a subtraction of the first and the second images $(B - A)$. The deformation is not axisymmetrical as in the resonant minima of the threshold acceleration curve. We identified this mode as being related to $\ell = 2$ and $m = 1$ and being characterized by two orthogonal lines of nodes as enhanced in orange on the third image of Fig. 2.6a. This highlights the existence of two fixed points located on the equator of the droplet. As the line of nodes does not follow the axisymmetric geometry, those fixed points move. More precisely, the plate gives a kick to the asymmetric drop which is set in rotation. The drop thus deforms itself following the mode Y_2^1 which turns around two fixed points which correspond to the intersection of the two lines of nodes. The rotation

enhances the regeneration of the air film and induces drop motion in a straight line. This is a way to observe the Y_2^1 mode of deformation, which is generally degenerated together with the Y_2^0 mode since Eq. 2.1 depends only on ℓ. At the first maximum, a droplet in the Y_2^0 mode cannot bounce while a droplet in the Y_2^1 mode bounces and rolls. As far as Rayleigh frequencies are concerned, we thus observed a break in the degeneracy of the modes Y_2^0 and Y_2^1 on the m parameter.

Some tracers, given by Yves, were placed in the droplet (cf. Fig. 2.6b). The reflection of the light on these particles allows the following of the inner fluid motion, which clearly reveals that the droplet is rolling over the bath surface. The speed v of the droplet which is observed to be constant was measured with respect to the forcing parameters (amplitude and frequency). A scaling law can be found when considering that the phenomenon can occur only above a defined cut-off frequency $f_0 \approx 103$ Hz and the amplitude threshold $A_b(f) = \Gamma_b(f)g/(4\pi^2 f^2)$ as

$$v = 2\pi\alpha(A - A_b(f))(f - f_0) \tag{2.2}$$

where α is a constant. The speed is represented versus the characteristic speed $v^* = (A - A_b(f))(f - f_0)$ in Fig. 2.7. The proportionality between the speed of the roller and v^* is remarkable.

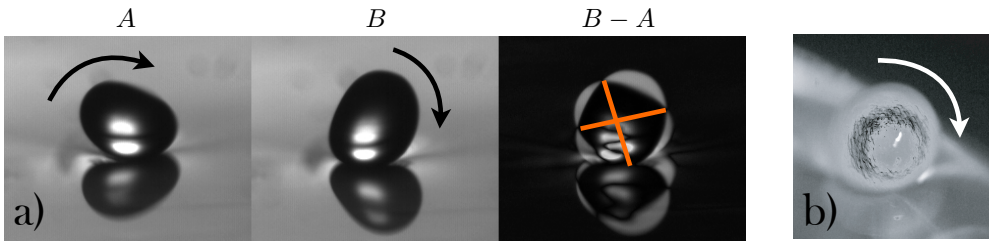

Figure 2.6: a) The rolling droplet deforms itself according to a deformation mode Y_2^1. The bouncing droplet ($\nu = 1.5$ cSt, $D = 1.53$ mm) is observed as a roller at $f = 115$ Hz and $\Gamma = 4.5 \geq \Gamma_b$. The two first snapshots are separated by half a period of the oscillating bath (~ 4.5 ms). The droplet rolls and moves towards the right. The third image which is a subtraction of previous ones reveals the two perpendicular lines of nodes (highlighted in orange). The roller turns around the two fixed points which correspond to the intersection of both lines of nodes. b) The rolling motion was revealed by small bright particles spread inside the droplet.

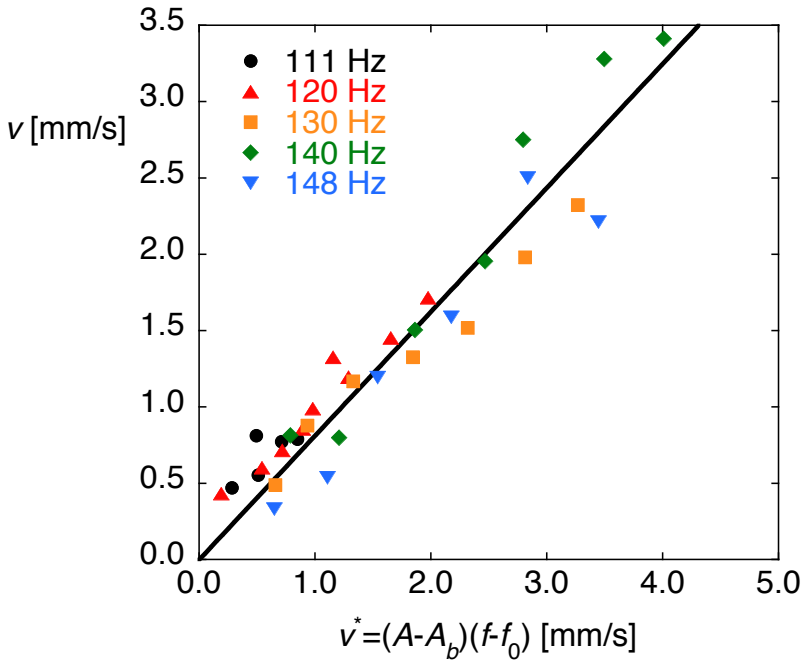

Figure 2.7: Speed of the roller for various frequencies (listed in the legend) as a function of the characteristic speed v^*. The droplet diameter is 1.53 mm while the viscosity is 1.5 cSt.

Three characteristic frequencies are involved in the rolling process : (i) the excitation time 100 Hz, (ii) the rotation of the liquid inside the droplet (about 10 Hz) and (iii) the translational motion (about 0.2 Hz) (Note that the droplet travels a distance corresponding to its circumference once every 5 seconds). The three processes are interrelated, i.e. the deformation induces the internal motion which in turn induces the rolling and translational motions.

2.1.5 Other deformation modes

Deformation modes such as Y_2^0, Y_3^0 and Y_4^0 are observed at the minima of the $\Gamma_b(f)$ curve just above the bouncing threshold acceleration. However, when we increase Γ and vary the frequency f, we can excite various deformation modes that can be described in term of spherical harmonics Y_ℓ^m. Let us remember that Y_ℓ^m defines the vibrational mode of a deformable sphere with m nodal meridians and $(\ell - m)$ nodal parallels. Brunet *et al.* [17] studied the deformation modes

of sitting puddles of water that are vibrating and built a phase diagram as a function of Γ and f. We chose to list all the modes of deformation that are predicted theoretically by Rayleigh [56]. These correspond to spherical harmonics with different ℓ and $m = \pm\ell$. These theoretical deformation modes are represented in Fig. 2.8a for ℓ ranging from 0 to 4. By varying the frequency f and the forcing acceleration Γ, we sought those deformation modes. Snapshots of the deformation modes that we observed experimentally are listed on Fig. 2.8b, the forcing parameters are noted on each snapshot. The first mode Y_0^0 cannot be encountered for liquid droplets as it is a mode of compression and decompression. The next modes Y_1^0 and Y_1^1 are simply modes of translation. The Y_2^0, Y_3^0, Y_4^0 modes and the roller mode Y_2^1 are indicated on the figure. We also observed modes Y_2^2, Y_3^1, Y_3^3 and one corresponding to one of the mode Y_4^1, Y_4^2 or Y_4^3. The Y_4^4 mode was also observed but not reported on the figure. Higher modes are difficult to identify. The bouncing droplets are an easy and relevant way to illustrate spherical harmonics.

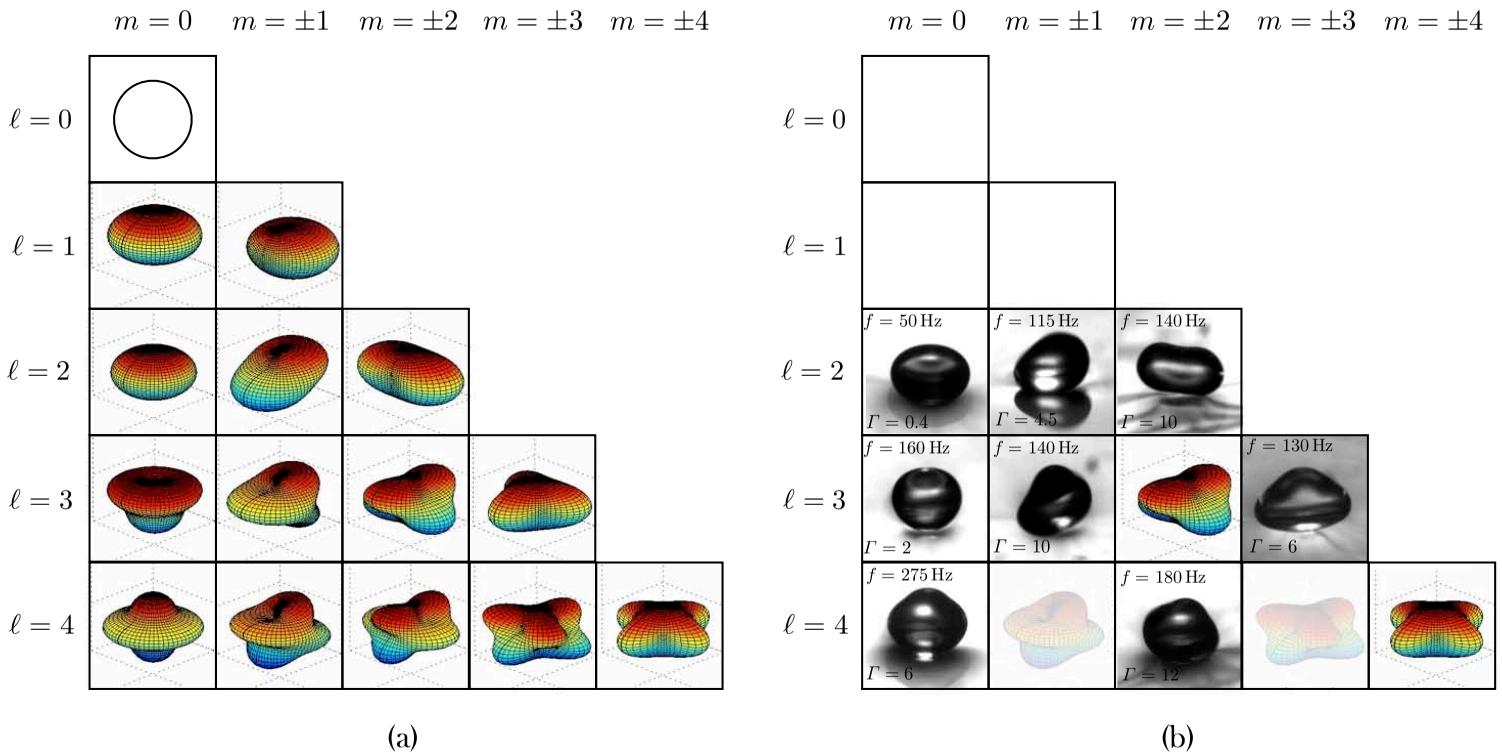

Figure 2.8: (a) List of snapshots of the theoretical deformation modes that can be excited on a deformable sphere. They are expressed in terms of spherical harmonics Y_ℓ^m. We limited our list to $\ell = 4$. (b) Experimental snapshots of the identified deformation mode Y_ℓ^m. The forcing frequency and acceleration are indicated for each snapshot.

2.2 Focusing on the deformation mode Y_2^0

In the previous section, we observed minima in the acceleration threshold curves as a function of the frequency which corresponds to different deformation modes. In this section, we focused on the first minimum corresponding to the deformation mode Y_2^0 and we investigated the stability around that threshold. Additional experiments were performed : they concern threshold measurements, lifetime measurements and air film thickness dynamics.

The stability of bouncing droplets was investigated above the threshold ($\Gamma > \Gamma_b$) for an homogeneous system, i.e. the droplets bouncing on a bath made of the same liquid [52]. Both were characterised by a low Ohnesorge number $Oh \sim 0.4$. The droplet vertical motion was shown to be periodic (as well as the evolution of the air film thickness). The droplets experience a finite lifetime that depends on the viscosity, the forcing parameters, etc. This fact has been related to the probability of an air film collapsing which is supposed to be linked to its thickness. An activated process like an Arrhenius law has been imagined [60,61]. Nevertheless, the droplets with $Oh \geq 1$ may bounce for a very long time that we considered to be infinite [1,25]. Below Γ_b, no significant lifetime was observed: the droplets coalesce quickly with the bath.

The situation is completely different in heterogeneous systems (i.e. low viscosity droplets on a highly viscosity bath). On a vibrating bath with $\Gamma > \Gamma_b$, the droplets lifetime exceeds 15 minutes and is thus considered infinite. However, when $\Gamma < \Gamma_b$, the droplet may bounce for a few tens of a seconds before coalescing. This finite lifetime depends on viscosity and forcing parameters (acceleration Γ and frequency f).

2.2.1 Bouncing threshold measurements of Y_2^0

We performed here some additional measurements of the bouncing threshold. Using a syringe, silicone oil droplets of diameter 1.53 mm with viscosities 1.5, 10, 50 and 100 cSt were placed on a vibrating bath of 1000 cSt silicon oil. The forcing frequency was tuned between 25 and 100 Hz. In this frequency range, the droplet deformation is accurately modeled by the spherical harmonics Y_2^0. The threshold Γ_b is determined experimentally as described in Section 2.1 : at a fixed frequency, a droplet is created on the bath at an acceleration high enough

to bounce and then the amplitude is decreased until coalescence (it can occur after a few tens of seconds). For highly viscous droplets of kinematic viscosity $\nu \geq 100$ cSt (Fig. 2.9d), the threshold acceleration is always higher than 1 and increases monotonically with the frequency (as predicted by Couder *et al.* [23]) but much more quickly than f^2. However, for lower droplet viscosities, the threshold can be lower than 1 and a minimum occurs in the $\Gamma_b(f)$ curve. At high frequencies, the $\Gamma_b(f)$ curve increases strongly with the frequency.

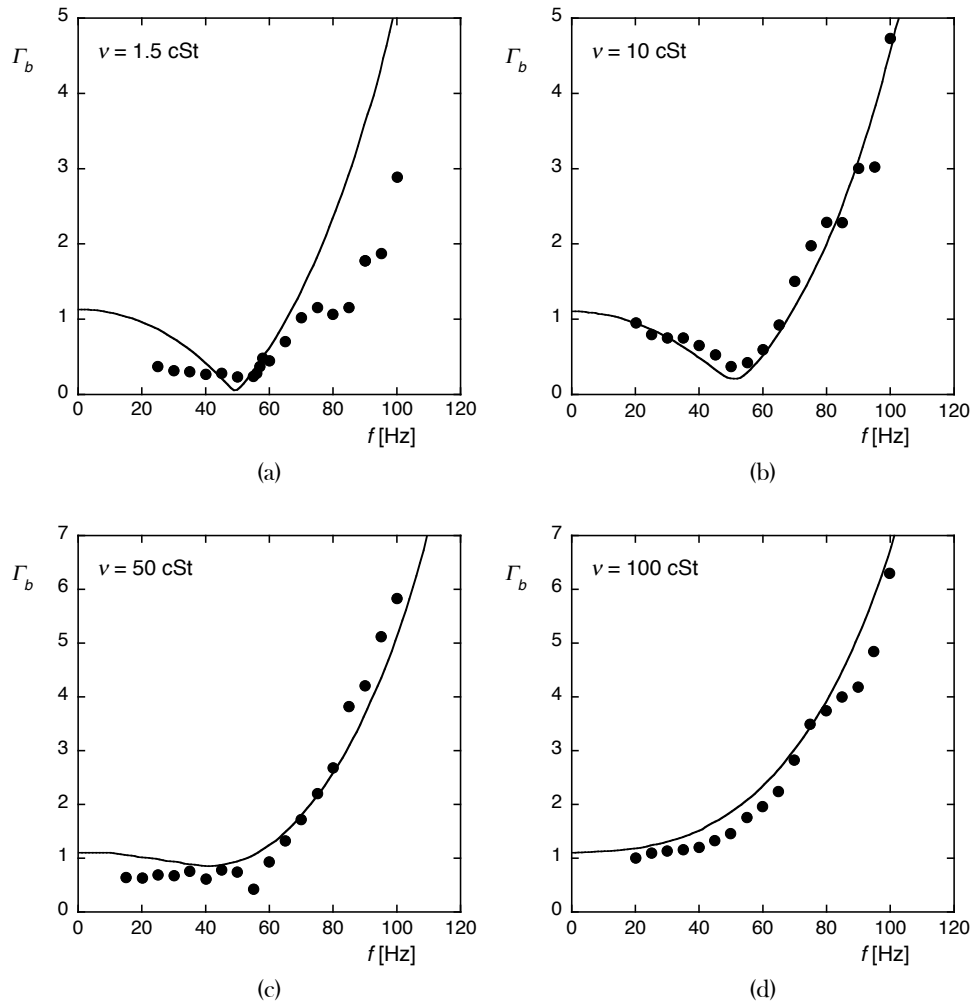

Figure 2.9: a) Acceleration threshold Γ_b required for the bouncing for various drop viscosities: (a) $\nu = 1.5$ cSt, (b) $\nu = 10$ cSt, (c) $\nu = 50$ cSt and (d) $\nu = 100$ cSt. The solid line corresponds to the model prediction, with coefficients $c_{L_2} = 17.5$, $c_K = 0.1$, $c_\sigma = 16\pi/5$ and $c_D = 3$ (cf. Section 2.3).

Information about the air film thickness can be obtained by using low pressure monochromatic sodium lights. The experimental setup is presented in Appendix B. Indeed, since the film thickness is typically micrometric, interference fringes are observed. According to [23,52], the number of fringes is related to a thickness of the film in a complex (but monotonic) way. These fringes are recorded from the top with a high-speed camera.

Above the threshold Γ_b, the evolution of the fringes is periodic which indicates that the droplet bounces periodically without aging, i.e. there is no thinning of the air film (on average). An aliasing technique, detailed in Appendix B, is used to overcome the 100 Hz oscillation of the lamp. On Fig. 2.10, snapshots of a droplet bouncing at $f = 26\,\mathrm{Hz}$ and $\Gamma = 0.92$ detail one bouncing event. Fringes appear when the droplet and the bath start to interact. A maximum number of fringes is visible when the air layer is minimum $e = e_{min}$. Interference fringes then disappear when the droplet lifts off.

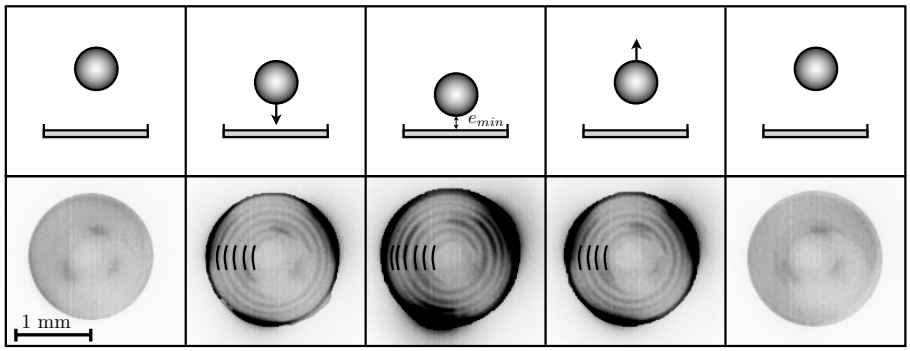

Figure 2.10: A droplet bounce - Successive snapshots of interference fringes (accentuated with black arcs) made by a bouncing droplet. The snapshots are separated by 8 ms. The number of observed fringes is directly related to the film thickness which varies between 100 nm and 10 μm. An increasing number of fringes is visible when the droplet lands and squeezes the air film (until the third column), then the number of fringes decreases as the droplet lifts off.

2.2.2 Lifetime below the bouncing threshold

Below the acceleration threshold the droplets are observed to bounce and coalesce after a period varying from a few seconds to a minute. The droplets are gently laid onto the vibrating bath set to an acceleration Γ between 0 and

$\Gamma_b(f)$ for 4 forcing frequencies, $f = 25$, 50, 75 and 100 Hz. They are subject to a low deformation, typically of about 5 to 10 % of their radius. The lifetime is measured starting from the first bounce on the bath. At least 18 droplets are used for each set of parameters. The standard deviation of the measured lifetime is reported as a typical error bar.

To begin with, we studied the statistical distribution of the lifetime of 10 cSt silicone oil droplets of diameter 1.68 mm at $f = 75$ Hz when the forcing acceleration is smaller than the threshold Γ_b. In Fig. 2.11, the cumulative distribution function is plotted for $\Gamma = 0.45$ ($\Gamma = 0.15\,\Gamma_b$) and $\Gamma = 1.8$ ($\Gamma = 0.6\,\Gamma_b$). Note that the mean lifetime $< \tau >$ is subtracted from measurements. Two cumulative distributions were fitted by error functions (the continuous lines on Fig. 2.11). These correspond to Gaussian distribution functions for the lifetime which are typical of an aging process. In general, we observe that the distribution of measured lifetimes is much narrower for the value of Γ that is the closest to the bouncing threshold Γ_b.

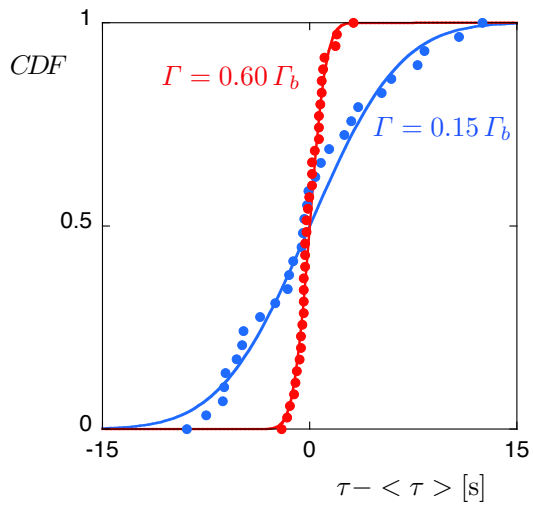

Figure 2.11: Cumulative Distribution Function *CDF* of the normalized lifetime of the bouncing droplets of diameter 1.68 mm ($f = 75$ Hz, $\nu = 10$ cSt) at various forcing accelerations (blue •) $\Gamma = 0.45$ ($\Gamma = 0.15\,\Gamma_b$), (red •) $\Gamma = 1.8$ ($\Gamma = 0.6\,\Gamma_b$). The lines represent fitted cumulative distributions function for Gaussian distribution which is typical of an aging process.

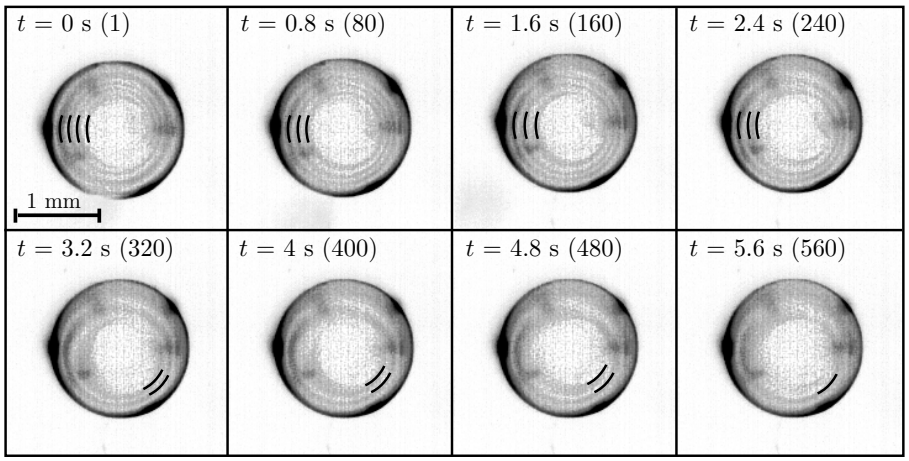

Figure 2.12: Below the bouncing threshold, the air film under a droplet thins at each bounce. Successive snapshots of the interference fringes (highlighted by black arcs) taken when the air film thickness is minimal, for a droplet bouncing at $f = 100$ Hz, $\Gamma = 0.22\Gamma_b$ and $\nu = 100$ cSt. The number of fringes decreases with time, indicating a progressive diminution of the average film thickness. The number of bounces from the start is indicated in brackets on each snapshot.

In order to connect the lifetime and the air drainage mechanism, the air layer thickness was observed while studying the interference fringes for $\Gamma = 0.5$ ($\Gamma = 0.22\,\Gamma_b$), $f = 100$ Hz and $\nu = 100$ cSt. In these conditions, the mean lifetime is about 20 s. Fringes are visible during the whole lifetime of the droplet. The film thickness is estimated to oscillate between 100 nm and 10 μm. In Fig. 2.12, fringes are shown for oscillating phases corresponding to the minimum in film thickness e_{min}. The number of fringes progressively decreases, which demonstrates that, even if the film is partially regenerated at each bounce, it drains out progressively and slowly.

Lifetime measurements of droplets of diameter 1.68 mm as a function of the forcing acceleration Γ are presented on Fig. 2.13a, b, c and d corresponding to the forcing frequencies $f = 25$, 50, 75 and 100 Hz, respectively. On each figure, three sets of data points are plotted corresponding to three droplet viscosities, $\nu = 10$, 50, 100 cSt. Measurements have also been made (but are not reported here) with a 1.5 cSt droplet, whose lifetime was less than 1 s when $\Gamma < \Gamma_b$. The vertical dotted lines correspond to the bouncing threshold Γ_b. Below Γ_b, at a fixed frequency, the lifetime curves present an optimum which increases with

the viscosity. Positions of these optima seem to depend only on the frequency in the same way as the bouncing acceleration threshold Γ_b. Nevertheless, it seems that the influence of viscosity cannot be assessed by simple scaling arguments. As seen on the error bars of Fig. 2.13 and confirmed by our statistical analysis (Fig. 2.11), the scattering of experimental data is very important when $\Gamma \ll \Gamma_b$, while the lifetime seems more predictable for larger values of Γ.

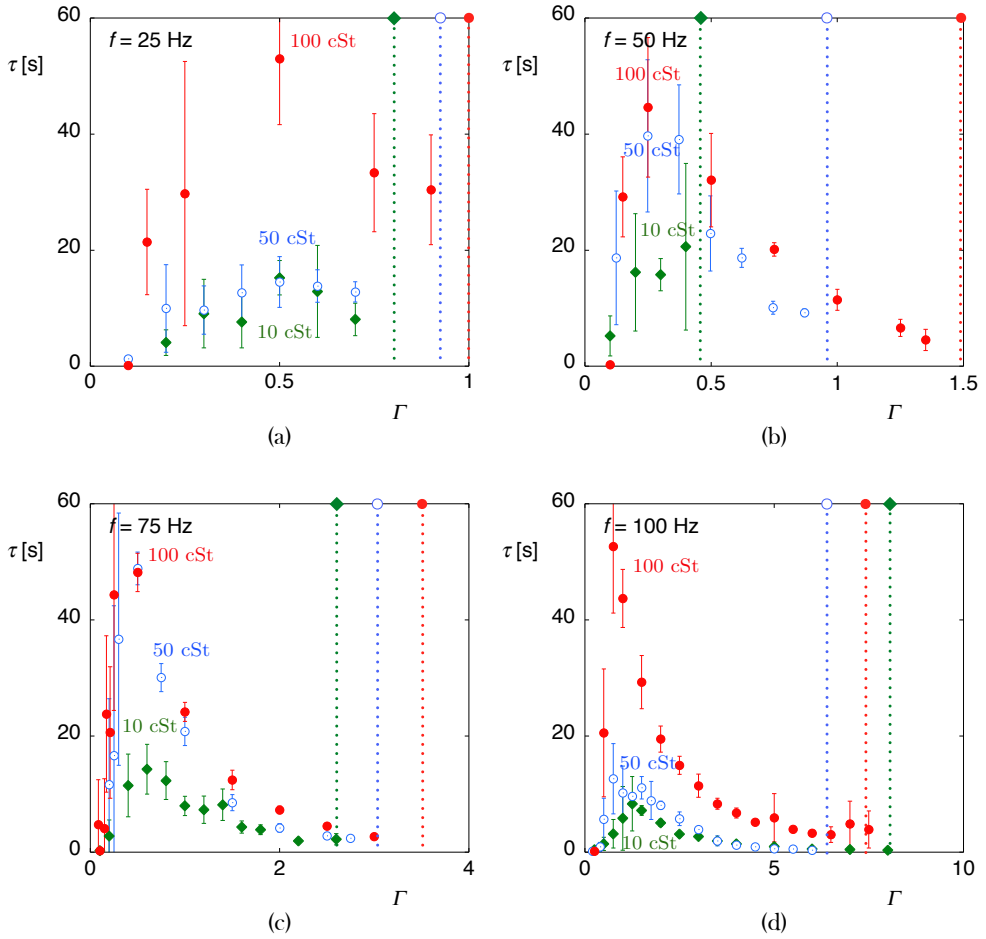

Figure 2.13: Lifetime τ of bouncing droplets of 1.68 mm diameter as a function of the forcing acceleration Γ for various droplet viscosities and forcing frequencies. The bath is made of 1000 cSt silicone oil. Symbols are (green ♦) $\nu = 10$ cSt, (blue ○) $\nu = 50$ cSt and (red •) $\nu = 100$ cSt. The vertical dotted lines are the bouncing thresholds Γ_b for the drops corresponding to each series of data points. Forcing frequencies are a) $f = 25\,\mathrm{Hz}$, b) $f = 50\,\mathrm{Hz}$, c) $f = 75\,\mathrm{Hz}$, d) $f = 100\,\mathrm{Hz}$.

2.3 Building up a model

We propose the following model in order to describe the Γ_b dependence on the forcing frequency f and the droplet viscosity ν. It explains also the finite lifetime below Γ_b. The idea being that a droplet stores energy in its successive deformations. During this process, the deformation influences the air film drainage. We can expressed the Newton equations for the droplet considering two external forces, the apparent gravity force and the lubrication force. Energy is dissipated by the viscosity in the fluid motion inside the droplet and in the air film through the lubrication force. In order to have a periodic bouncing, the energy loss has to be completely recovered by the vibrating bath through the lubrication force.

The motion of the droplet mass center (mass M) is confined to a vertical axis. The droplet bouncing can be modeled with two scalar ordinary differential equations describing the vertical position x_c of the mass center and the vertical deformation η of the droplet (Fig. 2.14a). As we work with a rigid bath, we consider the bath as a perfectly smooth solid. During its flight, the droplet experiences an apparent weight $Mg(\Gamma\cos(2\pi ft-1))$ in a frame moving with the bath. The droplet is stressed by the surrounding air, resulting in a vertical force F_L, which depends on the thickness e of the film and its rate of decrease $\dot{e}$ can be estimated by the lubrication theory [13].

The movements inside the droplet also have a significant influence on the air film drainage. The air flow is assumed to be axisymmetric and can be modeled by a Poiseuille flow between two parallel planar interfaces. In the frame of the bath, the bottom interface is at rest, while the upper moves with a vertical velocity equal to $\dot{e}$ and a horizontal velocity proportional to $\dot{\eta}r/R$, where r is the radial cylindrical coordinate, R the radius of the unstrained droplet and $\dot{\eta}$ the vertical deformation speed (Fig. 2.14b). Therefore, the lubrication force from the air film on the droplet is given by

$$F_L = c_{L_1}\mu_a R^4\left(c_{L_2}\frac{\dot{\eta}}{e^2R}-\frac{\dot{e}}{e^3}\right), \tag{2.3}$$

where c_{L_1} and c_{L_2} are positive constants and μ_a is the dynamic viscosity of the air. According to the lubrication theory, $c_{L_1}=3\pi/2$. The parameter c_{L_2} represents the influence of the flow inside the droplet on the flow in the air film. It cannot be estimated by simple arguments.

Newton's second law applied to the droplet is written as

$$M\frac{d^2x_c}{dt^2} = Mg(\Gamma\cos 2\pi ft - 1) + F_L. \tag{2.4}$$

For practical reasons, we use $e = x_c - R - \eta$ instead of x_c. The evolution of η is prescribed by an energy transfer balance in the frame of the mass center of the droplet:

$$\frac{d(K+E)}{dt} = -P_D - P_F, \tag{2.5}$$

where K is the kinetic energy of the motion inside the droplet, E is the potential interfacial energy and P_D is the power lost to viscous dissipation power inside the droplet. The power developed by F_L, called P_F, is supposed to be equal to $\dot{\eta}F_L$. A convenient way to estimate K, E and P_D as a function of η refers to the potential flow related to unimodal infinitesimal capillary waves at the surface of a droplet [9]. As we observed that only the mode Y_2^0 is present, coefficients are computed for this deformation mode and given in Table 2.1.

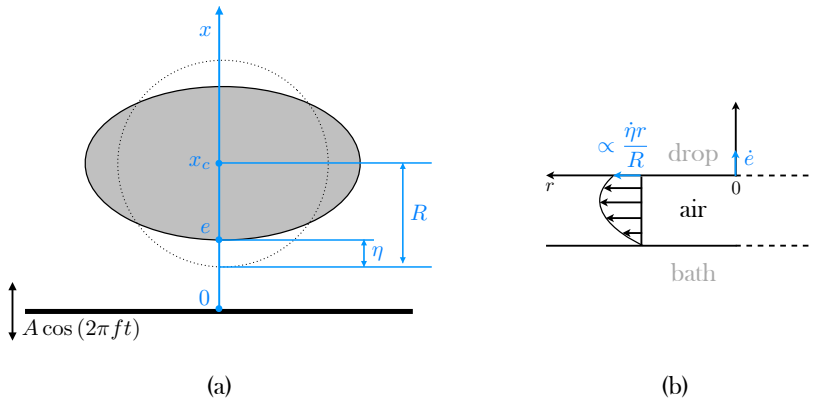

Figure 2.14: a) Geometrical variables of the bouncing droplet model : R is the radius of the undeformed droplet, x_c is the distance between the droplet center of mass and the bath, e is the air film thickness on the x axis and η is the vertical droplet deformation about the axis of symmetry. b) The air flow between the droplet and the bath is modeled by a Poiseuille flow between two parallel planar interfaces separated by a distance e. The lower interface behaves like a wall while the upper one moves with a horizontal velocity proportional to $\dot{\eta}r/R$ and a vertical velocity equal to $\dot{e}$.

Law	Y_2^0 mode
$K = c_K M\dot{\eta}^2/2$	$c_K = 3/10$
$E = c_\sigma \sigma \eta^2/2$	$c_\sigma = 16\pi/5$
$P_D = c_D \nu M\dot{\eta}^2/R^2$	$c_D = 3$

Table 2.1: Constitutive laws for the energy balance of the droplet deformation. The parameter ν is the kinematic viscosity of the droplet, and σ is its surface tension. The second column gives the theoretical coefficients c_K, c_σ and c_D for deformation modes Y_2^0.

2.3.1 At the bouncing threshold and beyond

We observed that the bouncing droplet motion is periodic beyond the acceleration threshold Γ_b and that the air film thickness decreases when the droplet does not bounce. Consequently, the solutions of the system should be periodic. Forcing the Eq. 2.4 and Eq. 2.5 to be periodic requires the following [48]:

- a mechanism of potential energy storage (droplet deformation) has to be taken into account to ensure the equations' periodicity. The droplet has to spend more time in an oblate state ($\eta < 0$) than in a prolate state ($\eta > 0$). This has been verified experimentally in [52];
- internal movements in the liquid phase, related to the deformation rate, must have a significant influence on the film drainage and the resulting lubrication force. A significant phase shift between the minimum film thickness and the maximum compression must be observed;
- this model is minimal, if one of the physical effects listed above is omitted, no periodic bouncing solution can be found; and
- there is a cut-off frequency $f_c^2 = \frac{1}{4\pi^2}\frac{c_\sigma}{c_K}$ above which the model cannot predict bouncing. This frequency corresponds to the natural resonance of the Y_2^0 deformation mode, when the droplet is directly excited (i.e. not excited through the air film dynamics).

In order to compare the model predictions with the experimental data shown in Fig. 2.9(a) to Fig. 2.9(d), we made a single fit on c_{L_2} and c_K while the theoretical values for the mode Y_2^0 are taken for $c_D = 3$ and $c_\sigma = 16\pi/5$ (c_{L_1} is

not present in equation to fit). The values obtained $(c_{L_2}, c_K) \sim (17.5, 0.1)$ are close to the values estimated theoretically (Table 2.1). Using results from the fit, we plotted the model prediction for the acceleration threshold on each curve of Fig. 2.9. The comparison with the experiments is acceptable, both qualitatively and quantitatively. The model reproduces all main features of the $\Gamma_b(f)$ curves including the minima for low viscosities and divergence for high frequencies. For an oil droplet with a diameter of 1.53 mm bouncing in Y_2^0 mode, resonance is observed at a maximum frequency of 51 Hz when the viscosity is less than 32 cSt, and the cut-off frequency is about 165 Hz. The quantitative discrepancies may be due to the fact that only a pure Y_2^0 deformation mode is considered in our model. A detailed formulation of the model has been published in Ref. [48].

2.3.2 Below the bouncing threshold

When $\Gamma < \Gamma_b$, the droplet does bounce but the air film is not completely renewed. The droplet behaves like a simple forced oscillator. The thickness of the air film $e(t)$ decreases with time and the droplet eventually coalesces when the film reaches a critical thickness. Considering this, the time τ necessary to reach the critical thickness can be derived from the model. The model parameters are set by the fits of the Γ_b measurements. Furthermore, τ is a function of a parameter τ_0 defined as the lifetime that could be obtain without forcing acceleration ($\Gamma = 0$). In Fig. 2.15, we represent a schematic illustration of the normalized lifetime τ/τ_0 as a function of the normalized acceleration Γ/Γ_b for a low frequency ($f \to 0$ Hz) and a high frequency ($f \sim 100$ Hz). The curves corresponding to intermediate frequencies are of the same shape and are located in between these two curves.

In Fig. 2.16a, the lifetime is plotted as a function of the forcing acceleration for various droplet viscosities and for $f = 100$ Hz. The acceleration is normalized by the threshold acceleration Γ_b. The lifetime decreases and tends to 0 with increasing Γ, then abruptly goes to very high values when Γ reaches Γ_b. The steepness of the curve clearly underlines that Γ_b represents a threshold to reach permanent bouncing. On the one hand, at $f = 100\,\text{Hz}$, the lifetime decay occurs for characteristic accelerations approximately $\Gamma \simeq 0.5\,\Gamma_b$, whatever the viscosity. On the other hand, we can see in Fig. 2.16b that the decay acceleration increases proportional to Γ_b when the forcing frequency is decreased, shifting the whole

lifetime curve to the right. This experimental fact, which cannot be explained by simple arguments, is rationalized by the model.

As seen in Fig. 2.16a and 2.16b, those curves correctly fit the decreasing part of the experimental data with the only fitting parameter being τ_0. The complex variation of τ_0 with the droplet viscosity, mass, etc. is unfortunately not predictable by the model. However, the model does correctly capture the slow decrease of the lifetime with increasing Γ, followed by a sharp divergence at the threshold acceleration Γ_b. As in experiments, the decay in $\tau(\Gamma)$ is right-shifted when the frequency is increased. The increasing trend of $\tau(\Gamma)$ for very small values of Γ is not predictable by the model. It is likely that other uncontrolled parameters (e.g. the residual flows created inside the droplet when it is laid on the bath) considerably influence the lifetime at very low forcing accelerations.

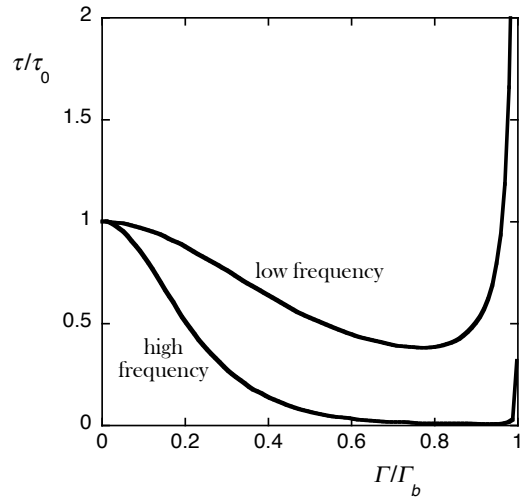

Figure 2.15: Schematic illustration of the normalized lifetime τ/τ_0 as a function of Γ/Γ_b, according to the bouncing model [53] for a low frequency ($f \to 0$ Hz) and a high frequency ($f \sim 100$ Hz). Curves corresponding to the intermediate frequencies are of the same shape and are located in between these two curves.

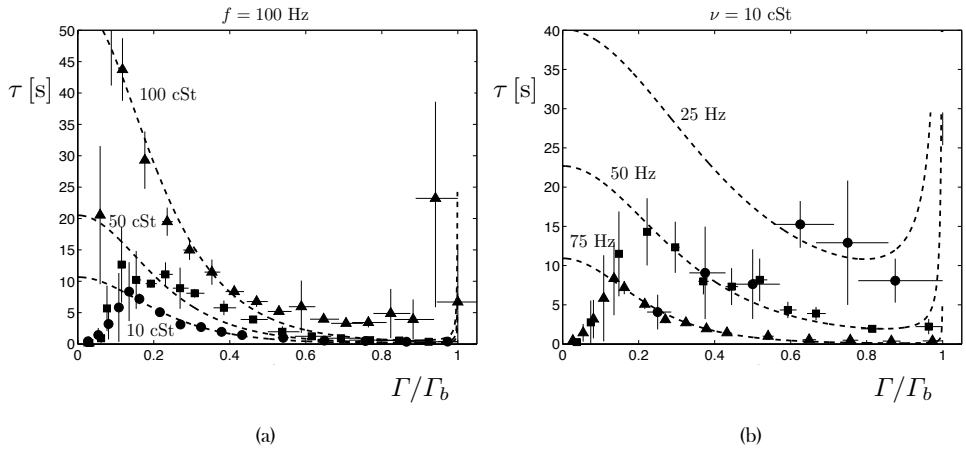

Figure 2.16: a) Lifetime τ of bouncing droplets, at $f = 100$ Hz, as a function of the normalized acceleration Γ/Γ_b for various droplet viscosities. (•) $\nu = 10$ cSt, (■) $\nu = 50$ cSt and (▲) $\nu = 100$ cSt. Solutions of the model are represented by dashed curves. b) Lifetime τ of bouncing droplets as a function of the normalized acceleration Γ/Γ_b for a droplet viscosity $\nu = 10$ cSt at various forcing frequencies. (•) $f = 25$ Hz, (■) $f = 75$ Hz and (▲) $f = 100$ Hz. Solutions of the model are represented by dashed curves.

2.4 A high deformation mode enabling a double emulsion

After observing various droplet deformations, we thought about taking advantage of them to perform some microfluidic process. As a matter of fact, droplets can be put into horizontal motion on the bath by tuning the frequency and exciting the roller mode (Y_2^1). Several bouncing droplets, possibly made of different chemicals, can coalesce and merge with each other. When two immiscible drops are put together, the liquid with the lower surface tension surrounds the other one. A compound drop laid on an oscillating bath can bounce. Additionally, a double emulsion, namely an emulsion inside an emulsion, can be obtained in a compound drop bouncing, on a highly viscous bath, far above the bouncing threshold. Indeed, large deformations are excited which are followed by non-linear behaviors. Using oil and water, we can create a sort of mayonnaise droplet. In the following section, we detail an experimental method to create such a double emulsion, oil in water in oil, starting from a single compound drop (water in oil).

We start by determining experimentally the parameters (forcing and mixture composition) required to produce a double emulsion from a compound drop. In order to rationalize these observations, we analyze the behavior of a compound drop impacting a static liquid surface. The link between experiments made with a static and a vibrating bath is finally made by measuring the trajectory of a bouncing oil drop on a vibrating interface.

2.4.1 The emulsions: motivation

Emulsion-producing companies start to show interest in the endless applications offered by double emulsions. Droplets of a liquid A are encapsulated in a drop of a liquid B, which is itself surrounded by a third immiscible liquid C (which can possibly be the liquid A). The liquid B is mainly used to protect A from C, or to delay the mixing of A with C. This strategy can be useful to the food industry [62] or in pharmaceutics for a prolonged delivery of drugs [63].

During the past few decades, the scientists have been concerned by the production, the complex structure and the possible metastability of compound drops and double emulsions. Their stability may be enhanced by the use of surfactant molecules [64,65] or microparticles [66]. The well-defined production

of these multiphasic objects is complicated. Loscertales *et al.* [67] presented a method to produce micrometer/nanometer compound drops using the action of electro-hydrodynamic forces. Chiu *et al.* and Chen *et al.* [68,69] produced compound drops with an outer diameter of about 700 to 1000 μm with the help of a piezoelectric generator and studied the results of their impact on a hot surface. Prunet-Foch *et al.* [70] investigated the impact of compound drops in simple emulsion on a solid substrate. Traditionally, double emulsions are formed in microchannels [71] or by shear-induced rupturing [72, 73], usually in two emulsification steps. This way, a first emulsion is created with two immiscible fluids and then this emulsion is again emulsified in a third continuous phase. More recently, some other fabrication processes were developed in order to generate relatively well-controlled double emulsions in one step [74]. Hereafter, we develop an original method to emulsify a compound drop which is based on the repeated impacts and rebounds of it onto a liquid interface.

2.4.2 Creating a compound droplet

The initial compound drop results from the merging of a distilled water drop (density $\rho_w = 1000$ kg/m^3 and kinematic viscosity $\nu_w = 1$ cSt) and a silicone oil (from Dow Corning) drop (density $\rho_o = 850$ kg.m^{-3} and kinematic viscosity $\nu_o = 1.5$ cSt). The surface tension of the oil (relative to the air) is $\sigma_{o/a} = 16.8$ mN.m^{-1}. In order to favor the deformations of the water/oil interface, an anionic surfactant, sodium dodecyl sulphate (SDS), is added in the water drop, at a concentration 10 times higher than the Critical Micellar Concentration (CMC). The resulting interfacial tension between oil and water is estimated according to the natural oscillations of a water drop immersed in oil [9,26]:

$$\sigma_{w/o} = \frac{3\pi m}{8T^2}\left[1 + \frac{2\rho_o}{3\rho_w}\right] = 7.1\,\text{mN.m}^{-1} \pm 1.0\,\text{mN.m}^{-1}, \tag{2.6}$$

where m is the mass of the drop and T is the period of its first mode of self-oscillation (spheroid). This estimation is in good agreement with a direct measurement ($\sigma_{w/o} = 8.6 \pm 1.0$ mN.m^{-1}) using the pendant drop method measured with an optical goniometer CAM200 (KSV Instruments).

The compound drop generation device consists of two syringes (one for each liquid) whose nozzles are connected by a thin copper wire curved downwards (cf. Fig. 2.17) [75]. The surfactant solution drop (light blue in Fig. 2.17),

created with the first syringe, slides along the wire and stops at the lowest point. Then, the oil drop is released from the second syringe (yellow in Fig. 2.17); it slides down and encapsulates the water drop. The resulting compound drop is sufficiently large to spontaneously detach from the fiber, fall and start bouncing onto the oscillating liquid surface, approximately 5 mm below. The bouncing motion was recorded at 1000fps with a fast video camera (IDT-N3).

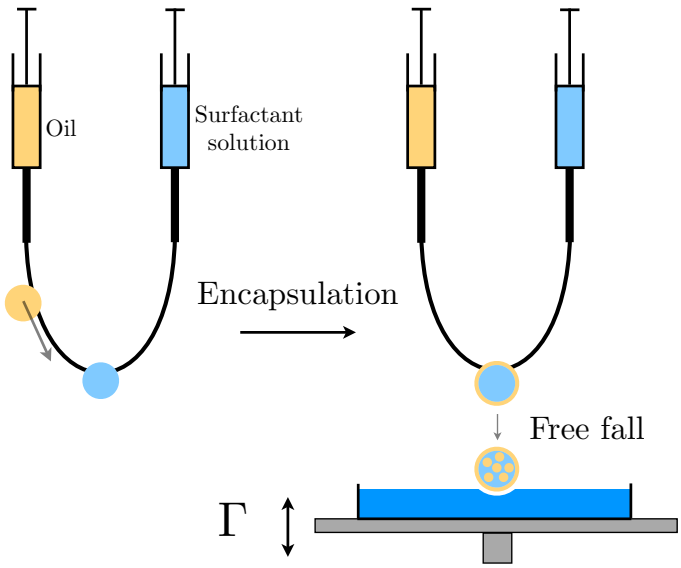

Figure 2.17: The compound drop is created by using two syringes connected by their ends by a thin copper wire. A water and an oil drop are respectively released from each syringe, they slide along the fiber and stop at the lowest point where they eventually merge. The compound drop detaches itself from the fiber and falls onto the oscillating liquid bath.

The volume of each drop is fine-tuned by selecting the needle diameter and the wire width [75]. We tested five compositions of millimetric compound drops (Table 2.2). In order to evaluate the influence of viscosity on the deformations, the Ohnesorge number $Oh = \nu\sqrt{\rho/\sigma D}$ has been successively estimated from the diameter D of the compound drop and the liquid properties of oil and water. In all cases, this Ohnesorge number is less than 0.01, so the drop deformations are slowly damped. Conversely, as the bath is made of 1000 cSt silicone oil, its deformations are quickly and fully damped by the viscous effects and so may be neglected.

Symbols	$\Omega_w[\mu\text{L}]$	$\Omega_o[\mu\text{L}]$	$\Omega_{cd}[\mu\text{L}]$	$D_{cd}[\text{mm}]$
⊠ □	1.1	1.05	2.15	1.60
◊	1.75	0.68	2.43	1.67
▽	1.29	1.29	2.58	1.70
△	1.42	2.10	3.52	1.89
○	2.99	1.15	4.14	2.00

Table 2.2: Composition and volume of the different tested compound drops (5 sizes). The columns represent, respectively, the water volume Ω_w, the oil volume Ω_o, and the total volume Ω_{cd} and diameter D_{cd} of the compound drop.

2.4.3 Bouncing threshold

As for single drops, we observed sustained bouncing of compound drops when the amplitude of the forcing vibration exceeds a threshold which value depends on the forcing frequency and the drop properties (surface tension, viscosity and size among others). For the frequencies investigated, 25 to 130 Hz, the relatively small deformations may be associated with the spherical harmonic function Y_2^0. We measured the bouncing threshold of compound drops of volume 2.15 μL (cf. composition in Table 2.2) by placing these drops on a vibrating bath and then decreasing the forcing amplitude until coalescence. The measurements (⊠) are reported on Fig. 2.18. The minimum in the bouncing threshold curve is clearly visible. As demonstrated in previous sections of this chapter, a minimum is a characteristic of the low viscosity bouncing droplets. It is a consequence of a resonance of a highly deformable droplet coupled with the drainage of the air film between the drop and the bath.

2.4.4 Emulsification threshold

We observed the spontaneous creation of a double emulsion for much larger forcing amplitudes, when the bouncing trajectory becomes chaotic. During vigorous impacts, the drop deformation may become so important that a tiny droplet of the oil layer is injected into the water drop. This phenomenon is shown in Fig. 2.19 for a compound drop of total volume 3.52 μL (△ in Table 2.2) and forcing parameters $(f, \Gamma) = (50\,\text{Hz}, 4.4)$. According to these snapshots, the drop flattens out as soon as it impacts the bath. The resulting capillary waves start

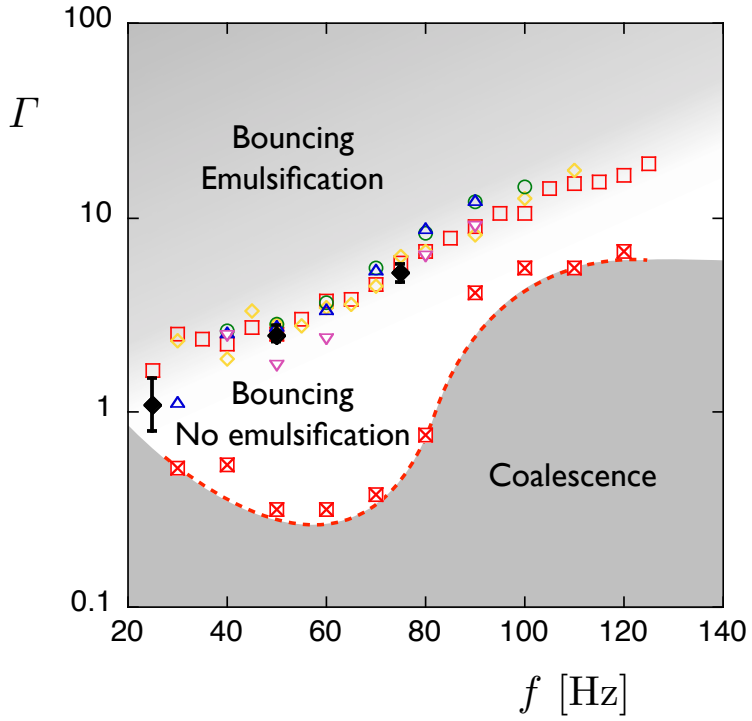

Figure 2.18: Bouncing threshold acceleration Γ_b (⊠) and emulsion threshold acceleration Γ_e (□, ◊, △, ○, ▽) as a function of the forcing frequency f. Symbols correspond to various sizes of the compound drop, as detailed in Table 2.2. Black diamonds are explained in Fig. 2.22 (cf. text).

propagating from the bottom to the top of the drop [76]. The convergence of these waves at the top locally pushes the oil shell inside the water interface and a pinch-off occurs so that an oil droplet is released in the inner water drop. This mechanism of droplet creation through wave convergence and pinch-off is similar to what is observed in the partial coalescence of low viscosity drops [11, 12]. By analogy, we may therefore expect a critical Ohnesorge number above which these waves are damped and the water-oil interface no longer pinches off. Each sufficiently strong impact creates an additional oil droplet into the water drop (cf. Fig. 2.20) and, by doing so, the initial compound drop progressively turns into a double emulsion. The process comes to a stop when the numerous oil droplets inside the water drop start to strongly dampen the capillary waves, therefore preventing any additional pinch off. The large impact velocities could weaken the air film and lead to premature coalescence of the emulsion with the underlying bath. Therefore, as soon as the emulsification is completed, the forc-

ing acceleration can be significantly decreased in such a way that the bouncing becomes smoother and much more stable. Then, the emulsified compound drop can be manipulated, e.g. by adjusting the forcing parameters in order to excite the so-called 'roller' mode of deformation, developed in Section 2.1, inducing a drop motion.

The emulsification behavior is only observed for high dimensionless forcing acceleration Γ. A second threshold value Γ_e, where $\Gamma_e > \Gamma_b$, exists, above which pinch-off occurs and the inner droplets are created. In order to measure this threshold, a compound drop is gently released onto the oil bath oscillating at an acceleration just above Γ_b. The forcing amplitude is increased step by step, the frequency being fixed. Three scenarios are observed: when $\Gamma < \Gamma_b$, the compound drop quickly coalesces with the bath; when $\Gamma_b < \Gamma < \Gamma_e$, the compound drop starts bouncing on the oil bath exactly as a monophasic drop [23,47,48]; and when $\Gamma > \Gamma_e$, a double emulsion starts forming. Γ_e is measured as a function of the forcing frequency for various drop sizes (cf. Table 2.2). The emulsion threshold $\Gamma_e(f)$ is reported in Fig. 2.18 for each of the 5 drop sizes that we investigated, while the bouncing threshold $\Gamma_b(f)$ is only reported for the 2.15 μL drop (⊠).

As we have already noted in Section 2.1, the bouncing threshold for a pure oil drop depends on the drop size. Because bouncing is ensured by the deformation of the oil drop, Γ_b only depends on the ratio between the forcing frequency and the natural frequency of the drop deformation. The latter scales as $\sqrt{\sigma_{o/a}/M}$, where M is the total mass of the compound drop. Conversely, the emulsion threshold Γ_e is not found to be much influenced by the drop size. The corresponding curves in Fig. 2.18 collapse on each other when they are represented as a function of f. While the volume is doubled from the smallest to the largest drop (and so is the square of the natural frequency), the emulsion threshold remains unchanged. Our conclusion is that the drop deformations are too large to be directly affected by the forcing frequency. The latter only influences the emulsion threshold by modifying the height of the jump and so the strength of impact. Nevertheless, it should be noted that emulsification is not possible for very large drops, for which even sustained bouncing is not possible. Indeed, it has been shown [24] that for a given frequency, there is a maximum size of drops that can bounce without coalescing.

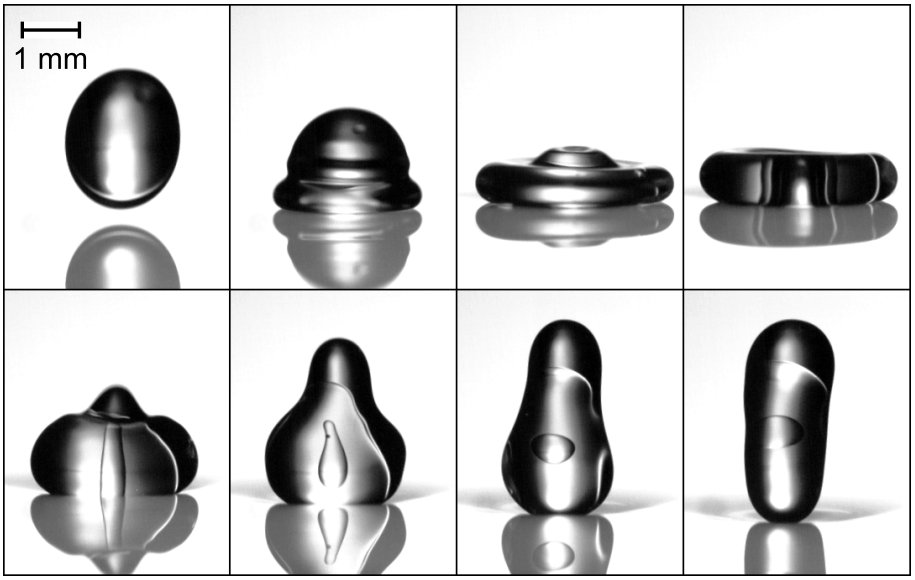

Figure 2.19: A compound drop ($\triangle$ in Table 2.2) bounces on a liquid surface vibrating sinusoidally at $f = 50$ Hz and $\Gamma = 4.4$. The convergence of capillary waves on the top of the drop pushes the oil layer inwards. The water-oil interface pinches off and a tiny oil droplet is released into the water core.

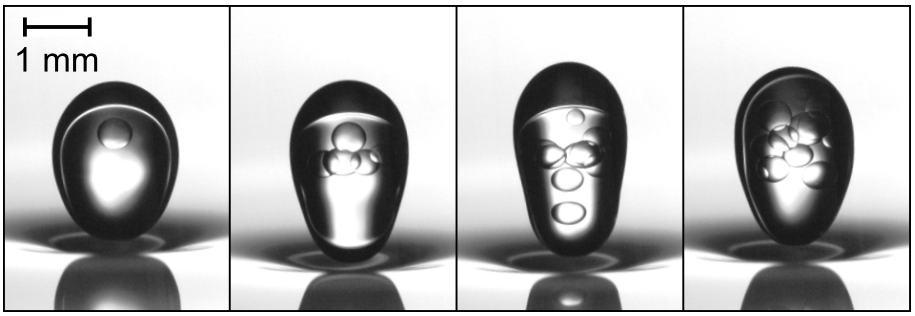

Figure 2.20: Each time the droplet impacts the bath with sufficiently high velocity, an additional oil droplet is injected into the inner water drop, progressively creating a double emulsion of oil droplets into a water drop surrounded by an oil shell. The four snapshots represent the same compound drop after 5, 20, 34 and 51 bounces.

According to our direct observations and the discussion of Fig. 2.18, the deformation of the compound drop plays a key role in the possible formation of a double emulsion. The energy required to deform the drop mainly comes from the kinetic energy released at impact. This energy originates from the relative velocity V_i between the drop and the bath and is transferred into surface energy just after the impact. Both the water/oil and the oil/air interfaces must be taken into account in the calculation of the surface energy . The ratio between the kinetic energy and the surface energy of the compound drop is given by the Weber number, as defined by Chiu *et al.* [68] :

$$We = \left(\frac{6}{\pi}\right)^{1/3} \frac{[\rho_w \Omega_w + \rho_o \Omega_o]}{\sigma_{o/a}(\Omega_o + \Omega_w)^{2/3} + \sigma_{w/o}\Omega_w^{2/3}} V_i^2, \tag{2.7}$$

The impact velocity V_i can be seen as the sum of the free fall velocity V_f of the drop and the velocity of the vibrating bath V_b, i.e. $V_i = V_f + V_b$. We have found interesting to calculate the maximum speed expected V_i. The free fall velocity is given by $V_f = \sqrt{2gh}$, where h is the maximum height reached during the flight $h = 0$ corresponds to the mean position of the bath. The velocity of the bath V_b varies between $-\Gamma g/(2\pi f)$ and $\Gamma g/(2\pi f)$, the most favorable case for generating an emulsion being $V_b = \Gamma g/(2\pi f)$. For typical values of Γ, $V_b \sim 0.3$ m/s, which is of the same order of magnitude as V_f. This confirms that both velocities must be taken into account in the definition of We.

In the following, we show that a single oil droplet can be created in the water core of a compound droplet which impacts a static bath ($V_b = 0$). The impact velocity being the free fall velocity V_f which is tuned by changing the falling height. A critical value $We = We_e$ exists above which the double emulsification is triggered. After that, assuming that the same threshold applies in the vibrating case, we rationalize the emulsification threshold Γ_e observed in Fig. 2.18.

2.4.5 Impact of compound drops on a static liquid surface

We investigated the influence of the impact velocity V_i (and so We) by releasing 60 compound drops (with various compositions, listed in Table 2.2) from different heights onto an oil bath at rest. In Fig. 2.21a, the probability to encapsulate an oil droplet in the water droplet is represented as a function of We. Data are

binned in classes of 1.25 of width. The droplet generation is not possible for low We and is systematic for high We. A smooth transition is observed in between, where the probability p of emulsification increases with We, a black line is used as a guide to the eye. We defined the critical Weber for emulsification We_e as being the Weber value for which the probability to create an oil droplet in the water droplet is 50%. We chose to characterize the width of the transition as being twice the size of one class, consequently we claim $We_e = 5.7 \pm 1.25$. The various compositions are presented together, since almost no effect of the relative sizes is evident in the experimental data. Nevertheless, we were expecting that highly different compositions/sizes would lead to different values of the critical We.

It is difficult to characterize the inner oil droplet formed at the impact of the compound drop on the static surface. The high curvatures of the air-oil and oil-water interfaces behave as a lens that alters the apparent size and shape of these tiny droplets. For a given composition, the relative size of the inner droplets

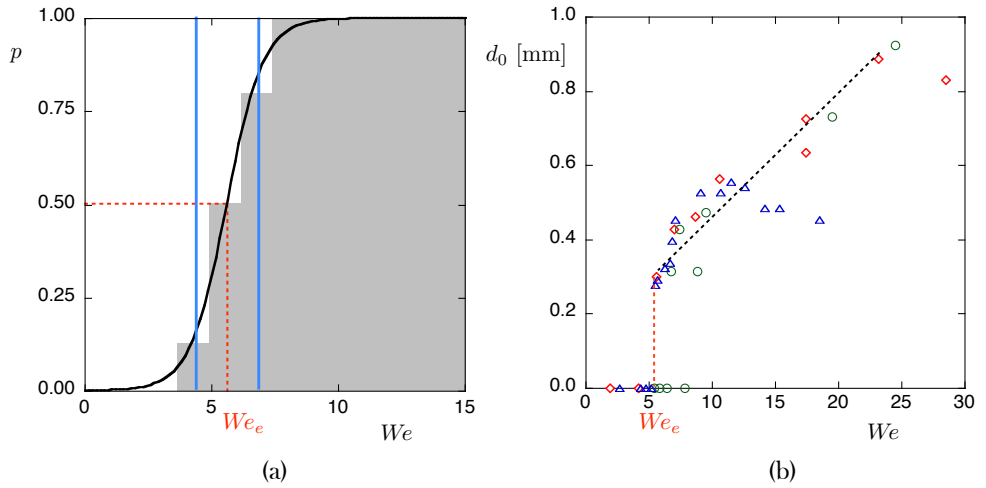

Figure 2.21: a) Probability p for encapsulating an oil droplet in the water drop by impacting on a static bath, as a function of the Weber number We. The black line is a guide to the eye. The water-oil interface pinches off when We is higher than a critical value $We_e \simeq 5.7 \pm 1.25$. b) Diameter d_o of the inner oil droplets as a function of We. The dashed lines are guides for the eyes. The symbols are the same as those used in Fig. 2.18 and are explained in Table 2.2.

can be estimated each time they pass through the center of the compound drop. In Fig. 2.21b, we report the measurements of the relative size of an inner oil droplet as a function of We. Only compound droplets of the same composition (i.e. having the same optical magnification) can be compared to one another. We observed that the diameter of the inner droplets increases with We.

2.4.6 Impact velocity on a vibrating liquid surface

It is reasonable to assume that the critical Weber number We_e does not depend on the motion of the bath, provided that the relative impact velocity $V_i = V_b + V_f$ is considered in Eq. 2.7. Keeping in mind that $V_b = \Gamma g/(2\pi f)$ at maximum, we can write that the emulsion threshold Γ_e is the dimensionless forcing acceleration for which the resulting $We = We_e$. Unfortunately, the height of the rebounds h, and consequently the free fall velocity V_f, also depend on Γ in a non-trivial way, exactly as in the classical bouncing ball problem [49, 77, 78].

To evaluate $h(\Gamma)$, we recorded the trajectory of a drop of the same size as the compound drops, but made only of oil (kinematic viscosity $\nu = 1.5$ cSt and volume $\Omega_o = 2.15\,\mu$L). The measurements were made for three forcing frequencies $f = 25$, 50 and 75 Hz. We checked that the compound drop had approximately the same restitution coefficient $\epsilon = \sqrt{1 - \Delta We/We} \sim 0.33$ as the pure 1.5 cSt oil drop, ΔWe being the difference in We before and after the bounce and We the Weber at impact. Therefore, the bouncing compound drop may adopt the same trajectory as the oil drop for a given set of forcing parameters (f,Γ). From the measurements of the heights reached by the droplet during the bouncing, we calculated the falling speed V_f, then deduced V_i and inserted these into the definition of the Weber number which, when rewritten for a pure oil droplet, can be expressed as

$$We = \left(\frac{6}{\pi}\right)^{1/3} \frac{\rho_o \Omega_o^{1/3}}{\sigma_{o/a}} V_i^2, \tag{2.8}$$

It is represented as a function of Γ for f equal to 25, 50 and 75 Hz in Fig. 2.22, each point corresponding to one bounce. We measured the height h experimentally, then V_f and We are calculated through Eq. 2.8. The diagrams of Fig. 2.22 are similar to the bifurcation diagram observed in the elastic bouncing ball problem [79,80]. The important deformations of the drop make the trajectory chaotic [81], leading to a large range of impact Weber numbers. We drew

the envelope curve in green on each diagram and represented the maximum impact Weber number expected for given forcing parameters (f,Γ).

The critical Weber number $We_e = 5.7 \pm 1.25$, measured in the static case, defines a range in Fig. 2.22 as indicated by two blue bold horizontal lines. Their intersection with the envelope curve indicates the minimum forcing amplitude Γ_e required to achieve double emulsification. According to Fig. 2.22, the emulsification transition occurs at $\Gamma_e \in [0.7, 1.4]$ for $f = 25$ Hz, at $\Gamma_e \in [2.4, 2.9]$ for

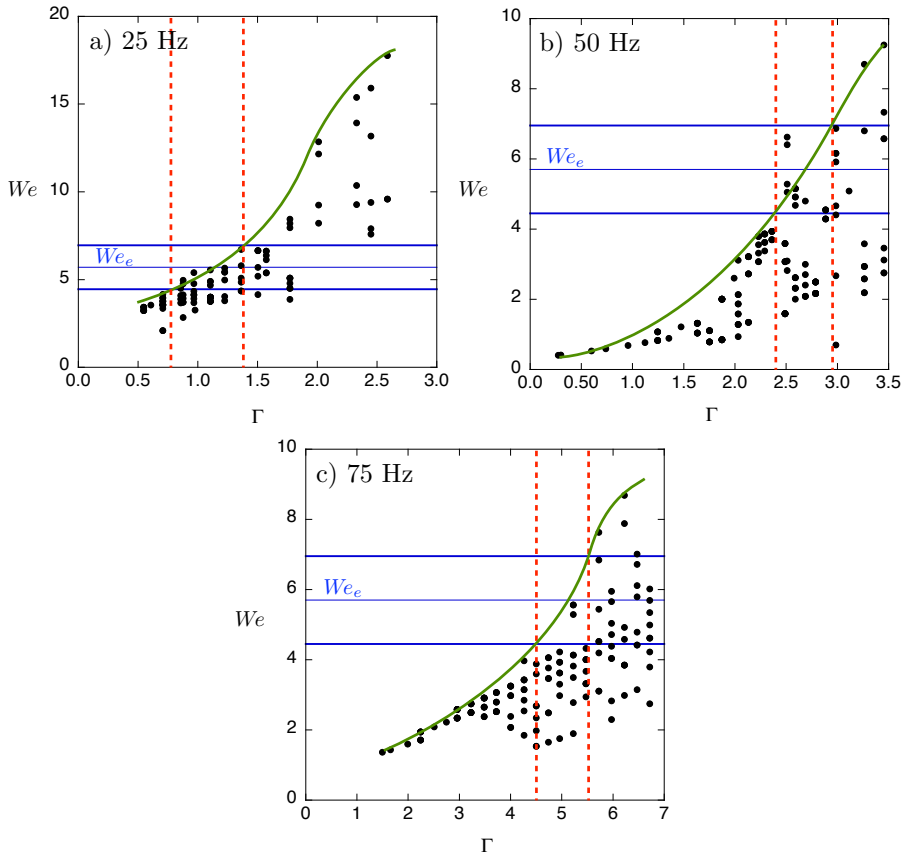

Figure 2.22: Relative Weber number We of an oil drop ($\nu = 1.5$ cSt, $\Omega_o = 2.15$ μL) impacting the bath vibrating at (a) 25 Hz, (b) 50 Hz and (c) 75 Hz, as a function of the forcing amplitude Γ. Compound drops are assumed to experience the same range of We for a given Γ. The emulsification is triggered when We is higher than We_e (range represented by the two blue bold horizontal lines). The dashed lines indicate the corresponding range of Γ_e.

$f = 50$ Hz and at $\Gamma_e \in [4.5, 5.5]$ for $f = 75$ Hz. These values are reported in Fig. 2.18 (black diamonds ♦ with error bars indicating the range). Their good agreement with the direct measurements of Γ_e confirms that the relative Weber number at impact is the relevant parameter to rationalize the emulsification threshold.

Summary

In this section, we have shown that double emulsions can be formed from a compound drop (surfactant solution surrounded by an oil layer) permanently bouncing onto a vibrating liquid surface. No contact with a solid part is involved in the emulsification process. Above a given threshold Γ_e in the dimensionless amplitude of the vibration, the oil shell penetrates the water drop and leaves a tiny oil droplet inside. As this phenomenon occurs at each impact, a double emulsion (oil in water in oil) is progressively formed. We note that Γ_e depends on the forcing frequency, but only weakly on the droplet size. The mechanism responsible for the encapsulation is the convergence of capillary waves to the top of the compound droplet.

In order to rationalize this emulsion threshold, we have investigated the impact of a compound drop onto a static liquid surface. We have observed the irreversible penetration of the oil shell within the water core above a critical Weber number We_e. Finally, we have shown that We_e may be related to Γ_e by considering the rebounds of the chaotic trajectory of the bouncing drop.

The bouncing ability of the compound droplet relies on the presence of a thin air film in between the droplet and the bath. Since the relatively large values of Γ required for emulsification could remove the air layer and lead to coalescence with the underlying bath, the forcing amplitude is usually decreased as soon as the emulsion is formed. The emulsified droplet can then be handled on the bath surface by changing the forcing parameters (amplitude and frequency). For example, it can be set into spontaneous motion [47], or several double emulsions can be merged together. Controlled droplets bouncing could be a promising way to manipulate liquids for microfluidic operations; this study proves that spontaneous emulsification is possible in that context.

Chapter 3

At the limit of small deformations

Contents

Our aim is to simplify the system to the maximum extent possible and to examine the influence of small deformations on the bouncing droplet trajectories. To achieve that, we considered droplets which deform only slightly during their bounce. We used a droplet dispenser (cf. Appendix C) to create small droplets of 20 cSt silicone oil impacting a highly viscosity bath. To begin with, we investigated the bounces of a droplet on a static bath. We measured the droplet deformation as a function of the impact speed as well as a restitution coefficient ϵ given by the ratio of the velocities after and before the bounce. In a second step, we extended this investigation to droplets bouncing on an oscillating bath. We proceeded as if the droplet was a bouncing ball. We reported droplet trajectories as a function of the frequency f and the bath acceleration Γ in order to obtain a bifurcation diagram with respect to Γ. For comparison, a typical bifurcation

diagram, the one of the inelastic bouncing ball ($\epsilon = 0$), is presented on Fig. 3.1. At low Γ, the ball simply bounces on the oscillating plate. At $\Gamma \approx 4$, the period of the ball doubles until the ball bounces one time each two periods of the plate. For higher Γ, the ball encounters more bifurcation and even chaos. Finally, using the results of the bouncing on a static bath, we developed a model based on the analogy between a spring and a droplet in order to explain the bouncing droplet phenomenon on a vibrating interface. We have analyzed this model numerically. It proved to be very efficient to reproduce the experimental results.

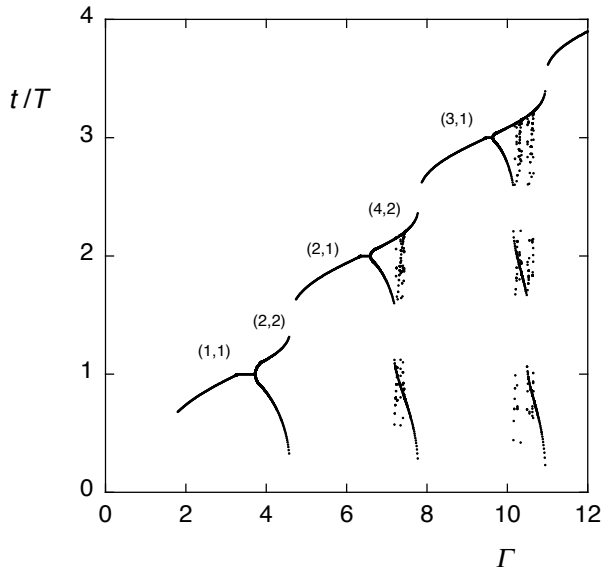

Figure 3.1: Bifurcation diagram of an inelastic ball ($\epsilon = 0$) bouncing on an oscillating plate [49, 82]. We represented the flight time t of the ball, normalized by a period of oscillation of the plate T, as a function of Γ. Note that this diagram is independent of the plate oscillation frequency and of the ball mass. Some particular modes, defined by two parameters (p, q), are noted on the diagram. The drop bounces q times while the bath oscillates p times.

3.1 A bouncing droplet on a static liquid surface

We chose to work with droplets smaller than those examined in Chapter 2. They were made of 20 cSt silicone oil which is an oil commonly used for the walking

droplets [1] and quantum-like experiments [2–5]. Using the dispenser, we made identical droplets, of diameter $D = 740\,\mu$m. These were dropped from different heights ($\sim 1\,$cm) on a static silicone oil bath of viscosity 1000 cSt and of depth 1 cm. The silicone oil parameters (surface tension σ, density ρ, viscosity ν) can be found in Appendix A. We observed that the droplets bounce several times on the bath before coalescing with it. Using a high speed camera, we recorded 12 experiments, from the side, at 2000 fps (frames per second), each of a single droplet falling and bouncing. The experimental setup is detailed in Appendix B and illustrated on Fig. B.1a.

On Fig. 3.2, a succession of droplet bounces is detailed. Based on movie images, we constructed a spatio-temporal diagram according to the method explained in Section 1.3.3 : the drop vertical centerlines of each image are juxtaposed. The time elapses from left to right, its scale is represented on the top right corner of the figure. On the figure, some snapshots illustrate the droplet shape at different moments along its trajectory. On each snapshot, the white vertical line indicates the pixel line represented on the spatio-temporal diagram. The vertical distance scale is also indicated on the top right corner of the figure. Before impact, the drop is spherical and has a diameter D. Then, it deforms due to the impact. The maximal droplet horizontal extension is denoted by $D + X$. After that, the drop, which returns to a spherical shape, takes off without entering in contact with the underlying liquid. Residual oscillations are then rapidly damped by viscosity. Generally speaking, a droplet, falling from a height of about 1 cm, bounces 2 or 3 times until it starts floating on the surface. Eventually, the droplet coalesces when the air film has drained out.

3.1.1 Deformation of a droplet during a bounce

For each bounce, we measured the maximal horizontal extension $D + X$ of an impacting droplet (cf. Fig. 3.2a) as a function of the impact Weber number $We_i = \rho D V_i^2/\sigma$, where V_i is the speed of the drop at impact, ρ and σ are the density and the surface tension of the droplet liquid. For each experiment, we established the impact speed before the first bounce by measuring the position of the drop at different times before the impact. We evaluated the impact speed of two next bounces by measuring the maximal height h that the drop reached between two successive bounces. It is important to note that the origin of the

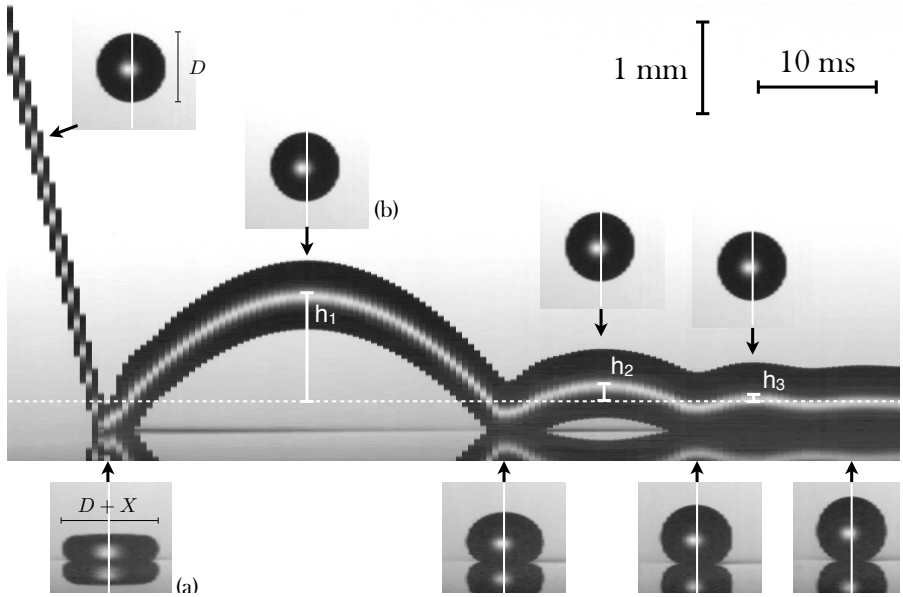

Figure 3.2: Spatio-temporal diagram of a droplet of a 20 cSt silicone oil of diameter $D = 740\,\mu$m falling on a static 1000 cSt silicone oil bath (highly viscous). Time elapses from left to right. The droplet experiences several bounces of heights h_1, h_2 and h_3. These heights are measured from the center of mass of the droplet when it is floating (white dotted line). The impact speeds of the bounces are $V_1 = 0.56$ m/s, $V_2 = 0.16$ m/s and $V_3 = 0.07$ m/s. Several snapshots illustrate the shape of the droplet at different moments of the bounce. (a) The droplet maximal deformation at impact is $D + X$. (b) The droplet retakes a spherical shape after lifting-off.

vertical axis is located at the center of mass of the floating droplet (just before coalescence), which is represented by the horizontal dashed line on Fig. 3.2. The two bounce heights h_1 and h_2 are measured, then respective impact speeds are calculated from $V_i = \sqrt{2gh}$. Oscillations of the drop are damped in a characteristic viscous time $\tau_\nu = \nu\rho D/\sigma \sim 0.7$ ms. Compared to the flight time after a bounce, typically a few tens of milliseconds, the oscillations do not affect the next bounce. Internal motions should also be rapidly damped by viscosity. On Fig. 3.3a, the measurements of the dimensionless extension X/D of the droplet are reported as a function of the impact Weber We_i for the three first bounces of each experiment. Error bars are estimated and indicated on each data point, and are huge for the measurements of the third bounce. Nevertheless, we plotted measurements for each of the 3 bounces of the 12 experiments and these data points were fitted by a power 1/2 law which is explained later.

In the vibrating case, droplets bouncing periodically on a bath oscillating at

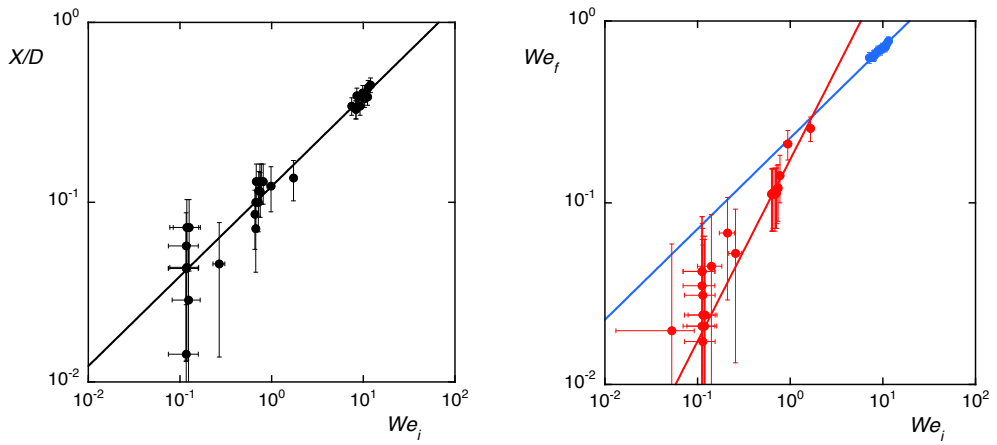

(a) (b)

Figure 3.3: (a) Maximal deformation X/D of a 20 cSt silicone oil droplet of diameter $D = 740\,\mu$m impacting a highly viscous bath as a function of the Weber number at impact We_i. A power 1/2 law is plotted on the data points. (b) Weber number after impact We_f as a function of the Weber number before impact We_i. Data points with $We_i < 1$ and $We_i > 1$ are represented in red and blue, respectively. A linear law is plotted in red on the data points ($We_i < 1$) indicating a restitution coefficient ϵ of 0.41 ± 0.02 which is independent on We_i. A power 1/2 curve is plotted in blue on the the second series of data points ($We_i > 1$) as a guide to the eye.

50 Hz and $\Gamma = 1$ usually reach a maximum height of 0.5 mm which corresponds to an impact speed of about 0.10 m/s. Moreover, they impact the moving bath whose speed is equal to $A\omega$ at maximum. As $A\omega$ is about 0.03 m/s for $\Gamma = 1$, the maximal impact speed for those bouncing droplets is about 0.13 m/s ($We_i = 0.6$). This corresponds roughly to the 2nd bounce shown on Fig. 3.2 for which $V_i = 0.16$ m/s.

The range of impact speeds of our measurements of falling droplets on a static bath is 0.05 to 0.6 m/s. For this series of speeds, since the Weber number range is $We = 0.1$ to 10, kinetic energy is of the same order of magnitude as the surface energy. Surface energy dominates when V_i is smaller than

$$V_W = \sqrt{\frac{\sigma}{\rho D}} \sim 0.17\,\mathrm{m/s}. \tag{3.1}$$

For velocities lower than V_W ($We < 1$), deformations are small during contact and the shape can be modeled by an oblate spheroid of major axis $D+X$ [83,84]. When $X \ll D$, the increase in surface of the oblate spheroid is proportional to X^2. We can write a simple energy balance between kinetic energy and surface energy,

$$\rho D^3 V_i^2 \sim \sigma X^2 \tag{3.2}$$

which yields,

$$X \sim D\, We_i^{1/2}. \tag{3.3}$$

This scaling rationalized our measurements of the droplet maximal deformation during a bounce and is presented on Fig. 3.3a. Okumura *et al.* [83] measured the maximal extension of droplets impacting a hydrophobic surface and found the same scaling law with a prefactor estimated being 0.13. Note that we found a prefactor of 0.12 which is similar to their value. They rationalized their measurements by the same energy arguments, starting from the Euler equation. They noted that Eq. 3.3 is valid in the case where capillarity dominates gravity. Indeed, a floating or sitting drop is deformed by gravity by an amount $\delta \sim D^3/8\kappa^{-2}$ as discussed by Mahadevan *et al.* [85]. The condition is thus written as $X \gg \delta$: the impact speed should be larger than a characteristic speed which, in our problem, is evaluated as

$$V_c \sim \sqrt{gD^3/\kappa^{-2}} \sim 0.04\,\mathrm{m/s}. \tag{3.4}$$

The corresponding characteristic Weber number is equal to $We_c = 6.10^{-2}$. In our system, impact velocities of bouncing drops on a static or an oscillating liquid bath are always larger than the characteristic speed V_c.

For velocities much higher than V_W ($We \gg 1$), the impacting drop takes the shape of a pancake. The higher the Weber number, the thinner the pancake. Clanet *et al.* [86] observed that the maximal deformation diameter $D+X$ of low viscosity droplet impacting a hydrophobic surface, at high speed, scale as $We^{1/4}$. They explained that, during the impact, the drop is subjected to an acceleration much higher than the gravity, i.e. about 100 g. The latter is the cause of the flattening of the drop and dictates its maximal extension. During the impact, the initial kinetic energy is not only transferred to the surface energy but also to the internal kinetic energy; indeed, vortices were observed at the edge of the pancakes.

3.1.2 Restitution coefficient

In order to compare a bouncing droplet with a bouncing ball, the coefficient of restitution of the droplet has to be defined, even if that coefficient is not perfectly appropriate. Successive heights, reached by the droplet during an experiment, decrease. Actually, the droplet has an initial kinetic energy that is converted in surface energy during the bounce (cf. Fig. 3.2a). The surface energy is then restored and converted into kinetic energy of the center of mass of the droplet and into kinetic energy of the internal liquid motion. The latter is eventually dissipated by the viscosity while the kinetic energy of the center of mass is converted into gravitational potential energy which is maximal when the maximal height of rebound h is reached (cf. h_1, h_2 and h_3 on Fig. 3.2b). By measuring this potential energy, we found the impact speed of the next bounce. For each bounce of the 12 experiments, we calculated the Weber numbers before and after. We reported on Fig. 3.3b, the resulting Weber numbers after impact We_f as a function of the Weber numbers We_i just before impact (in red for $We_i < 1$ and in blue for $We_i > 1$). Error bars have been estimated and indicated on the figure. We observed that we have two dynamics depending on the impact Weber number We_i. When $We_i < 1$, the Weber number after impact We_f is proportional to We_i. A linear curve is fitted on the red data points. That indicates that the restitution coefficient ϵ, the ratio between the speed of the

droplet V_f after and the speed V_i before the bounce, is constant. We measured a restitution coefficient of about 0.4. When $We_i > 1$, the restitution coefficient depends on We_i. A power 1/2 curve is plotted in blue on the data points ($We_i > 1$) as a guide for the eyes.

Richard *et al.* [84] experimentally explored millimetric water droplets impacting a highly hydrophobic solid. They reported measurements of the restitution coefficient ϵ as a function of the impact speed V_i. They observed that for low velocities, ϵ is about 0.9 and is independent of the impact speed. If there was no loss of energy during the impact this coefficient ϵ should be equal to 1. They demonstrated that this loss comes from the internal motions that are generated and persists after impact. They rejected the contact angle hysteresis and the effects of viscosity during impact as they used water droplets. When $We_i < 1$, we found a restitution coefficient of 0.41 ± 0.02 (our error is estimated as the standard deviation of the weighted fit) which is substantially smaller than their value of 0.9. This difference could come from a dissipation by viscosity during impact (our droplet viscosity is 20 times larger) but also from a dissipation in the air film. Assuming that the flow in the air film is a combination of Poiseuille, dissipation can occur due to the air viscosity and velocity gradients. An effect already highlighted in droplets bouncing on a soap film [26].

Biance *et al.* [87] investigated impacts of water droplets on a hot surface, they observed Leidenfrost droplets that bounce on their own vapor. The authors showed that for $We_i \gg 1$, ϵ decreases as $We_i^{-1/2}$ which suggests that We_f is constant and does not depend on We_i. This observation has been rationalized by a bouncing spring model in the case of high deformations, i.e. the maximal deformation of the droplet $D+X$ at impact is proportional to $We^{1/4}$ (pancake).

For $We > 1$, we observed that We_f scales as $We_i^{1/2}$ thus $V_f \propto V_i^{1/2}$. This is in contradiction with what Biance [87] observed. This could come from the fact that our measurements are limited to a We of about 10 and we did not observe the pancake behavior (high deformation regime). This is confirmed by the scaling found for the maximal deformation when $We > 1$. The dynamics that we observed could be transient dynamics between the pancake regime and the low deformation regime.

For $We > 1$, we should note that the contact time τ_c of bouncing droplets on a hydrophobic solid surface is constant [88]. However, for $We < 1$, τ_c decreases

with We_i [83]. This value can be doubled when $We \ll 1$. We also observed that the contact time scales as $D^{3/2}$ [88]. This is easily understandable when we take into account that the droplet bounces on the solid in a time inversely proportional to its natural frequency. The latter is given by Eq. 2.1. The contact time τ_c thus scales as $1/f_c = \sqrt{\sigma/M}$ where the mass M is equal to $\pi\rho D^3/6$.

What to keep in mind is that the typical speed at impact of droplets bouncing on a vibrating bath has an impact Weber number $We_i < 1$ (at least just above the bouncing threshold Γ_b). For $We_i < 1$, we observed that the coefficient of restitution ϵ of droplets bouncing on a static bath is constant ($\epsilon = 0.4$) and does not depend on We_i. The kinetic energy $\rho D^3 V_i^2$ available just before impact is stored in surface energy σX^2 and dissipated by the viscosity in the droplet and by the viscosity in the air film.

3.2 Bifurcation diagram of a bouncing droplet

Small droplets are laid on the highly viscous bath that is oscillating vertically. We measured the bouncing threshold Γ_b for several sizes of droplets made with the droplet dispenser (cf. Appendix C). The $\Gamma_b(f)$ curves are presented on Fig. 3.4 and scale as the capillary frequency f_c as demonstrated in Chapter 2. We can also observe that droplets are permanently bouncing for acceleration lower than the gravity ($\Gamma_b < 1$). At the threshold, droplets are simply bouncing, i.e. one bounce per oscillation of the bath, following the mode of deformation Y_2^0. The energy loss of the droplet at each bounce is compensated by an energy input coming from the oscillation of the bath.

When Γ is increased, the droplets experience complex trajectories that can be periodic over a few bath oscillations. Indeed, according to the phase, some extra energy can be used for a higher bounce and at the next bounce the energy given could be lower. However, on average the energy loss at each bounce has to be balanced after a number q (an integer) of periods. These differences in bouncing heights are characterized by different times between successive bounces which can be measured. We investigated the bouncing droplet trajectories as a function of the forcing parameters of the oscillation of the bath. Firstly, the forcing frequency f and the size of the drop D were fixed and the trajectories

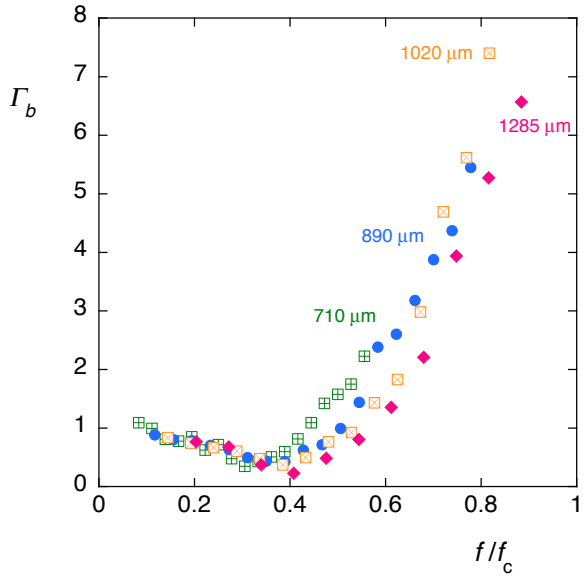

Figure 3.4: The bouncing threshold acceleration Γ_b measurements for 4 different droplets with respective diameters $D = 710\,\mu$m (green ⊞ symbol), $D = 890\,\mu$m (blue •), $D = 1020\,\mu$m (orange ⊠), $D = 1285\,\mu$m (magenta ♦). The $\Gamma_b(f)$ curves rescale with the capillary frequency $f_c = \sqrt{\sigma/M}$. The corresponding capillary frequencies are $f_{c,710} = 342\,$Hz, $f_{c,890} = 242\,$Hz, $f_{c,1020} = 197\,$Hz, $f_{c,1285} = 140\,$Hz.

of a droplet were studied as a function of the forcing acceleration Γ. We highlighted several bouncing modes. Secondly, we studied the dependance of these trajectories on the droplet size and forcing frequency.

Using a drop of $890\,\mu m$ on a bath oscillating at $f = 50$ Hz, we recorded the trajectory from the side with a fast video camera at 1000 fps. A horizontal wire glued on the bath indicated its position during time. Stable bouncing modes are sought by varying the initial conditions of the bounce for bath accelerations between $\Gamma_b = 0.9$ and $\Gamma = 5$ by steps of approximately 0.1. Each movie represents about 50 bath oscillations. The center of mass of the droplet and the bath positions are tracked over time.

On Fig. 3.5, we present different characteristic periodical trajectories that corresponds to different forcing accelerations Γ. The position of the bath and the center of mass of the droplet are drawn in blue and red, respectively. The bath follows a sinusoidal motion. Trajectories of the center of mass of the

droplet are vertically translated for better visualization. Note that the droplet is **not** bouncing instantaneously, it deforms itself when interacting with the bath which lasts about one third of a bath oscillation period. We define the droplet "contact" with the bath as the minimum in the trajectory of the center of mass of the droplet.

The modes are referred by two parameters (p, q) according to the classical notification. The drop bounces q times while the bath oscillates p times. On Fig. 3.5a, the first bouncing mode (1,1) is a mode which presents even bounces at each period of the oscillation of the bath. Furthermore, it is characterized by the same time interval between droplet "contact" with the bath. For the same set of forcing parameters, depending on the initial conditions, another bouncing mode also denoted by (1,1) can be observed on Fig. 3.5b. The main differences reside in the bouncing heights and the contact phases which are different. When Γ is increasing to $\Gamma = 1.7$, the droplet experiences a large bounce followed by a smaller one during two oscillations of the bath which is denoted by (2,2) on Fig. 3.5c. When Γ is further increased, a wide variety of periodic modes can be observed. They are presented on Fig. 3.5d-h. The corresponding mode is written on each figure. Note that the mode (2,1) on Fig. 3.5f shows a droplet bouncing once every two oscillations of the bath. The mode on Fig. 3.5h is described by the same set of parameters (2,1) even if the bouncing phase and heights are different. In fact, these two parameters do not describe unequivocally the droplet trajectories[1].

We define $\Delta T_{\min}$ as time intervals between two successive "contacts" of the droplet with the bath and h as the height of successive bounces which is defined as the difference of height in between a maximum and the previous minimum of the droplet trajectory. These two parameters are illustrated on Fig. 3.5e. The measurements of $\Delta T_{\min}$ are normalized by the oscillation period of the bath T. We have measured $\Delta T_{\min}/T$ and h as a function of the forcing Γ on each of the experimental movies. These measurements are reported on Fig. 3.6a-b.

On Fig. 3.6a, all $\Delta T_{\min}/T$ measurements are reported as a function of Γ.

[1] The mode (2,1) is known to be the characteristic mode of the walker droplets presented in Chapter 1 [44]. The latter are observed in the region "W" of the phase diagram of droplet bouncing on a 50 cSt silicone oil bath on Fig. 1.7. The modes observed in regions "bouncers" and "PDB" are similar to modes (1,1) and (2,2), respectively (cf. Chapter 4).

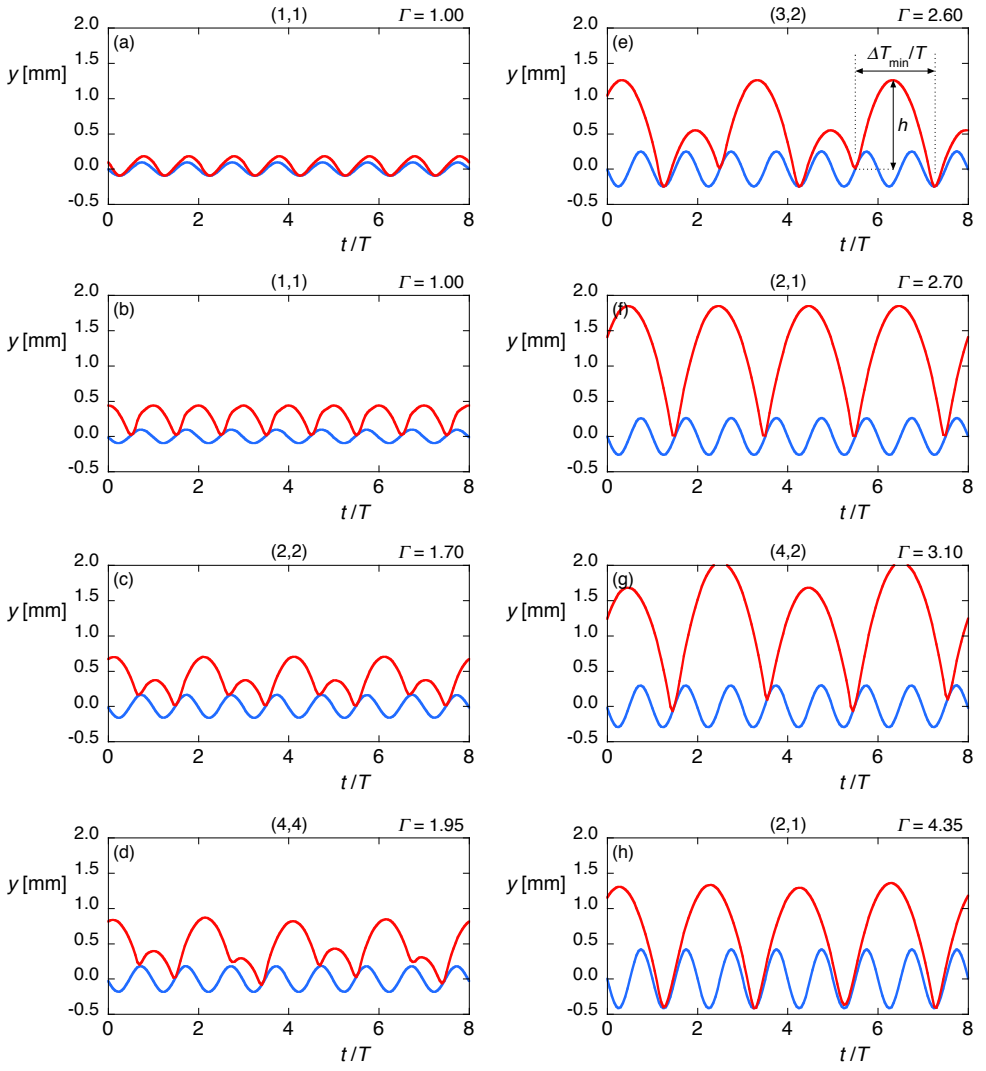

Figure 3.5: Experimental trajectories of a 20 cSt silicone oil droplet of diameter $D = 890\,\mu$m bouncing on a bath oscillating at a frequency of 50 Hz for various accelerations Γ. The bouncing mode (p, q) and the forcing acceleration Γ are indicated on each figure. The time interval $\Delta T_{\min}$ between two successive bounces and the bouncing heights h that are measured on each trajectory are illustrated on figure (e).

Red data points are related to the droplet trajectories observed as periodic while the grey data points are related to the chaotic trajectories, no periodic motion was observed on these movies. The bouncing modes are indicated above their corresponding red data points.

Using the same experimental data, we represented the bouncing height h as a function of Γ on Fig. 3.6b. Data symbols are the same as on the previous figure. This bifurcation diagram gives more information on the observed bouncing modes. The first mode (1,1) is characterized by two distinct possible heights. The lower data points are characteristic of a mode (1,1) that we called "low (1,1)", of the type presented on Fig. 3.5a whereas the upper series of data points are of the type presented on Fig. 3.5b called "high (1,1)". The height of the low (1,1) type varies with Γ while the "contact" phase remains fixed. Conversely, the height of the high (1,1) type remains fixed while the "contact" phase adapts itself with Γ. According to the initial conditions, a trajectory at a fixed Γ can be either stable or chaotic. Note that a trajectory, under certain conditions, can alternatively pass from stable to chaotic and vice versa. We can observe the same difference for the mode (2,1) as for the mode (1,1). Both types of mode (2,1) are represented on Fig. 3.5f and h, where we observe that they occur for different Γ. They are characterized by a same time interval between the minima. However, the bouncing height of the mode occurring at higher Γ increases with Γ as long as the contact phase remains constant. The other mode (2,2) is characterized by a constant height for an increasing Γ when the contact phase varies.

We have observed that a droplet permanently bounces on a bath oscillating at an acceleration $\Gamma > \Gamma_b$. At Γ_b, the droplet bounces simply on the bath following a mode (1,1). When Γ is increased, the bouncing droplet reaches a bifurcation ($\Gamma = \Gamma_{PDB}$), above which two successive bounces become uneven, corresponding to the mode (2,2). After that, when Γ is increased further, a succession of bifurcations and modes (4,4), (3,2), (2,1) and (4,2) emerge. These modes can be interspersed with chaotic zones. An important observation is that a mode denoted by the same parameters can hide two different bouncing trajectories which differ depending on the bouncing heights and phases. Indeed, two different modes (1,1) can be encountered for the same Γ just above Γ_b, the selected mode depends on initial conditions. The same remark can be made for

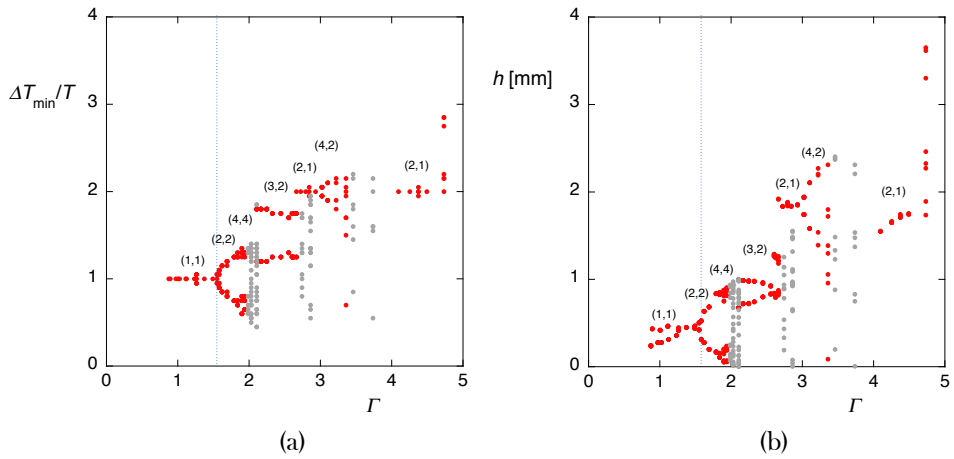

Figure 3.6: Experimental trajectory characterization of a droplet of diameter 890 μm bouncing on a highly viscous bath oscillating at 50 Hz for various forcing accelerations Γ: (a) measurements of the time intervals $\Delta T_{\min}$, normalized by the oscillation period of the bath T, between two successive bounces and (b) measurements of the bouncing heights h. The different bouncing modes (p, q) are indicated on the figure. Error bars are typically of the symbol size.

the two modes (2,1); however, they occur at different forcing accelerations.

3.3 Spring model

Based on these observations, a model can be imagined to reproduce these bouncing modes. They are observed to be linked to the frequency and size of the droplets. A natural bouncing model would be the inelastic or elastic bouncing ball which reproduces this kind of phase diagram (cf. Fig. 3.1). This model is characterized by an instantaneous contact solely governed by the restitution coefficient ϵ of the ball. However, such a model does not highlight a finite contact time. Let us remember that the term "contact" is improper because the droplet and the bath are never in contact. A droplet is considered to take off when the lubrication film is sufficiently thick for the force it exerts to be neglected. Gilet and Bush [26, 89] faced the same issue as they observed droplets bouncing on a vibrating soap film. They developed a theoretical model based on the second Newton law to predict trajectories. Depending on the shape of the soap film, they could deduce the force acting on the droplet. Similarly, Eichwald *et*

al. [90] investigated the phase diagrams of a solid bouncing ball on an elastic membrane that oscillates. Note that in their works the bouncing motion is due to the deformation of the membrane or of the soap film.

In Section 2.1, we demonstrated that a droplet behaves as a forced harmonic oscillator, the surface tension providing the restoring force and viscosity the damping. We reinforced our statement by performing additional experiments in Section 3.1. For $We_i < 1$, the droplet stores energy in surface energy which scales as σX^2, where X is the length increment of the droplet at impact. We can thus, naturally, propose a 1D model for the droplet as a system of two masses linked by a spring which is characterized by a stiffness k in parallel to a dashpot with a damping ratio ξ (cf. Fig. 3.7a). The behavior of the spring system is governed by the Newton laws written for both masses. This kind of model has already been applied to infer a bouncing criteria and a restitution coefficient to inviscid droplets impacting an hydrophobic surface at high speed (corresponding to high deformation) [87]. On our side, we studied this system at the limit of small deformation ($We < 1$). Futhermore, we investigated the dynamic of the system bouncing on a static as well as on an oscillating plates. We started by studying numerically the behavior of a spring falling on a static plate. Then, we compared the results to the experimental data of Section 3.1 in order to adjust the spring parameters k and ξ. Finally, we evidenced the bouncing modes of this spring bouncing on an oscillating plate. We then made a comparison with our own experimental bifurcation diagram (cf. Fig. 3.6).

We take y as the vertical coordinate (positive upward), y_1 and y_2 are the coordinates of the upper mass m_1 and of the lower mass m_2. The spring is characterized by a spring constant k and a damping coefficient c. At rest and in free fall, the length of the spring $y_1 - y_2$ is L.

On Fig. 3.7b, we represented the gravity forces $F_{g1} = -m_1 g$ and $F_{g2} = -m_2 g$ that act on both masses. The spring exerts also forces on each mass, they are $F_{s1} = -k(\Delta y - L)$ and $F_{s2} = k(\Delta y - L)$ with $\Delta y = y_1 - y_2$. When the lower mass m_2 is in contact with the plate, it experiences a normal force N_2 from the plate. The normal force N_2 is calculated through molecular dynamics when there is contact and is null when there is no contact (cf. Appendix D). We add a viscous dissipation force which is proportional to the speed of elongation of the spring, with a viscous damping coefficient of proportionality c. Newton laws

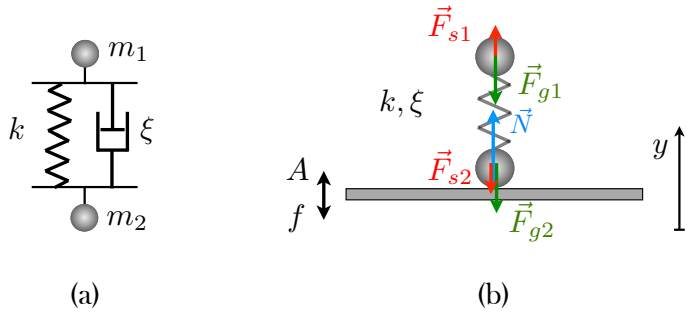

Figure 3.7: (a) The droplet is modeled by two masses linked by a spring of stiffness k in parallel to a dashpot with a damping ratio ξ. (b) The spring system is in contact with the plate oscillating at a frequency f and amplitude A. As m_2 is in contact with the plate, a normal force $\vec{N}$ acts from the plate on m_2. In this case the spring is compressed ($\Delta y < L$), the two masses feel outwards spring forces $\vec{F}_{s1}$ and $\vec{F}_{s2}$ in addition to the gravity forces F_{g1} and F_{g2}.

can be written for both masses as

$$m_1\ddot{y}_1 = -m_1 g - k(y_1 - y_2 - L) - c|\dot{y}_1 - \dot{y}_2|, \tag{3.5}$$

$$m_2\ddot{y}_2 = -m_2 g + k(y_1 - y_2 - L) - c|\dot{y}_1 - \dot{y}_2| + N_2. \tag{3.6}$$

We choose to spread the mass of our droplet M on both masses, $m_{1,2} = M/2$. The length of the spring L is set to 0.74 mm which is the typical size of our droplet. The spring constant k models the surface tension $\sigma \sim 0.02$ N/m. This constant k determines the undamped frequency of the spring given by $\omega_0/2\pi = \sqrt{2k/M}$. The damping coefficient c is estimated via the damping ratio $\xi = \frac{c}{2\sqrt{2kM}}$ which compares the spring damping effect with the restoring effect. This parameter ξ models the Ohnesorge number Oh for droplets which is about 0.14. In Table 3.1, we compare the spring system and the droplet.

	mass	stiffness	damp. coeff.	damp. ratio	length at rest
droplet	$\pi\rho D^3/6$	σ	ν	Oh	D
spring system	$m_{1,2}$	k	c	ξ	L

Table 3.1: Comparison of a system of two masses m_1 and m_2 linked by a spring with a droplet of diameter D.

The behaviors of the damped harmonic oscillator of mass m depend on the value of ξ which can be listed as follows:

- when $\xi = 0$, the system is undamped and oscillates at its natural frequency $\omega_0 = \sqrt{k/m}$;
- when $0 < \xi < 1$, the system is underdamped and oscillates at a frequency ω_d lower than ω_0. Its amplitude decreases with time and more rapidly when ξ approaches 1. The frequency ω_d is given by

$$\omega_d = \omega_0 \sqrt{1 - \xi^2}; \tag{3.7}$$

- when $\xi = 1$, the system is critically damped and returns to its position of equilibrium without oscillating. The amplitude decays exponentially in a characteristic time equal to $1/\omega_0$; and
- when $\xi > 1$, the system is overdamped and returns also to its position of equilibrium without oscillating. The deformation decays exponentially in a characteristic time larger than in the critically damped case. This time becomes larger when ξ is larger.

This model depends on two parameters only, ξ and k, which are of the order of magnitude of Oh and of σ, respectively. We can fine tune them in order to reproduce the bouncing droplet trajectories as accurately as possible. This is done by comparing the numerical simulation of a spring laid on a static plate with the experimental results of a droplet laid on a static bath, this has been developed in Section 3.1.

3.3.1 Determination of the spring parameters

As demonstrated in Section 3.1, the relative impact velocities of droplets bouncing on an oscillating plate just above the threshold are about 0.15 m/s. These velocities are similar to the impact velocities of the second bounce of the experiments performed in that section. On Fig. 3.8, we present the first and the second bounce of one of the experiments. In fact, it is a part of Fig. 3.2. The green dots are the measurements of the center of mass of the droplet. We adjusted both spring parameters k and ξ in order to reproduce this succession of bounces as accurately as possible.

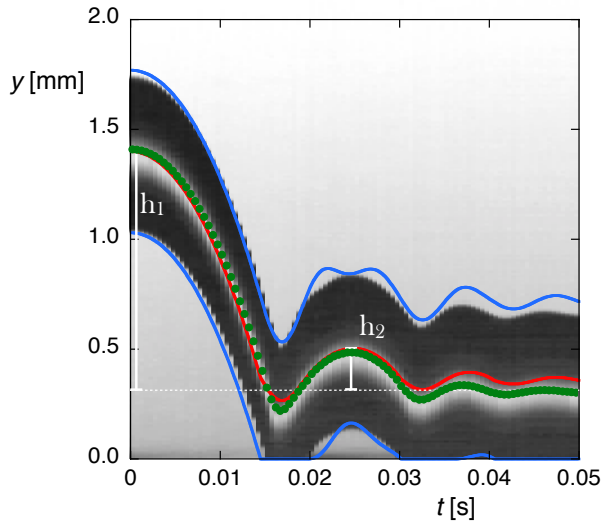

Figure 3.8: Zoom on the spatio-temporal of Fig. 3.2. The measurements of the center of mass are represented by black dots. The simulation of a falling spring system, from a height of $h_1 = 1.1$ mm, with parameters $k = 0.072$ N/m and $\xi = 0.25$, is represented by blue and red lines. The central red line is the trajectory of the center of mass and both outer blue lines are the trajectories of the masses m_1 and m_2.

We performed numerical simulations of the spring system laid from the height of $y_1 = h_1 + D/2 = 1.46$ mm on a static plate ($V_i = \sqrt{2gh_1} = 0.15$ m/s and $We_i = 0.8$). That is the spring constant k that mainly governs the maximal deformation of the droplet during the bounce. We adjusted this parameter by setting ξ to 0 and dropping the spring system on the static plate. After comparing the numerical and experimental deformations at impact, we adjusted the spring constant k to 0.072 N/m. The damping ratio ξ imposed mainly the height of the next rebound and thus the restitution coefficient ϵ. The latter decreases when ξ increases. We adjusted ξ to 0.25 in order to find h_2 the height of the next bounce. We note that these two parameters do not have independent effects. But this method was very satisfying to adjust the parameters in order to reproduce the succession of bounces. On Fig. 3.8, we draw the results of the simulation in red and blue. We have drawn the trajectory of the center of mass of the spring system in red while the trajectories of the masses m_1 and m_2, assimilated to points, are drawn in blue. After comparing simulations with experiments, we note that the trajectories of the center of mass are in good

agreement. We observe that the floating drop (at the end) has a lower center of mass than the prediction of the simulation. This could be due to the fact that the highly viscous bath was not completely rigid, so that the droplet created a small hole in it. Another difference is the additional oscillation of the spring system during the bounce which has, however, no influence on the next bounce.

3.3.2 The spring system bouncing on an oscillating plate

Considering the two parameters $\xi = 0.25$ and $k = 0.072$ N/m for the model, we performed numerical simulations of the spring system bouncing on a 50 Hz oscillating plate. We started by dropping the spring system, from a height of 1 mm, on a plate oscillating at a frequency of 50 Hz and with an amplitude such that $\Gamma = 1$. The real time simulation was set to 11 seconds (~ 550 oscillations of the plate). We then increased Γ by steps of 0.1, without break between the simulations. We repeated the process until reaching $\Gamma = 5$. After that, we decelerated by decreasing Γ by steps of 0.1 until reaching $\Gamma = 0.5$. We then processed the data of the center of mass of the spring system in the same way as we processed the data displayed on Fig. 3.6. For each Γ value, we measured each bouncing height h and each time interval $\Delta T_{\min}$ between the two minima of the center of mass trajectories.

On Fig. 3.9a, we reported the different intervals of time $\Delta T_{\min}$ between two successive bounces of the center of mass as a function of Γ. For each Γ value (increasing and decreasing phase), N measurements of $\Delta T_{\min}$ were binned in classes of 0.1 ms of width (step of the simulation) and 0.05 of height (experimental error). We defined n_i as the number of events in the bin i corresponding to time within the interval $0.1\,i$ and $0.1\,(i+1)$ ms. On Fig. 3.9a, the measurement recurrences n_i/N in each bin i are then represented in a grey level corresponding to $(1 - n_i/N) \times 255$ where a value of 255 is white and a value of 0 is black. A 100 % black bin means that all of the measurements corresponding to the acceleration Γ are located in the considered bin. Taking bins of 0.1 of width and 0.05 mm of height, we proceeded the same way with the measurements of h. These are plotted on Fig. 3.9b. We identified the different bouncing modes on both diagrams. They are indicated on each figure. To enable comparison with experimental data we transferred Fig. 3.6a-b on Fig. 3.9c-d just below the simulation results.

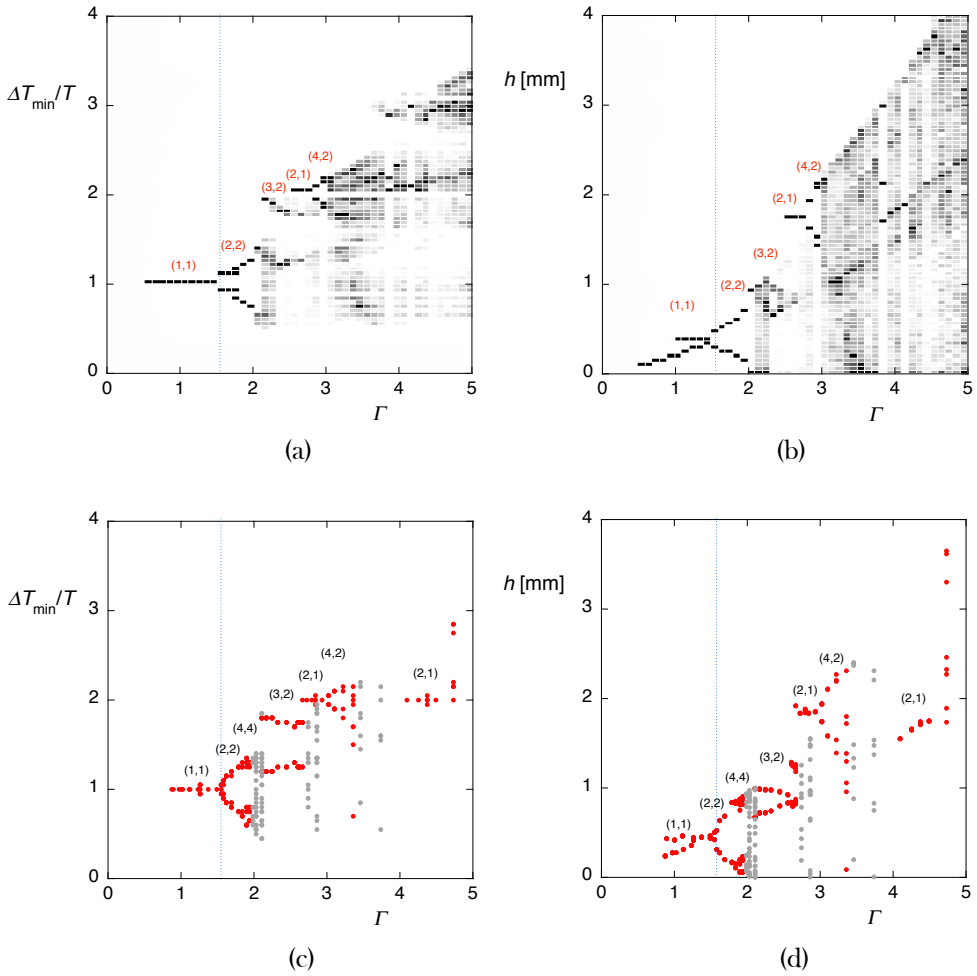

Figure 3.9: Trajectory characterization of the spring model ($k = 0.072$ N/m and $\xi = 0.25$) and the experiments (cf. Fig. 3.6) for a droplet of diameter 890 μm bouncing on a solid plate oscillating at 50 Hz for various forcing accelerations Γ: (a) simulation measurements of the time intervals $\Delta T_{\min}$, normalized by the oscillation period of the bath, between two successive bounces; (b) simulation measurements of the bouncing heights h; (c) experimental measurements of the time intervals $\Delta T_{\min}/T$; and (d) experimental measurements of the bouncing heights. The different bouncing modes (p, q) are indicated on the figure.

The agreement between the simulations and the experiments is remarkable. The first bifurcation from (1,1) to (2,2) is located at the same $\Gamma_{PDB} = 1.6$ value. For $\Gamma < \Gamma_{PDB}$, the two different trajectories characterized by the same mode parameters (1,1) are observed in the simulations. The (3,2) mode is also observed and it is overlying the mode (2,1). In fact, the (3,2) mode was observed during the simulations when Γ increased and the (2,1) mode was observed in the simulations during the decreasing phases. Thus, depending on the initial conditions one or the other mode can be observed. The bifurcation to the mode (4,4) is also observed for nearly the same acceleration Γ. The second mode (2,1) observed experimentally at $\Gamma = 4.4$ was detected when analyzing the trajectories of the simulations; however, it was not stable for more than several periods, which is why it does not appear on the figure.

Guided by our observations of Section 2.1 and 3.1, we modeled the droplet by two masses linked by a spring of stiffness k in parallel with a dashpot of damping ratio ξ. These two parameters were adjusted during experiments performed on a static bath before extending the study to an oscillating bath. We used the same strategy in Section 2.4. We thus simulated the spring system on an oscillating bath and found the bifurcation diagram that we observed experimentally in Section 3.2. The agreement between the experiments and the simulations is good. This shows that the spring system is an excellent model for bouncing droplets.

Chapter 4

Only the bath can be deformed

Contents

In the previous chapter, we investigated slightly deformable droplets on an oscillating highly viscous bath. Depending on the forcing parameters, we observed different trajectories that we rationalized using a spring model. We were able to reproduce accurately bifurcation diagrams using this model. In the present chapter, we investigate droplets bouncing on a low viscous bath instead of a highly viscous one. This deformable bath changes the properties of the rebounds. In Section 4.1, similarly to our investigation in the previous chapter, we begin by investigating bounces on a static bath, which allows us to extract the basic properties of the bouncing. In Section 4.2, we report measurements of the bouncing and of the Faraday thresholds. We then construct, in Section 4.3, phase diagrams of bouncing modes of droplets of different sizes. These allow us to discuss the behavior of the droplets as a function of the experimental parameters. We are extending here an investigation that was initiated by the Couder's team in 2005 [7, 44]. They observed walkers capable of moving on the surface

owing to the waves emitted on the liquid bath. This amazing behavior is the main subject of quantum-like experiments. The origin of this motion is however still not fully understood. Therefore, we analyze trajectories and bifurcation diagrams of so called walkers in Section 4.4. The speed of these walkers is then correlated with the bouncing mode.

4.1 Bouncing on a static bath

We made droplets of 20 cSt silicone oil and of diameter $D = 770\,\mu$m using the droplet dispenser (cf. Appendix C for details). We laid these, from different heights ($\sim$ 1 cm), on a static 20 cSt silicone oil bath of 1 cm depth (deep bath conditions). We recorded movies from the side, at 2000 fps, with a high speed camera (IDT-Y4L) (cf. Appendix B). We present a spatio-temporal diagram of one of these movies on Fig. 4.1. We detail our construction method in Section 1.3.3 and 3.1.

The initial speed at the first impact on the static bath is about 0.5 m/s which is similar to the impact speed of the droplet impacting a highly viscous bath presented in Fig. 3.2. The resulting bounce heights are however significantly smaller than for highly viscous baths and only two successive bounces are observed, as we can see on Fig. 4.1. The droplet makes a crater in the bath which which can no longer be neglected. The size of this crater depends on the size and impact speed of the droplets. After a bounce, the liquid bath oscillates a few milliseconds before returning to rest. In this case, we cannot draw a parallel with the bouncing ball since the interaction of the droplet with the bath is complex. This is an issue already encountered by Gilet *et al.* [26,89] and Eichwald *et al.* [90]. They had to evaluate the forces acting on the droplet or on the solid ball during the bounce in order to solve the second Newton law. The coefficient of restitution is like a black box which predicts the speed after the impact given the initial impact speed. While, we could determine this coefficient of restitution on the rigid bath, it is difficult to do so here. Nevertheless, we can conclude that an oil bath with a viscosity of 20 cSt instead of 1000 cSt induces more dissipation during the bounce, i.e. more energy is dissipated in the bath deformation.

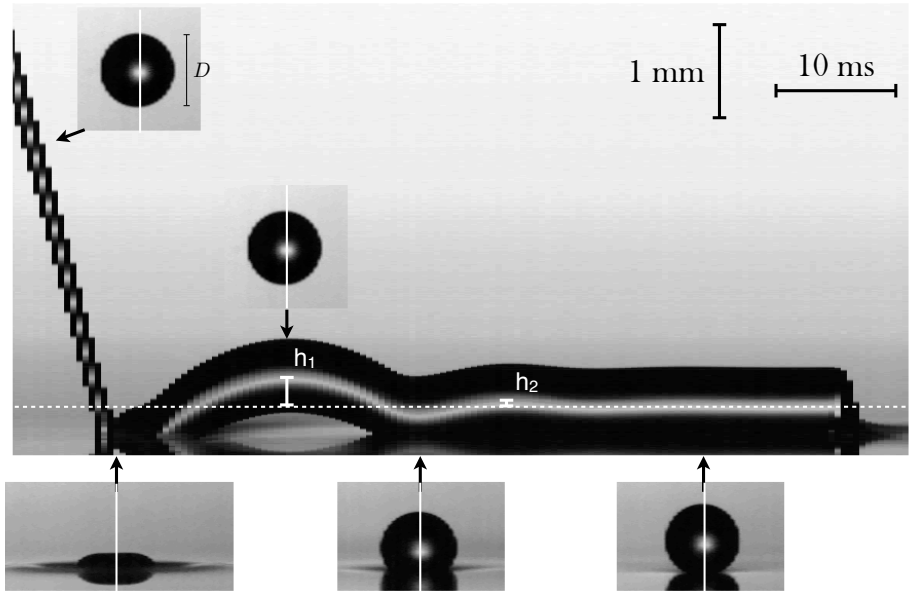

Figure 4.1: Spatio-temporal diagram of a 20 cSt silicone oil droplet of diameter $D = 770\,\mu$m falling on a static 20 cSt silicone oil bath. The time elapses from left to right. The droplet experiences two bounces of heights h_1 and h_2. These heights are measured from the center of mass of the droplet when it is floating (white dotted line). The impact speeds of the bounces are $V_1 = 0.51$ m/s and $V_2 = 0.08$ m/s. Five snapshots illustrate the shape of the droplet at different typical times of the bounce.

4.2 Bouncing on an oscillating bath

Using the droplet dispenser, we laid droplets on an oscillating 20 cSt silicone oil bath. We measured the bouncing acceleration threshold Γ_b following the method that we explained in Section 2.1.1. These measurements are reported on Fig. 4.2a for droplet sizes ranging from $D = 665\,\mu$m to $1500\,\mu$m. The Γ_b curves present a minimum, lower than 1. The smaller the droplet, the higher the frequency of the minimum. As the viscosity of the bath is relatively small, we observe Faraday waves that occur above the acceleration threshold Γ_F defined by Eq. 1.8. The Faraday threshold Γ_F is proportional to the viscosity ν and increases according to a power law, $f^{5/3}$. Experimental measurements of Γ_F are represented, on Fig. 4.2a, by red squares that are fitted by a 5/3 power law (the red line). As the Γ_b curves are shifted upwards when considering larger droplets, we found that there is a maximum size not to be exceeded for the droplet to bounce on the bath. We cannot increase the acceleration Γ beyond Γ_F without disturbing the surface of the liquid bath by exciting Faraday waves. For a 20 cSt silicone oil bath, the largest droplet that can bounce, such as $\Gamma < \Gamma_F$, has a maximum diameter $D \sim 1500\,\mu$m.

On Fig. 4.2b, the frequencies of the measurements presented on Fig. 4.2a are normalized by the capillary frequency $f_c = \sqrt{\sigma/M}$, where M is the droplet mass. All the Γ_b curves collapse on a master curve as we have demonstrated in Section 2.1. The first minimum of about 0.5 is observed at a value of $f/f_c \sim 0.21$ (cf. inset in Fig. 4.2b) while the first minimum for these droplet bouncing on a 1000 cSt silicone oil bath is about 0.3 at $f/f_c \sim 0.38$ (cf. Fig. 3.4). For this value, the coupling between the dynamics of the air film and the dynamics of the deformation is favorable for bouncing. Also, the Γ_b curves increase much more rapidly with the 20 cSt bath than with the 1000 cSt one. There is also a slight inflection at $f/f_c \sim 1.25$ indicating another resonant mode being excited. This was also observed, on Fig. 2.1, for larger droplets of 100 cSt silicone oil bouncing on an oscillating highly viscous bath.

4.3 Phase diagrams

Droplets are observed to bounce for acceleration Γ higher than the bouncing acceleration threshold Γ_b. At higher accelerations, the bouncing droplets are

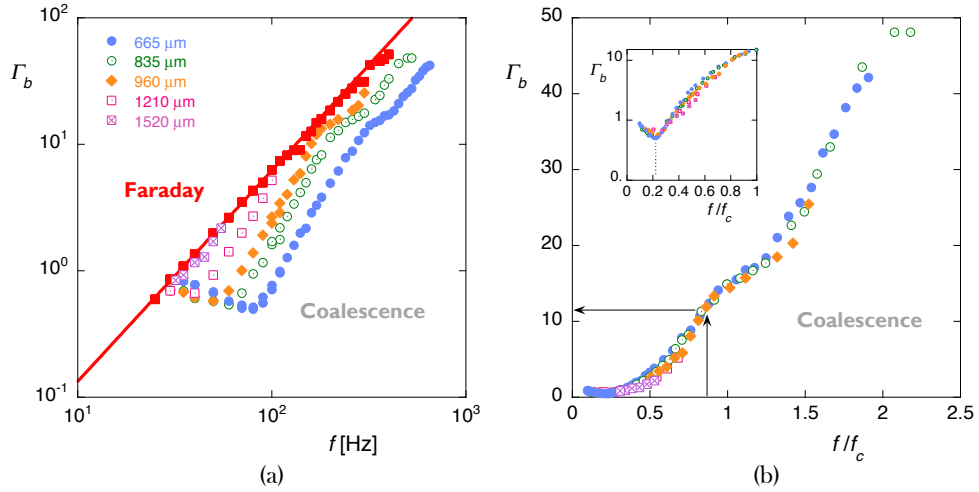

Figure 4.2: The bouncing threshold acceleration Γ_b measurements for different droplet sizes ranging form $D = 665\,\mu$m to $1520\,\mu$m (diameters are indicated in the legend). (a) The Γ_b threshold is represented as a function of f. The Faraday threshold measurements are represented by red square symbols which are fitted, in red, by a power law, $5/3$ of the frequency. (b) The Γ_b measurements are represented against the normalize frequency f/f_c where f_c is the capillary frequency. The arrows are explained in the text. A zoom of the first minimum of the $\Gamma_b(f/f_c)$ curve is presented in the inset.

limited by the triggering of the Faraday instability which occurs at Γ_F. Between these two accelerations, the droplets can bounce following different trajectories. These trajectories were highlighted for the 50 cSt silicone oil and a frequency $f = 50$ Hz in [44]. This diagram was presented on Fig. 1.7. We built the diagram for a liquid of 20 cSt silicone oil at $f = 80$ Hz in Ref. [7], it is presented, for a liquid bath of thickness 3 mm, on Fig. 4.3a (for a better visualization, axes are inverted with respect to Fig. 1.7). In those studies, the forcing frequency was fixed, and the droplet trajectories were characterized as a function of the forcing acceleration Γ and the droplet diameter D.

The bouncing mode phase diagram, presented on Fig. 4.3a, is divided in regions of different colors, each region corresponding to a specific bouncing mode (p, q) similar to those represented on Fig. 3.5. Each color matches a mode. Above the $\Gamma_b(D)$ curve, which is represented by the purple bullets (the dotted line is a guide for the eyes), the region "B" describes droplets bouncing in the

mode (1,1). The region "PDB → P2" is a zone where it is really difficult to differentiate between a mode (2,2) and a mode (2,1). Nevertheless, the periodicity of the rebounds is equal to two periods of the oscillating bath. We will get back to this later. Just below the Faraday threshold, droplets can spontaneously be set into horizontal motion where they become the "walkers" detailed in Section 1.3.6. According to [44], the walkers are bouncing in a mode (2,1). When a droplet is too large or too small it can can experience chaos before becoming a walker or reaching the Faraday instability at $\Gamma_F \approx 4.2$. The bullets on Fig. 4.3a are experimental data points detected as being the transition between different regimes.

The $\Gamma_b(D)$ curve observed on Fig. 4.3a can be readily predicted by the bouncing acceleration threshold $\Gamma_b(f/f_c)$ presented on Fig. 4.2b. Indeed, since we work at a fixed frequency ($f = 80$ Hz), we can determine the bouncing acceleration by calculating the ratio $f/f_c = f(\sigma/\rho)^{1/2}D^{3/2}$ for the desired diameter D. This value can then be reported on Fig. 4.2b and using the master curve, as suggested by the arrows, Γ_b can be found out as a function of D.

We made the same kind of phase diagrams after varying the forcing parameters Γ and f for several sizes of droplets. We selected three typical diagrams for the droplets of size $D = 695\,\mu$m, $810\,\mu$m and $870\,\mu$m, these are represented on Fig. 4.3b, 4.3c and 4.3d, respectively. The regions are named as on Fig. 4.3a. Similarly to Fig. 4.2a, the red squares are the experimental measurements of the Faraday threshold and the red curves $\Gamma_F(f)$ are fits of a power 5/3 law as predicted by Eq. 1.8. The bullets are the measurements of the transition between the different regions. The $\Gamma_b(f)$ curve on Fig. 4.3c is an extrapolation from the measurements of Fig. 4.3b and 4.3d. The (Γ, f) and the (Γ, D) diagrams can be seen as the 2D projections of a the 3D phase diagram (Γ, f, D). The intersections of the (Γ, D) with the three (Γ, f) diagrams are represented by dotted vertical lines on each of the diagrams.

Let us focus on the "W" area. The smallest droplet, $D = 695\,\mu$m (cf. Fig. 4.3b), cannot walk efficiently when in this "W" region. It does not always move in a straight motion and its horizontal speed is always too low compared to an efficient walker [44]. The phase diagram of an efficient walker is represented on Fig. 4.3c. The walker moves horizontally on the surface in a straight motion at a speed of about 15 mm/s. This size of drop is typically the size of

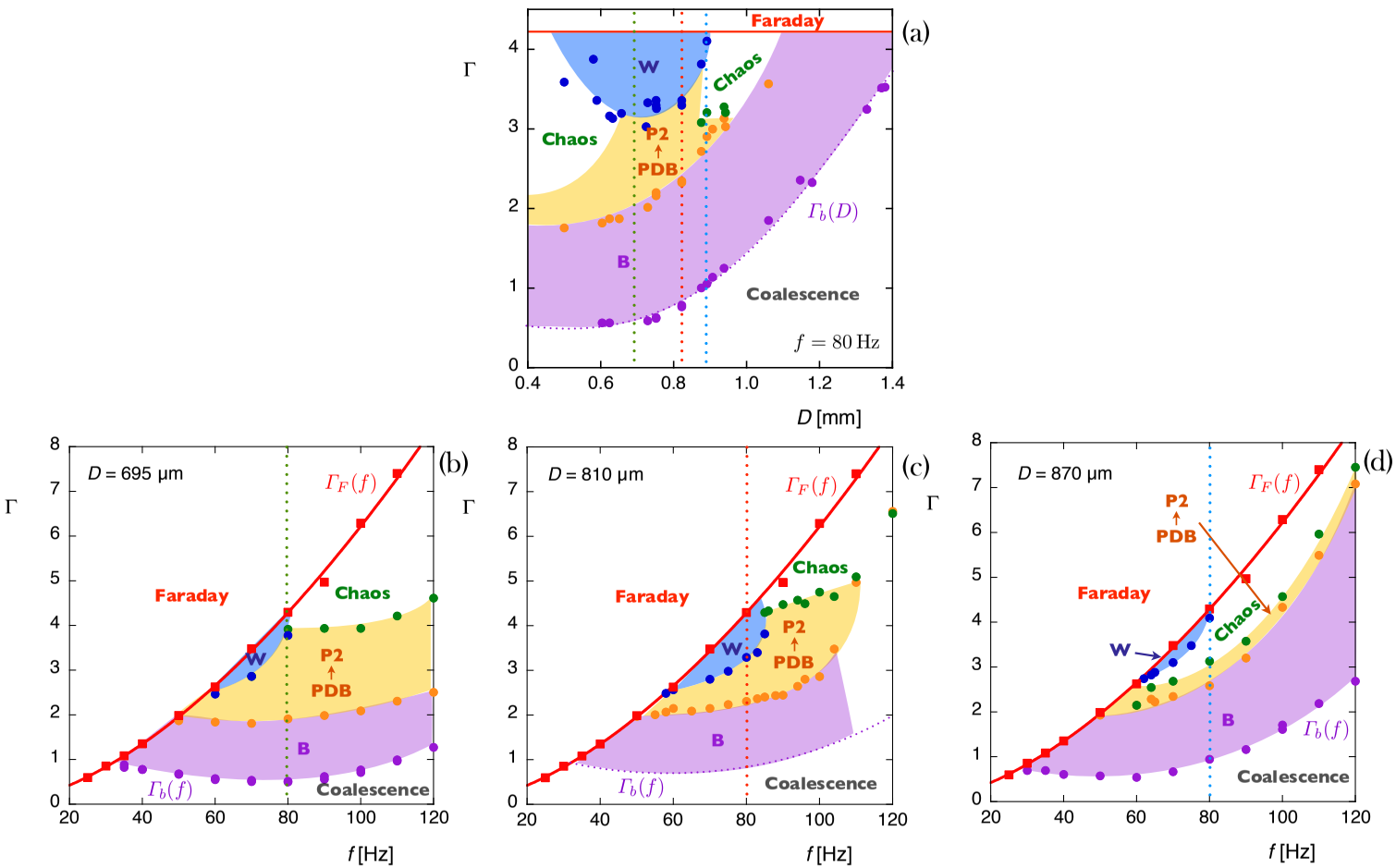

Figure 4.3: The (Γ,f) and the (Γ,D) phase diagrams of a droplet of diameter D bouncing on an oscillating bath. Both liquids are 20 cSt silicone oil. The droplet sizes are (b) $D = 695\,\mu$m, (c) $D = 810\,\mu$m and (d) $D = 870\,\mu$m. The oscillating frequency of (c) is $f = 80$ Hz. The regions are explained in the text.

the 20 cSt silicone oil walkers for the quantum-like experiments [2,3,5]. For a bigger droplet, $D = 870\,\mu$m (cf. Fig. 4.3d), the "W" region is much smaller. When Γ is increased, this droplet experiences a chaotic behavior before eventually walking. Moreover, these are observed to be intermittent walker. They start walking when a little kick on the surface is provided but they stop after some distance. In fact, the bouncing mode of the walker is unstable and the droplet returns to a chaotic bouncing mode.

The region where walking takes place has been investigated by Protière *et al.* [25] as a function of the viscosity. Walkers are observed for droplets with a viscosity ranging from 10 cSt to 100 cSt. They always occur for acceleration just under the Faraday threshold Γ_F which increases more rapidly with the frequency when the viscosity is increased. Thus, the range of frequencies where walkers can be observed is shifted to lower frequencies when the viscosity is increased. Furthermore, it is observed that the mean droplet size of an efficient walker decreases with the viscosity.

On the phase diagrams of Fig. 4.3, we observed that a necessary condition for becoming a walker is to be able to experience at least a period doubling in order to excite Faraday waves. This ability varies with the droplet size as suggested on Fig. 4.4, the accelerations Γ_{PDB} of transition from the "B" to the "PDB" region are plotted for droplets of different sizes. The Γ_{PDB} curves increase with the frequency and more rapidly for larger droplets. The droplet of diameter $D = 810\,\mu$m (cf. Fig. 4.3c) was observed to be the most efficient one. Let us now focus on this droplet.

Meeting the period doubling bouncing mode condition is not sufficient for walking. Indeed, the other required condition is to be able to excite Faraday waves of large amplitude. This condition is only met close to Γ_F [7,29]. The amplitude of the Faraday waves emitted depends also on the size of the bouncing drop. Indeed, the wave field structure emitted by a bouncing drop is not trivial. Eddi *et al.* [4] investigated the wave field that is produced by the impact of a rigid sphere on an oscillating liquid surface near the Faraday threshold. They observed that the dynamics of the wave field can be divided into two phases: a capillary wave packet is emitted and progresses outwards from the impact (first phase) which leaves a stationary wave behind, corresponding to Faraday waves, whose amplitude decays slowly (second phase). The ability to excite

Faraday waves of large amplitude depends on the structure of the emitted wave packet during the first phase. A wave packet is a polychromatic wave that leaves the wave behind oscillating at the Faraday frequency. The persistence of the Faraday waves depends on how much energy is available for the Faraday regime. The structure of the wave packet depends on the size of the impacting object in a non trivial way. Starting from the hydrodynamical equations, Eddi *et al.* [4] simulated numerically the wave field emitted by perturbations of different sizes. They demonstrated that the amplitude of a stationary wave depends on the size of the perturbation, so there should be an optimal size for the drop. This is in agreement with what we observed and described above.

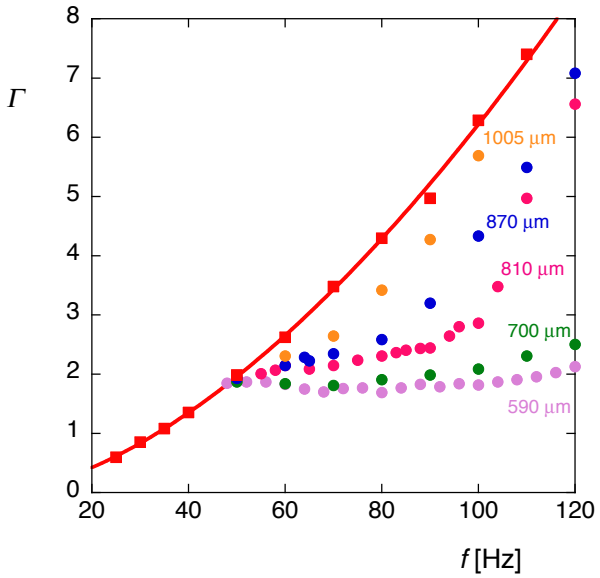

Figure 4.4: The acceleration threshold Γ_{PDB} (transition from a mode (1,1) to a mode (2,2)) as a function of the frequency for several droplet diameters which are indicated on the figure. The Faraday threshold measurements are represented by red square symbols which are fitted, in red, by a power 5/3 of the frequency.

4.4 Bifurcation diagram of a bouncing droplet

Following the same method as in Section 3.2, we built a bifurcation diagram of a 20 cSt silicone oil droplet bouncing on an oscillating bath made of the same liquid. We chose the droplet size $D = 810\,\mu$m and the forcing frequency at 80 Hz

in order to get an efficient walker. The (Γ,f) phase diagram corresponding to this droplet size is reported on Fig. 4.3c. By following the vertical dotted line, the behavior of our bouncing droplet can be determined as a function of Γ. Using the high speed video camera (IDT-N3), we recorded movies at 1000 fps of the bouncing drop for bath accelerations ranging from Γ_b to Γ_F. In each movie, we measured the bouncing heights h and the interval of time between two bounces $\Delta T_{\min}/T$, where T is the period of the oscillation of the bath. Both parameters are defined in Section 3.2 and illustrated on Fig. 3.5e. Let us remember that a bounce is defined as a minimum in the trajectory of the center of mass of the droplet. For a walking droplet, we had to follow the droplet horizontally to make the measurements. These measurements are reported on Fig. 4.5a and 4.5b. The region "B" and "PDB $\rightarrow$ P2" characterizing the bouncing modes are indicated as colored areas in Fig. 4.5. Note that the "W" region is not indicated as it does not defined a bouncing mode but the fact that the droplet moves horizontally on the surface (horizontal speed $v \neq 0$). On Fig. 4.5a and 4.5b, we observed a bifurcation at $\Gamma_{PDB} \approx 2.30$. Below Γ_{PDB}, it bounces in a mode (1,1) and beyond Γ_{PDB}, the droplet bounces in mode (2,2). The smaller bounce seems to vanish at $\Gamma \approx 2.7$ when the mode becomes, according to our definition of the bounce, a mode (2,1). The height of the larger bounce continuously increases with Γ. When $\Gamma_W = 3.60$, Faraday waves are triggered, the droplet starts walking on the liquid surface and the bouncing height increases more rapidly with Γ. We measured the horizontal speed v of the droplet ($D = 810\,\mu$m) as a function of Γ. The speed measurements are reported on Fig. 4.5c. The horizontal speed of the droplet is always null or negligible until $\Gamma_W = 3.60$ is reached. Above Γ_W, the droplet starts walking and the speed increases with Γ, finally saturating at a value of about 13 mm/s. Our measurements are in good agreement with the measurements reported by Protière *et al.* [44].

The first bifurcation is similar to the one observed on the highly viscous bath on Fig. 3.6 of Section 3.2. However, for larger accelerations, the mode (2,2) evolves continuously into a mode (2,1) which is not observed for the droplet bouncing on the highly viscous bath. This smooth evolution, from a mode (2,2,) to a mode (2,1), is much more a characteristic of the inelastic ball for which a bifurcation diagram is presented in Fig. 3.1. As we observed for the static bath (cf. Section 3.1 and 4.1), the "coefficient of restitution", if we can

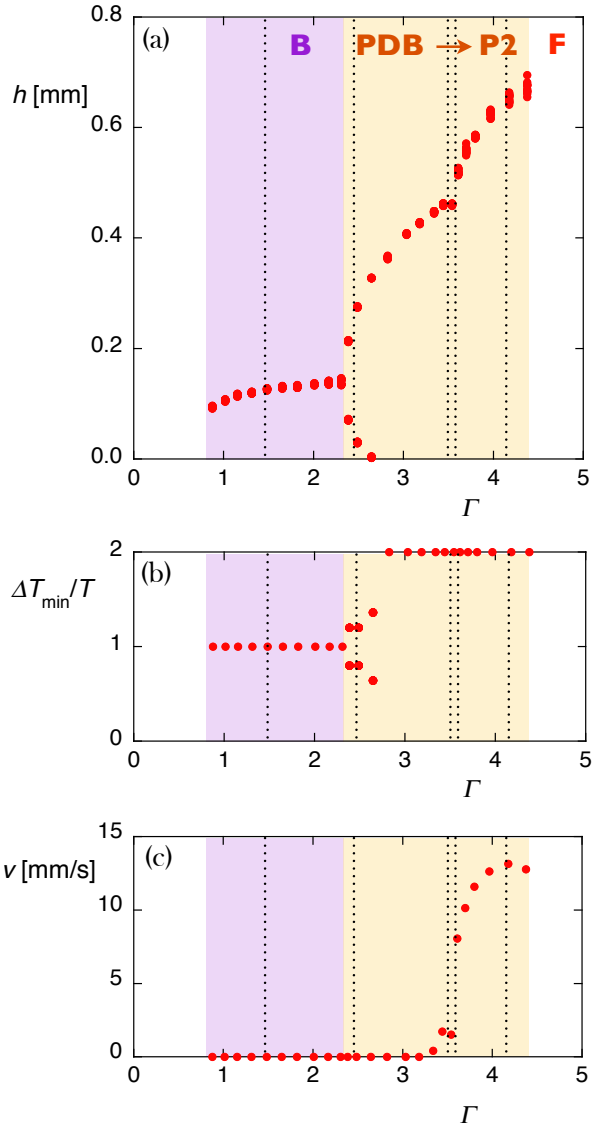

Figure 4.5: Bifurcation diagram of a droplet of diameter $D = 810\,\mu$m bouncing on an oscillating liquid bath at $f = 80$ Hz. Both liquids are 20 cSt silicone oil. (a) measurements of the bouncing heights h. (b) Measurements of the time intervals $\Delta T_{\min}/T$ between two successive bounces. (c) Horizontal speed v of the droplet as a function of Γ. The five dotted lines on each figure represent the selection of movies that are analyzed (cf. Fig. 4.6 and 4.7). Error bars are typically of the symbol size.

define it, is smaller for the low viscosity bath than for the highly viscous one. It results in a higher Γ_{PDB} value but not as high as in the inelastic bouncing ball; consequently, the elasticity of the rebound has to be taken into account in order to rationalize the phase diagram.

Let us have a closer look at the trajectories analyzed on the diagrams of Fig. 4.5. We selected 5 movies respectively corresponding to a droplet bouncing in a mode (1,1) ($\Gamma = 1.48$) and in a mode (2,2) ($\Gamma = 2.48$), a non walking droplet in a mode defined as (2,1) ($\Gamma = 3.54$), a low speed walking droplet ($\Gamma = 3.61$) and a high speed walking droplet ($\Gamma = 4.17$). These modes are highlighted by dotted lines on Fig. 4.5. For each movie, we constructed a spatio-temporal representation (cf. Section 1.3.3). These five plots are presented on Fig. 4.6a. On such an image, we can observe the droplet bouncing and its reflection on the bath that is perturbed by the waves. Below each image, we added another spatio-temporal image of the wire moving with the bath indicating the position of the plate. On each movie, we tracked the position y of the droplet center of mass and the plate. From the trajectories, we deduced the vertical velocity v_y and the vertical acceleration a_y of the droplet and the bath. The vertical positions[1], velocities and accelerations are presented, for the five movies, in Fig. 4.6b and 4.6c, and in Fig. 4.7a, 4.7b and 4.7c.

The measurements of the vertical velocity and the vertical acceleration of the droplet allow us to deduce when the droplet interacts with the bath and when it is in free fall. We should be careful when handling the acceleration curve as the acceleration is a second derivative of the position which has been sampled at 1000 Hz (samples are spaced by $\Delta t/T = 0.08$). Anyway, we can clearly determine when the droplet interacts with the bath and for how long. These "contact" periods are highlighted by grey areas on Fig. 4.6 and 4.7. In free fall, the acceleration of the droplet is observed at $a_y/g = -1$. In the mode (1,1) (cf. Fig. 4.6b), the droplet starts to interact with the bath when the bath is at a minimum and starts moving upwards. It stops interacting with the bath when the latter is at a maximum and starts moving downwards.

In the mode (2,2) (cf. Fig. 4.6c), the same bounce is observed during the upwards motion of the bath. As the amplitude of the oscillation is larger, it

[1]The relative positions of the droplet center of mass and of the bath have been adjusted for a better visualization.

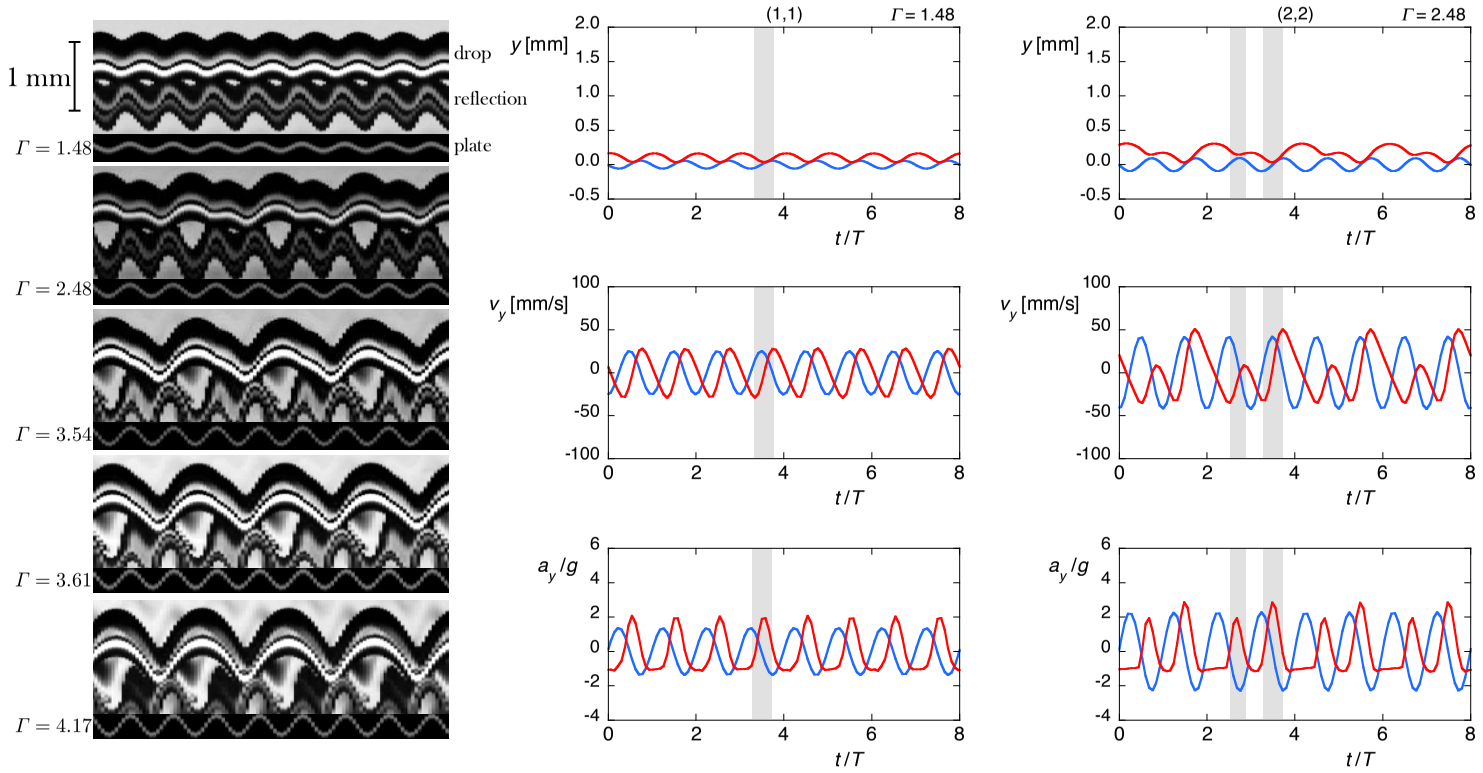

Figure 4.6: The 5 selected movies presented in Fig. 4.5 are analyzed. (a) Spatio temporal plots of the movies at different Γ which are indicated at the left of each plot. (b-c) The vertical position y, the vertical speed v_y and the vertical acceleration a_y of the droplet (in red) and the bath (in blue) are reported as a function of the normalized time t/T. The grey areas indicate intervals of interaction with the bath. (b) $\Gamma = 1.48$ and (c) $\Gamma = 2.48$. The three other movies are presented on Fig. 4.7.

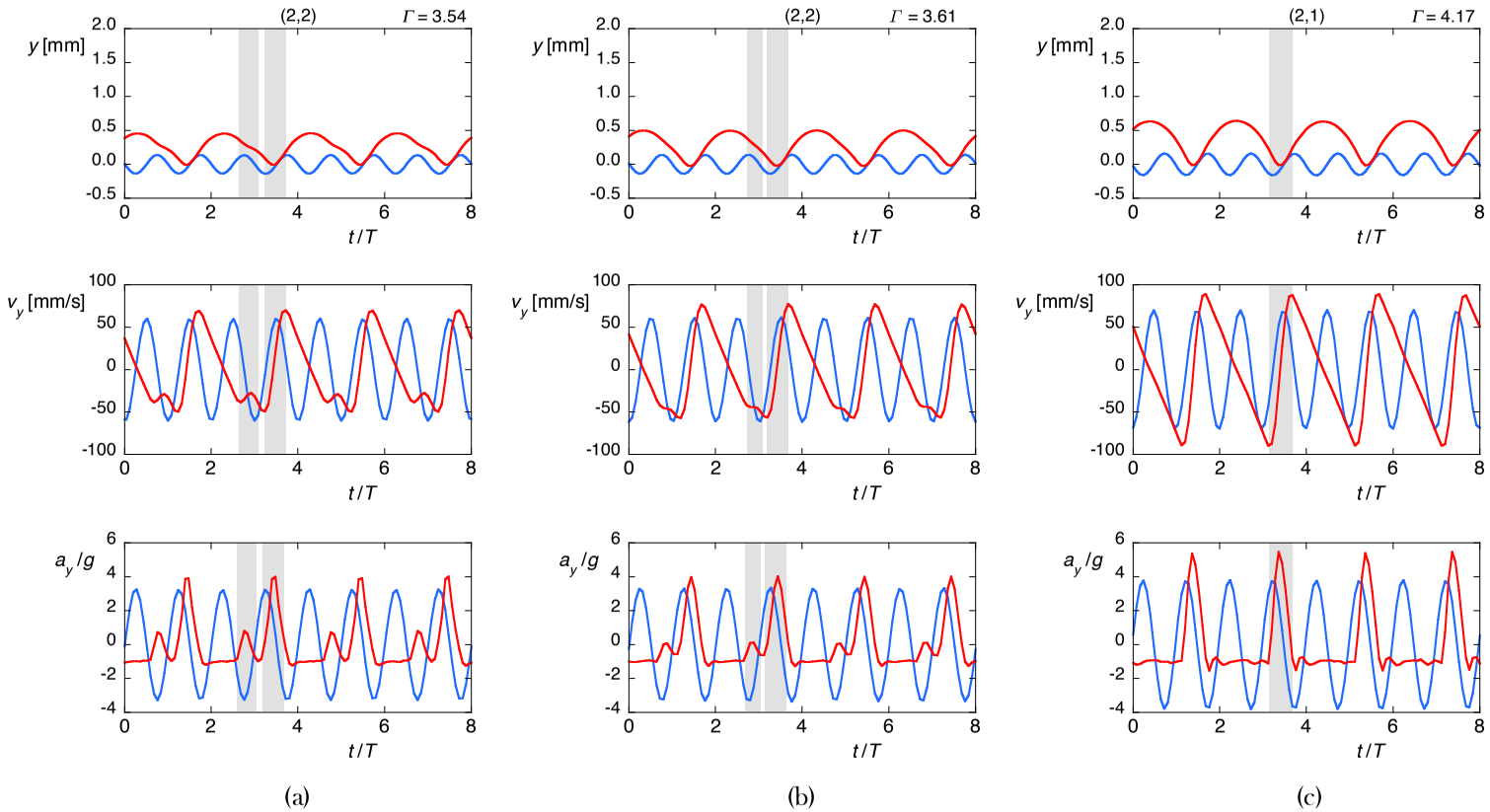

Figure 4.7: Continuation of Fig. 4.6. (a) $\Gamma = 3.54$, (b) $\Gamma = 3.61$ and (c) $\Gamma = 4.17$. Bouncing modes (p, q) are indicated at the top of each series of plots according to the new definition of the bounce (see text).

results in a larger bounce. Consequently, the droplet "lands" on a maximum of the bath and interacts with it during a shorter time. The second bounce is thus smaller. The height of the largest rebound increases with Γ while the smallest bounce keeps on decreasing. On Fig. 4.7a, the mode of the droplet is defined as (2,1). However, we observed that even if the droplet is not "bouncing", a decrease of the downwards speed is noticed ($a_y/g > 1$). This indicates an interaction with the bath during a defined span of time.

Until now, the "contact" with the bath was defined as the minimum in the trajectory of the center of mass of the droplet. We have thus to **redefine** this "contact" as any interaction with the bath perturbing the free fall of the droplet, i.e. when the droplet acceleration a_y/g becomes higher than -1. The bouncing mode notification (p, q) is also redefined as a period of q interactions with the bath while it oscillates q times. The interactions were difficult to determine until we tracked the droplet trajectories. That is the reason why we regrouped the bouncing modes (2,2) and (2,1) in one region "PDB $\rightarrow$ P2" on Fig. 4.3.

On Fig. 4.6c, 4.7a and 4.7b, the intensity of the smallest interaction of the mode (2,2) decreases until completely disappearing. The mode remains (2,2) as the droplet interacts twice with the bath during two periods. In the movie taken at $\Gamma = 3.61$ (cf. Fig. 4.7b), the small interaction is still present and the droplet **starts to walk** on the surface (cf. Fig. 4.5c). Then the intensity of the small interaction keeps on decreasing while the velocity of the walker is increasing. The speed of the walker saturates when the small interaction has completely disappeared and the droplet starts bouncing in a mode (2,1) (cf. Fig. 4.5c). This saturation was already observed in [44] but another explanation was given. In [44], they proposed a simple model based on the balance between two forces : a driving force and a friction force. The driving force comes from the momentum income of the droplet when bouncing on the slope of the Faraday wave emitted at the previous bounce. The friction force comes from the friction with the air that occurs when the droplet interacts with the bath. They found a transition from the non-walking to walking motion. The velocity is observed to increase as the square root of the distance to the walking threshold Γ_W. This model is however based on droplets bouncing in a complete bouncing mode (2,1) (without the smaller bounce).

We propose the following explanation. A drop can walk as soon as one jump

releases enough energy to trigger Faraday waves and this jump must occur in a $(p, 2)$ mode with $p = 1$ or 2. More precisely, in the (2,2) mode, since one of the bounce is higher than the other, the condition for triggering is satisfied. Note that we observed a droplet of diameter $D = 690\,\mu$m walking in a mode (2,2) (with the small bounce clearly visible) at an horizontal speed $v = 2.3$ mm/s on an oscillating bath at 58 Hz, just below the Faraday threshold. The trajectory of this walker is reported on Fig. 4.8. We considered a driving bounce (the large interaction) and a friction bounce (the small interaction). The driving bounce excites a local Faraday wave and induces the horizontal momentum of the walker when it lands (in average) on the slope of the wave emitted at the previous bounce. This idea is reinforced by the fact that droplets bouncing in a mode (2,2) are already used as source of Faraday waves in [7, 29]. The small bounce does not excite any Faraday wave. As a consequence, the walker reaches its maximum speed which saturates when the droplet bounces in a complete mode (2,1). The ability for a mode (2,2) or (2,1) to excite sub-critically Faraday waves is directly linked to the distance to the Faraday threshold. This is the key of the second model developed for the walker by Eddi *et al.* [4].

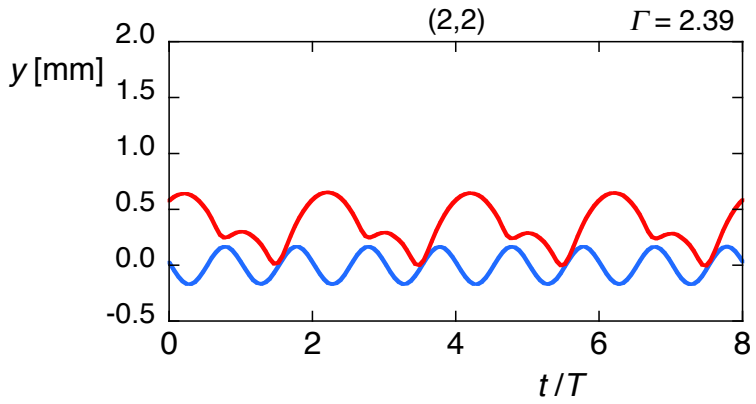

Figure 4.8: A droplet of diameter $D = 690\,\mu$m is walking in a bouncing mode (2,2) on a liquid bath oscillating at 58 Hz at $\Gamma = 2.40$ (just below the Faraday threshold). Both liquids are 20 cSt silicone oil. The vertical position y of the droplet (in red) and bath (in blue) are reported as a function of the normalized time t/T.

Summary

In this chapter, we investigated small droplets bouncing on a deformable liquid bath. Both liquids are 20 cSt silicone oil. We started with the observation of droplets falling on the bath when it was static. In comparison with the experiments on the static highly viscous bath (cf. Section 3.1), we observed that the droplets bounce at a smaller height when they have the same amount of energy at impact.

The bath was then set in oscillation and we studied the bouncing droplets on it. We built phase diagrams based on two pairs of parameters: the forcing parameters (Γ,f) and (Γ,D). In both series of diagrams, we measured the bouncing acceleration thresholds $\Gamma_b(f)$ and $\Gamma_b(D)$ that are shown to depend on each other. We discussed the appearance of the walking region as a function of the frequency f and the droplet size D. This region can be put in relation with the appearance of the mode (2,2) ("PDB $\rightarrow$ P2" region on Fig. 4.3) at an acceleration Γ_{PDB}.

Analysis of a bifurcation diagram of a walking droplet revealed that, we had to reformulate our definition of the bounce in terms of interaction rather than the minimum of the center of mass of the trajectory of the droplet. Within the region named "PDB $\rightarrow$ P2" on the phase diagrams, the bouncing mode (2,2) evolves continuously in a mode (2,1). This was not observed for the highly viscous bath (cf. Fig. 3.6). The walking motion was shown to appear when the droplet is still bouncing in a mode (2,2), which contrasts with the mode (2,1) required by previous studies [4,44]. These droplets bouncing in a mode (2,2) excite Faraday waves as far as they are in the vicinity of the Faraday threshold [7,29]. This could be a new perspective for the explanation of the increasing droplet speed when the walking threshold Γ_W is crossed. Indeed, the large bounce excites Faraday waves and occurs on a slope of the wave emitted by the previous bounce. This large bounce is the driving bounce. The smaller bounce prevents the Faraday waves from being excited, but its effects diminishe with its height when Γ is increased. Moreover, when the droplet interacts with the bath, the walker slows down due to the friction with the air film. The walker speed saturates when the smaller bounce/interaction has completely disappeared and the walker bounces in a complete (2,1) mode.

General conclusion

This thesis is a fundamental study of an original way to manipulate droplets. We chose to interact with bouncing droplets and to tackle the problem from the point of view of their **deformations**.

In Chapter 1, we placed the bouncing droplet question in its scientific context by summarizing some relevant works on the subject. We pointed out, in Section 1.4, some lack in the understanding of this phenomenon that we have decided to investigate. In Section 1.5, we established a strategy to answer a number of fundamental questions. We considered that the bouncing droplet problem is two-fold: the droplet itself and the bath and we decided that each entity could be studied independently. Using different liquids for the droplet and the bath, we can highlight the deformation of the droplet, of the bath, the deformations of both or no deformation at all. To do so, we chose the Ohnesorge number as the key parameter. This number compares the viscosity effects with the surface tension effects and allows us to find out whether the deformations are of importance or not. This number can be increased, causing the deformations to be more damped by the viscous effect, by increasing the liquid viscosity or by decreasing the droplet size. We chose to plot our work on the bouncing droplet as well as the one of others on a map defined by the Ohnesorge numbers Oh_b of the bath and Oh_d of the droplet (cf. Fig. 1.12b) and to explain our strategy on the road map of Fig. 1.12a.

In Chapter 2, we made large droplets of low viscosity silicone oil on an oscillating highly viscosity bath that is not deforming. Depending on the forcing frequency f, we measured a bouncing acceleration threshold Γ_b that can be smaller than 1 and which exhibited different deformation modes. These deformation modes are shown to correspond to the spherical harmonics introduced by Rayleigh [56]. The fundamental deformation mode is excited for low frequen-

cies (<100 Hz) and is the one observed in all previous studies on the walker and the bouncing droplet exposed in Chapter 1. Therefore, we focused on the bouncing threshold Γ_b of this mode. We observed that above Γ_b, the bouncing is periodic and below the droplets can only bounce during a certain time. As a consequence, we developed a theoretical model of the droplet deforming on a rigid bath that is oscillating. In this model, the deformation of the droplet influences the air film dynamics and thus the lubrication force that prevents the droplet from coalescing with the bath. With this model, we explained the minimum observed in the curve of the bouncing acceleration threshold $\Gamma_b(f)$ and the observed lifetime when $\Gamma < \Gamma_b$. Indeed, below Γ_b the droplets can bounce on the bath but the air film is not completely regenerated at each bounce and decreases in average. In the last section of this chapter, we investigated compound droplets, made of a water core and an oil layer, bouncing on a highly viscous bath. Exciting a specific mode of deformation, we demonstrated that it is possible to make a double emulsion in the droplets. At successive bounces, small oil droplets coming from the oil layer enter one by one in the water core. We modeled the acceleration threshold $\Gamma_b(f)$, but we did not explain the complex trajectories that the droplet can experience when bouncing at $\Gamma > \Gamma_b$.

In Chapter 3, we simplified the problem by considering small droplets made of 20 cSt silicone oil. These droplets are laid on a highly viscous bath (rigid) and are shown to deform slightly. We highlighted several periodic trajectories that can be compared to the bouncing ball problem. By investigating droplets impacting a static bath, we identified that a droplet stores energy into deformation similarly to a spring that is compressed. We thus developed a model based on two masses linked by a spring of stiffness k in parallel to a dashpot of damping ratio ξ. These parameters were adjusted on the observation of a droplet impacting the static bath. Then, we investigated numerically this spring system bouncing on a solid plate. Comparing both numerical and experimental trajectories, the model turned out to be very efficient.

In Chapter 4, we extended our investigation to a deformable bath. We considered droplets as in Chapter 3 bouncing on a bath made of 20 cSt silicone oil (deformable bath). We started by comparing the droplet impacts on the static deformable bath and on the static rigid bath. We observed that the bath dissipates more energy in the deformable case. Even if we showed the

limitations of the restitution coefficient and the bouncing ball parallelism, we observed bouncing trajectories on the oscillating bath that were much closer to the inelastic ball behavior. We constructed the phase diagrams for different droplet sizes and showed that the appearance of the walker is linked to the period doubling transition of the droplet and to the Faraday acceleration threshold. By analyzing a bifurcation diagram of the walker droplet, we showed that it was necessary to redefine how a bounce is detected. We managed to determine when the bath and the droplet interact. Doing so, we demonstrated that droplets can start walking in a period doubling mode characterized by a large bounce (large interaction) and a small bounce (small interaction). This is a generalization of the walker which is characterized in previous studies [1, 4, 44] by a mode (2,1) (one bounce every two bath oscillations). We observed that the speed decreases when the small interaction decreases and saturates when the small interaction has completely disappeared. We proposed a walker mechanism based on a driving bounce (the large bounce) and a friction bounce (the small one) which governed the horizontal speed of the walker. This could be a new element to consider in models of the walker [4, 44].

Perspectives

Here are some perspectives that we should consider in the near future.

Attempting to change the structure of the mayonnaise droplet

Just after the publication of our works on the double emulsions in a compound droplet [54,55], we have been contacted by Professor B.P. Binks, a well known chemist of the University of Hull (UK), who studies silica-stabilised emulsions. He proposed to use silica nanoparticles as the stabilizer instead of a surfactant. The silica particles are more or less fumed with SiOH, to make them hydrophobic or hydrophilic. We tried to put some fumed silica particles with 75 % SiOH, at 2 wt% in the water core to replace the SDS surfactant. The surface tension of the air/water interface does not seem to vary significantly when these particles are added to the water [91]. Compound droplets made with a water core with silica particles in dispersion were able to emulsify while it did not emulsify with pure water. Do these particles change the dynamics of emulsification ? It is possible to change the structure of the compound droplets, e.g. an oil core and a water layer ?

A self-propelled mode in the non-investigated area

During a discussion with Suzie Protière about the roller droplets. She mentioned to us that they have observed a similar behavior for a large droplet of several millimeters bouncing on a bath, droplet and bath both made of 100 cSt silicone oil, oscillating at 100 Hz. This research is located in the "not already investigated area" ($Oh_b \ll 1$ and $Oh_d \ll 1$) of our exploration map presented on Fig. 1.12b. The droplet moves horizontally on the surface and its speed increases until reaching the edge of the bath and collapsing, such a droplet is presented on

Fig. P.1. This droplet seems to move as a roller [47] and to emit waves as a self-propelled ratchet [7]. It would be interesting to investigate a droplet that combines both modes of self-propulsion.

Fig. P.1: Top view of a droplet of several millimeter bouncing on an oscillating liquid bath at 100 Hz. The two liquids are made of 100 cSt silicone oil. This droplet is moving towards the top right corner [Credit: S. Protière]. It exhibits the characteristics of two self-propelled modes: the ratchet and the roller [7,47].

Test the limit of the spring system model

In Chapter 3, we developed a model to mimic a droplet bouncing on an oscillating highly viscous bath based on two masses linked with a spring. We compared both experimental and numerical bifurcation diagrams at a fixed frequency of 50 Hz. The model proved to be very efficient to reproduce a number of bouncing periodic modes that were observed. One can seek the limitations of this model. Can it reproduce the variation of the trajectory with the frequency and the droplet sizes? Preliminary results are shown on Fig. P.2. The transition from a bouncing mode (1,1) to a mode (2,2) measured at Γ_{PDB} and the transition to a mode (2,1) measured at Γ_{P2} vary with the size of the droplet and the frequency. On the one hand, we observe that the Γ_{PDB} transition does not seem to depend on the size of the droplet nor on the frequency. This transition Γ_{PDB} is observed until a cut-off frequency, depending on the size of the droplets, is reached. On the other hand, the acceleration Γ_{P2} does not depend on the droplet sizes at low frequency. This transition increases with the frequency at high frequency and to depend on the droplet size.

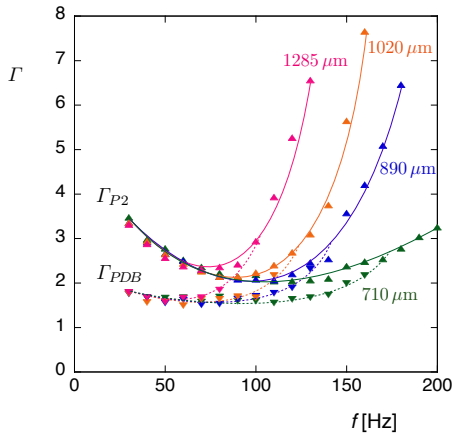

Fig. P.2: The transition accelerations Γ_{PDB} (▼ symbol) and Γ_{P2} (▲ symbol) are measured for 4 different droplets which sizes are $D_{\text{green}} = 710\,\mu\text{m}$, $D_{\text{blue}} = 890\,\mu\text{m}$, $D_{\text{orange}} = 1020\,\mu\text{m}$, $D_{\text{pink}} = 1285\,\mu\text{m}$. Diameters are indicated on the figure. The plain and dashed lines are guides for the eyes.

Extend the spring model to the deformable bath

In order to reproduce the observed bifurcation diagrams, a second spring model can be proposed for droplets bouncing on a low viscous bath. Starting from the design developed in Section 3.3, we add, on the oscillating plate, a spring linked to a mass m_b to model the deformable bath (cf. Fig. P.3b). The mass m_b represents the fluid of the bath that is set into motion when a droplet impacts the bath [92–94]. This mass m_b is linked to the oscillating plate with a spring of stiffness k_b in parallel to a dashpot of damping ratio ξ_b (cf. Fig. P.3a). These parameters represent the elasticity of the liquid surface and the dissipation in the bath by the viscosity.

The model is a bit more complicated than the previous one because we have to adjust 3 additional parameters: the mass m_b, the stiffness k_b and the damping ration ξ_b. We can keep the parameters of the spring (k and ξ) and the masses (m_1 and m_2), which characterize the droplet, like they have been fixed for the rigid surface in Section 3.3. To adjust the stiffness k_b, one can observe a droplet floating on the liquid surface and deduce the sinking depth of the droplet δ by comparing $k_b\delta \approx Mg$ where M is the mass of the droplet. Then, by analyzing a bouncing droplet on a static, low viscosity bath, we can

adjust the fluid mass m_b that is accelerated and the dissipation in the bath ξ_b. When all simulation parameters are determined, we can simulate the droplet with a bouncing spring on the oscillating spring as shown on Fig. P.3b in order to reproduce our observations detailed on Fig. 4.3.

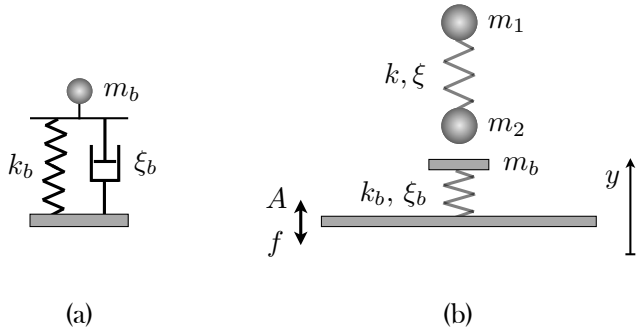

Fig. P.3: (a) The bath is modeled by a mass m_b linked to the oscillating plate with a spring of stiffness k_b in parallel to a dashpot of damping ratio ξ_b. (b) The droplet is mimicked by a spring system as detailed in Section 3.3 which itself bounces on the model bath.

Appendix A

Silicone oils properties

In a vast majority of cases, we used in this thesis Dow Corning silicone oils. Silicone oils are pure and low volatile liquids. Interactions in between molecules are of the Van der waals type which simplifies the expression of the long range forces. Surface tension is low which prevents surface contamination and is thus stable in time. By changing the length of the molecules, it exists a wide range of viscosities. The physical properties kinematic viscosity ν, density ρ and surface tension σ of Dow Corning silicone oils are reported at 25 $^{\circ}$C in Table A.1.

ν (cSt)	σ (mN/m)	ρ (kg/m^3)
0.65	15.9	761
1	17.4	818
1.5	16.8	850
10	20.1	934
20	20.6	949
50	20.8	960
100	20.9	960
1000	21.2	971
100 000	21.5 (extr.)	975 (extr.)

Table A.1: Dow Corning silicone oil physical properties. (extr.) means extrapolation.

Appendix B

Lighting and image acquisition

A fast video camera (up to 5000 fps) combined with an appropriate lighting are required to visualize millimetric droplets bouncing at frequencies over 20 Hz. Several fast video cameras were available all along this thesis but we mainly used the N3 and the Y4L from Integrated Device Technology, Inc. (IDT). Fast video cameras demand a powerful lighting, we used, for example, several sets of 7LED-cluster from IDT.

In Fig. B.1a, we present an experimental setup used to track the vertical trajectory and the shape of a bouncing droplet along the time. The droplet is illuminated from the back with a light and its shape is captured by a camera. The light, the droplet and the camera are aligned.

The electromagnetic shakers are GW-V55 or GW-V20. The acceleration of the plate is recorded by an accelerometer represented in red in the figures. All the acceleration values in this manuscript are given with an error of 2 %.

In Fig. B.1b, we detail a setup used to observe with great precision the waves launched on the surface by a bouncing droplet. The bath is illuminated by a perpendicular light fixed above it, the reflected beam from the bath and the drop is then reflected to the camera via a 50 % beam sampler. It is really important to make sure that the light and the camera are placed on a same axis.

In Fig. B.1c, we describe a setup used to observe the dynamics of the air film. Several low pressure sodium lamps are placed around the droplet. A monochromatic light allows us to visualize the interference fringes produced by the thin air film located between the droplet and the bath. The liquid bath is

bound by a transparent container raised above the plate. Below the container a mirror at 45 ° reflects the interfered light coming from the air film to the high-speed video camera. The number of fringes gives information about the thickness of the air film [95, 96].

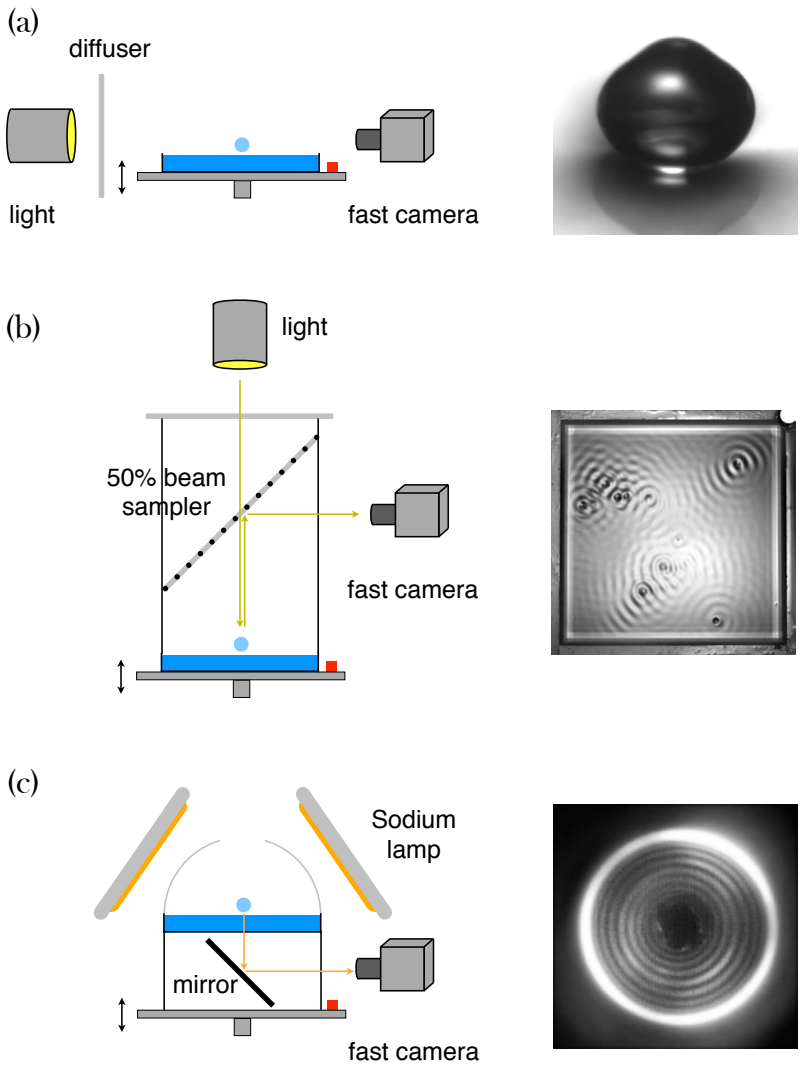

Figure B.1: Sketches of three experimental configurations used during this thesis.

Aliasing technique

The sodium lamps are oscillating at 100 Hz (alternative tension) this is a problem when recording movies with a high speed camera. Considering a periodical motion, we propose a method to record the motion during several periods and reconstruct a detailed single one. We choose to capture a picture every 10 ms (100 Hz), this allows us to obtain enough brightness and to decrease the shutter time. If each period is identical and that we want to obtain 50 images along one period, images will be separated by a constant phase $100/(50f)$. For instance, that can be possible when the frequency of the shaker is fixed to 26 Hz if we consider 13 periods. Doing so, it is possible to reconstruct one single period by superposing the 13 periods. Similar results may be obtained by considering f = 46, 74, and 98 Hz and 23, 37, and 49 periods, respectively.

Appendix C

Droplet generators

Droplets on demand can be generated in different ways. First, they can be made with a syringe using needles of different diameters to produce droplets of various sizes. Using this method, the smallest diameter for silicone oil droplets is roughly 1.5 mm.

For smaller droplets, a rod can be dipped into the bath and then extracted, a capillary bridge is forming at the tip of the rod that leaves a droplet when it breaks. Selected diameters depend on the rod width and the extraction speed [97], diameters are thus measured *a posteriori*. An automatic device can be built to produce droplets of reproducible diameters [98]. A limitation of this method is that the liquid of the drop and the bath must be identical.

A third method entails the use of a drop dispenser, a shock wave is launched, via a piezoelectric chip, in a small container with a hole filled with a liquid (cf. Fig. C.1 and C.2). A drop is ejected from the hole and its diameter is related to the one of the hole. With this technique, we are able to produce repeatedly droplets of silicone oil or water of the same diameter in a range of 100 μm to a few millimeters.

The dispenser setup is presented on Fig. C.1. A piezoelectric chip is glued on the top of a small cylindrical container and a small hole is drilled in the middle of the bottom wall (cf. Fig. C.2). The hole has been especially designed with an excimer laser (cf. Fig. C.2.c), the diameter is 600 μm with a groove around which pins the contact line of the liquid. The container is connected to a tank filled with liquid in which the air pressure is finely controlled using

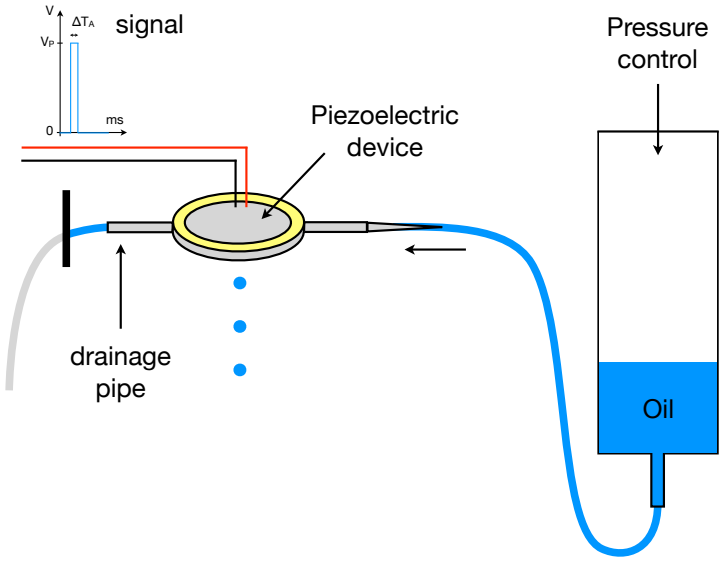

Figure C.1: Schematic illustration of the droplet dispenser.

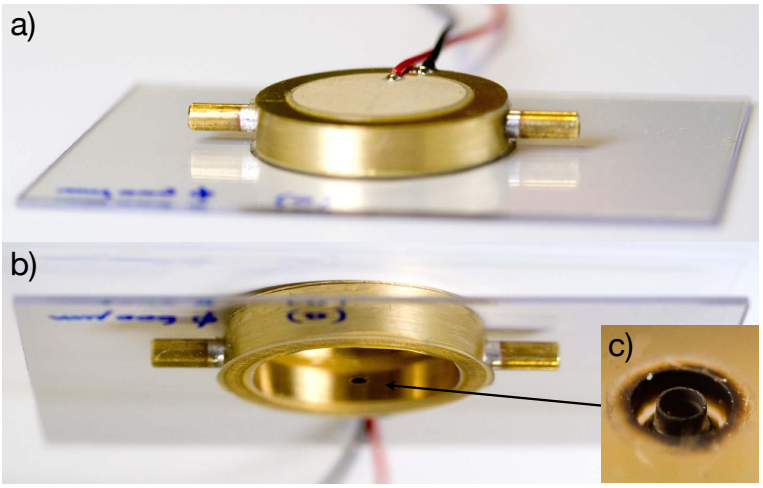

Figure C.2: Pictures of the droplet dispenser.

a pressure pump (Furness controls FCO502). The dispenser is fully filled with liquid from the tank and remaining air bubbles are evacuated by the drainage pipe before closing it. Then, using the air pump the pressure in the dispenser is finely adjusted so that the liquid surface into the hole is just at the level of the exit hole. No liquid may drain out nor air bubble may enter the container. The piezoelectric chip (MULTICOMP ABT-441-RC) is connected to a pulse generator that produces a square pulse of 0 to 100 V tension and of a few milliseconds width. Typically we use a square signal of 80 V in tension and 5 ms in width which produces a shock wave in the liquid that leads to the generation of a droplet. Multiple droplets can be produced by series of pulses. With 20 cSt silicone oil and a 600 μm nozzle, droplets of 700 μm diameter $\pm 3\,\%$ are produced. By changing the tension of the square signal from 50 to 80 V we produced droplet raging from 650 μm to 750 μm, the droplet size increasing with the tension. In order to generate droplets of much more different diameters, holes of various diameters can be used. One can also merged droplets on the bath in order to study different droplet sizes.

Appendix D

Molecular dynamics simulations

The numerical simulations are performed following the Molecular Dynamics method. This method considers deformable spheres which can interact through impacts that are governed by repulsion(normal) and friction (tangential) laws. Using this method, the individual trajectories of the spheres are calculated by integrating their equations of motion. This method has been widely developed in the field of granular matter by computational experts [99]. The Molecular Dynamics method is well explained in these two Ph.D thesis [100, 101]. Here is a summary. The method is divided into four steps :

1. the positions and the translational and rotational velocities are initialized;
2. the forces acting on each body are calculated, i.e gravitational, frictional and normal forces;
3. the equations of motion are integrated at the same time for each spheres; and
4. the new positions and the new translational and rotational velocities are recorded;

Steps 2 to 4 are repeated until reaching the time defined for the duration of the simulation.

In our simulation, the normal force $\vec{N}$ between the lower mass m_2 of the spring and the plate is estimated as follow. The contact between the plate and the mass is seen as 2 spheres that can interpenetrate, of a distance δ. A Hooke law is used to calculate the normal force:

$$N = k_c \delta. \tag{D.1}$$

Impacts are most of the time inelastic, a dissipative force should then be considered while the two spheres are interacting:

$$F_v = -c_c \frac{d\delta}{dt}. \tag{D.2}$$

In our simulation, we wanted to avoid interpenetration of the mass m_2 and the plate, the constant k_c is thus set to a higher value than the stiffness k of the spring modeling our drop. The droplet bounces on the plate because it stores energy in deformation during impact that is restored later. We thus wanted the most inelastic impact for the mass m_2 with the plate in order to have no effect on the bounce. We thus considered a really high value for c_c (as high as permitted by the numerical computation).

Appendix E

Selection of publications

In this appendix, we present two publications that have been written during two internships, the first one at the "Laboratoire Matière et Systèmes Complexes", in the team of Yves Couder, at the Université Paris Diderot-Paris 7 (France) and the second one in John Bush's Group at the MIT - Massachusetts Institute of Technology (USA).

The first work *"Wave propelled ratchets and drifting rafts"* is about droplets of uneven size bouncing on a low viscous bath. They interact with the wave field they emit to form a bound state that moves horizontally on the liquid surface. This self-propelled system is due to the asymmetry in the emitted wave field. By varying the forcing amplitude, the droplet bouncing mode can be changed inducing a reversal of the direction of this ratchet-like system. This mechanism of self-propulsion can be generalized to rafts of several droplets.

The second publication *"Tibetan singing bowls"* presents a study of fluid-filled singing bowls, originating from the Himalayas, which produce a myriad of droplets when they sing. The ejection of droplets out of the bowl is shown to come from the breaking of Faraday waves that are excited when the bowl is rubbed and is singing. In certain conditions, small droplets are observed to bounce periodically on the liquid surface.

A Letters Journal Exploring the Frontiers of Physics

May 2008

EPL, **82** (2008) 44001
doi: 10.1209/0295-5075/82/44001

www.epljournal.org

Wave propelled ratchets and drifting rafts

A. Eddi[1(a)], D. Terwagne[2], E. Fort[3] and Y. Couder[1]

[1] *Matières et Systèmes Complexes, Université Paris Diderot, CNRS - UMR 7057 Bâtiment Condorcet, 10 rue Alice Domon et Léonie Duquet 75205 Paris cedex 13, France, EU*
[2] *GRASP-Photopôle, Institut de Physique B5, Université de Liège - B-4000 Liège, Belgium, EU*
[3] *Matériaux et Phénomènes Quantiques, Université Paris Diderot, CNRS - UMR 7162 Bâtiment Condorcet, 10 rue Alice Domon et Léonie Duquet 75205 Paris cedex 13, France, EU*

received 24 January 2008; accepted in final form 26 March 2008
published online 7 May 2008

PACS 47.55.D- – Drops and bubbles
PACS 05.65.+b – Self-organized systems
PACS 05.45.-a – Nonlinear dynamics and chaos

Abstract – Several droplets, bouncing on a vertically vibrated liquid bath, can form various types of bound states, their interaction being due to the waves emitted by their bouncing. Though they associate droplets which are individually motionless, we show that these bound states are self-propelled when the droplets are of uneven size. The driving force is linked to the assymetry of the emitted surface waves. The direction of this ratchet-like displacement can be reversed, by varying the amplitude of forcing. This direction reversal occurs when the bouncing of one of the drops becomes sub-harmonic. As a generalization, a larger number of bouncing droplets form crystalline rafts which are also shown to drift or rotate when assymetrical.

Introduction. – The self-propulsion of particles moving in a spatially periodic, assymetrical potential has been widely studied recently. Several physical systems have been proposed, aimed at providing models for the motion of biomolecular motors in which the energy input is the Brownian motion [1,2]. In these model systems an assymetry is needed which can have various origins. i) It can come from the substrate: it was shown, for instance, that Leidenfrost drops bouncing on an assymetrically structured medium translate spontaneously [3]. ii) It can be introduced in the moving object as, *e.g.*, when it is formed of an assymetrical assembly of two different structures [4]. iii) Finally, in non-linear systems the breaking of symmetry can be spontaneous and due to a bifurcation [5]. In a recent work [6,7], we showed that the latter phenomenon was responsible for the spontaneous horizontal displacement of a liquid drop on a vertically vibrated bath of the same fluid. In general the drop bounces at the forcing frequency and is otherwise motionless as described in [8–10]. Near the Faraday instability threshold, the bouncing becomes sub-harmonic and the drop becomes the source of a localized Faraday wave packet. By interaction with its own wave, the drop becomes a self-propelled "walker" moving on the surface at constant velocity [7]. In the present letter we investigate, in the same type of experiment, the behaviour of self-assembled assymetrical bound states. Each element is here individually motionless: the motion comes from the assymetry of their assembly.

Experiment. – The experiments are performed on a liquid bath of thickness $h_0 = 3\,\mathrm{mm}$ submitted to a vertical oscillating acceleration $\gamma = \gamma_m \cos(2\pi f_0 t)$. In the following the control parameter of the system will be the non-dimensional amplitude of the forcing acceleration: $\Gamma = \gamma_m/g$. The liquid is silicon oil with viscosity $\mu_1 = 20 \times 10^{-3}\,\mathrm{Pa \cdot s}$, surface tension $\sigma = 0.0209\,\mathrm{N \cdot m^{-1}}$ and density $\rho = 0.965103\,\mathrm{kg \cdot m^{-3}}$. The forcing frequency $f_0 = 80\,\mathrm{Hz}$ is fixed. The drops are created by swiftly removing a pin dipped in the oscillating bath. The breaking of the liquid bridge between the pin and the bath can generate drops with diameters $0.1 < D < 1.5\,\mathrm{mm}$. When the forcing amplitude is large enough, typically when γ_m becomes larger than g, the drop lifts off at each period. The air film, which separates the drop from the substrate, is renewed at each period so that the bouncing can be sustained indefinitely [8,10]. The detail of their bouncing can be observed and recorded using a fast video camera (1000 images/s).

Bound states. – When two drops are present on the interface they "condense" into a stable bound state, a distance d_{bd}^0 separating them. The non-local interaction between drops is provided by the damped capillary waves

(a) E-mail: antonin.eddi@univ-paris-diderot.fr

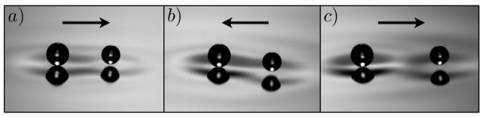

Fig. 1: Photographs of self-assembled bouncers forming self-propelled bound states. The two droplets have diameter of $D_1 = 0.73\,\text{mm}$ and $D_2 = 0.89\,\text{mm}$, respectively. Γ is the vertical acceleration normalized by g. In case a) ($\Gamma = 2.6 < \Gamma_1$), the two droplets are simple bouncers and the ratchet is pushed by the larger droplet. In case b) ($\Gamma_1 < \Gamma = 3.3 < \Gamma_2$), the smaller droplet has a period-doubled bouncing and has become the pusher. In case c) ($\Gamma_2 < \Gamma = 3.6$), the motion has reversed again as both drops have become period-doubled bouncers. See also the supplementary multimedia material `Ratchet_motion.mov`.

they emit. When a drop hits the bath, the collision forms a small crater in the surface. When the drop lifts up, the wave created by the shock evolves freely, the edge of the crater forming the crest of a circular wave propagating radially. In a bound state, each drop falls on a surface disturbed by the circular wave emitted during previous periods by its neighbour. With two drops of identical size, the system self-organizes in such a way that, during its collision with the bath, the horizontal impulse given to each drop is zero. This equilibrium can be obtained at a distance between drops $d_{bd}^0 = \lambda_0 - \epsilon$, where λ_0 is the wavelength of the surface waves at the forcing frequency [7], and ϵ is an offset due to finite duration of the collision. With more than two drops the condensation leads to the formation of stable rafts with a crystalline lattice of the same periodicity d_{bd}^0. With drops of identical size both the bound states and the clusters are motionless. When they are formed of drops of different sizes, they have a spontaneous drift motion.

We first focus on the association of two drops of diameter D_1 and D_2 (with $D_1 < D_2$). For low values of $\Gamma = \gamma_m/g$ the bound state they form is observed to translate, the large drop pushing the small one. This is the mode 1 shown in fig. 1a. In fig. 2, we have plotted the velocity of several bound states as a function of Γ; mode 1 being associated to negative velocities. The bound state's velocity is a function of both diameters of the drops. Relatively fast translation motions are observed as, *e.g.*, $V = 3\,\text{mm/s}$ for drops with $D_1 = 1\,\text{mm}$ and $D_2 = 1.12\,\text{mm}$.

When Γ is increased, the velocity of the pair becomes at first larger, then a reversal of the direction of motion is observed so that the small drop now pushes the large one (mode 2, fig. 1b). This transition, observed for all pairs of drops, occurs at a value Γ_1 which is a function of the diameter D_1 of the smaller drop (fig. 2).

When the two droplets have diameters in between $D = 0.5\,\text{mm}$ and $0.9\,\text{mm}$, a more complex sequence of behaviors is observed, characterized by two new thresholds, Γ_2 and Γ_3. Over the value Γ_2 there is a second reversal in the direction of motion (transition to mode 3, fig. 1c). In this case the large drop pushes again the small one. One can

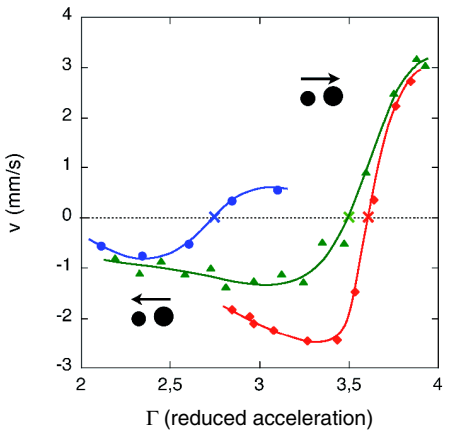

Fig. 2: The velocity of 3 couples of droplets as a function of Γ. The dots correspond to a couple of bound drops with $D_1 = 0.87\,\text{mm}$ and $D_2 = 0.96\,\text{mm}$, the triangles to $D_1 = 1\,\text{mm}$ and $D_2 = 1.12\,\text{mm}$ and the rhombs to $D_1 = 1.03\,\text{mm}$ and $D_2 = 1.23\,\text{mm}$. The continuous curves are simple interpolations. The crosses correspond to the reversal threshold Γ_1.

note that, after this transition, the distance d_{bd} between the two drops becomes larger. Finally, the third threshold is reached at $\Gamma = \Gamma_3$, when the drops begin orbiting around each other.

Before giving an interpretation of these effects we must first characterize the bouncing of a single droplet. In our fixed experimental conditions (*i.e.* viscosity and forcing frequency being fixed) the types of observed bouncing are a function of the droplet diameter D and of the reduced acceleration Γ [7]. Figure 3a is a phase diagram which summarizes the behaviors observed for a single droplet. In the region B of this diagram, the drop bounces at the forcing frequency. When Γ is increased the successive jumps become alternatively large and small, so that the period of the motion doubles (in region PDB of fig. 3a). The transition to this period doubling strongly depends on the drop's size. Larger drops do not lift away so easily because their deformation increases the size of their zone of near contact. Both the simple bouncing and the period doubling occur for larger values of Γ. This is related to the deformation of the drop during its collision with the substrate. This deformation depends on the drop's size D since it is characterized by the Weber number: $We = (\rho V^2 D)/(2\sigma)$, the ratio of the kinetic energy of the drop to its surface energy. For drops of intermediate size, $0.5 < D < 0.9\,\text{mm}$ the period doubling can become complete so that the drop touches the surface once in two periods. Correlatively, it becomes a "walker" (in the region W in fig. 3a) moving at a constant velocity in the horizontal plane. The walkers were already investigated elsewhere [7].

We can now return to pairs of interacting drops. They form stable bound states at a well-determined distance

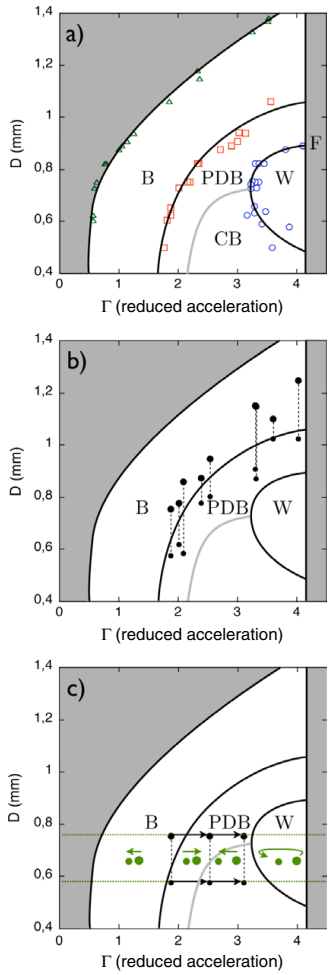

Fig. 3: a) Phase diagrams of the droplet's behaviour as a function of their diameter D and of the reduced acceleration Γ. The viscosity of the silicon oil used is $\mu = 20 \times 10^{-3}$ Pa·s and the forcing frequency $f_0 = 80$ Hz. The various zones correspond to the different behaviors of a single droplet: in B it bounces at the forcing frequency, in PDB the bouncing has undergone a period doubling, in CB the bouncing has become chaotic through a period-doubling cascade. In region W the droplets become walkers with a spontaneous horizontal displacement at a constant velocity. Region F is the Faraday instability zone. Panel b) shows, on the same phase diagram, the transition value Γ_1 for nine bound states. Two droplets forming a bound state are linked by a vertical dashed line. Their diameters are given along the ordinate axis. The abscissa at which they are represented is the value of Γ_1 for each bound state. Panel c) shows, with the same principle, the three thresholds observed for one single pair of droplets with diameters $D_1 = 0.57$ mm and $D_2 = 0.75$ mm.

d^0_{bd} from each other. Their non-local interaction is due to the surface wave they emit by their bouncing. The observed drift motion of uneven drops signifies that the forces exerted by the droplets on one another are not symmetrical: action appears to be different from reaction. In order to understand this drift we can first consider the motion of each droplet, then we will return to a global description of the system.

Local behavior. – The fast camera at a large magnification (see fig. 1) reveals images of the drops forming the ratchet in the three different regimes. In mode 1 both drops oscillate at the same frequency. However, the drops being unequal, neither the lift-off, nor the collision after the free flight, are simultaneous. At each period, the small drop hits the interface later than the large one. Being close to it, the small drop falls on the outer slope of the ridge of the crater formed by the larger drop. It thus receives a forward kick. Correlatively, the crater of the large drop becomes assymetrical by the collision of the small drop. As a result, at lift-off, the large drop also moves forward. Both drops thus receive a kick in the same direction and propagate together.

Where does the reversal in the motion direction come from? Just over the transition the small drop has undergone period doubling so that its successive collisions become uneven. One out of two shocks is weak and uneffective. During the other collision, the small drop hits the interface before the large one and repells it (see fig. 1b). This is confirmed by direct observation with a fast video camera. In fig. 3b, we have used the previous phase diagram, fig. 3a, of the individual droplets to represent the threshold values of Γ_2 for pairs of droplets. Γ_2 is systematically slightly larger than the value of Γ for which the smaller drop has entered the region of period doubling.

Global considerations. – The two drops receive energy from the vibration generator but, as the imposed vibration is vertical, it does not directly provide a driving force. The motion is due to the initial asymmetry resulting from the different size of the droplets. This is natural: considered as a whole the two drops do not form an isolated system because they emit waves which propagate away. The waves are carrying away a flux of momentum which can be estimated. Observing the waves far from the bound state, one can assume that they are locally travelling plane sinusoidal waves with surface elevation $\zeta = a\cos(\omega t - kx)$, a being the wave's amplitude, ω its pulsation and k its wave number. Such waves possess an average momentum $1/2(\rho\omega a^2)$ per unit surface, with ρ the fluid density [11,12].

This action reaction effect between the droplets and the waves explains the ratchet motion. However, it should be recalled that there is no exact momentum conservation in our system, because of dissipation. Consequently, it is not possible to make this argument more quantitative. Besides dissipation is needed. The emitted waves are

damped by viscosity before reaching the boundaries so that no reflected wave returns to the ratchet. If dissipation vanished, waves would reflect on the borders and accumulate on the whole bath. The droplets would then have a chaotic motion on those waves. In a finite cell the breaking of time symmetry by dissipation thus appears necessary to propulsion. Note that in an infinite system dissipation should not be needed, causality being sufficient to give a direction to the wave propagation.

We can now consider the flux of momentum due to each of the droplets. At low forcing acceleration, observation with a fast camera shows that both drops oscillate at the forcing frequency f_0. Because of the difference of their masses the waves emitted by the two drops have different amplitudes, the larger the mass, the larger the amplitude. The reaction, resulting from the emission of momentum by the waves, pushes the bound state, the large droplet being behind.

With the increase of Γ, the bouncing of the smaller drop undergoes a period-doubling transition while the larger drop continues bouncing at the forcing frequency.

After period doubling, the small drop begins to emit surface waves of frequency $f_0/2$. This is the Faraday frequency, which is the least damped by the system, because of the proximity of the Faraday instability threshold. Independent measurements enable us to measure the amplitude of the waves. In the typical situation shown in fig. 4, the amplitude of the wave emitted by the small droplet is approximately five times greater than the amplitude of the wave emitted by the larger drop. Thus, the assymetry of the wave emission is reversed and the flux of momentum carried away by the emitted wave is larger on the side of the small drop. The resulting reaction pushes the bound state, the small drop being behind. Figure 3b confirms that Γ_1 corresponds to the value for the period doubling of the smaller drop.

When the two droplets have diameters in the narrow range between $D = 0.5\,\mathrm{mm}$ and $0.9\,\mathrm{mm}$, at a value Γ_2 the distance d_{bd} between the two droplets increases and correlatively the direction of motion changes again. The plot in fig. 3c confirms that Γ_2 corresponds to the value for the period doubling of the larger drop. In this case, both droplets emit waves at the Faraday frequency. The distance d_{bd} changes accordingly to reach $d_{bd}^1 = \lambda_F - \epsilon$, where λ_F is the wavelength of the surface waves at the Faraday frequency (see fig. 1c). Finally, the third threshold Γ_3 is reached where the drops begin orbiting. This corresponds to the situation when one of the drops achieves a complete period doubling and enters the W region of the phase diagram (see fig. 3c).

Drifting and rotating aggregates. – The existence of aggregates has been previously investigated [7,13,14]. However, we show here a new behaviour relying on the same physical effect as the spontaneous motion of a two-droplets bound state. When the drops forming the aggregate are of uneven size, a slow spontaneous displacement of the whole cluster is observed. The nature of the motion depends on the symmetry of the system. The global shape of the small agregates is dominated by the trend to form a triangular lattice. It is combined with a trend for an aggregate formed of a given number of particle to minimize its outer perimeter.

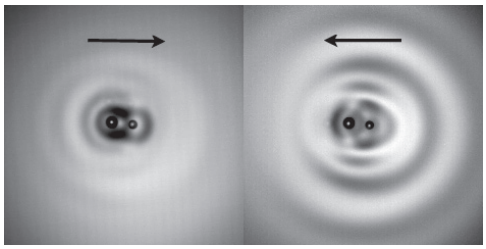

Fig. 4: Two top views of the same ratchet. Left: below Γ_1 the larger drop emits a wave of larger amplitude. Thus the bound state propagates to the right. Right: over Γ_1, the smaller droplet has undergone a period doubling and emits a Faraday wave of larger amplitude: the bound state propagates to the left.

The simplest possibility is the case of three drops. This type of bound state, with either a small drop and two large ones or the reverse situation, present the same first reversal. If we consider larger aggregates, in first approximation, each drop located at the periphery emits a wave, which can only propagate in the free surface. The reaction to the emission of the wave by each droplet placed at the periphery will be perpendicular to the local facet or if it is located at a vertex, along the bisector of the wedge under which it "sees" the free surface. If the direction of emission passes through the center of mass of the aggregate, the reaction will generate a drift, if not it will create an angular momentum and the cluster will rotate. Figure 5 shows two rotating aggregates. For drops which have diameter D in between $D = 0.5$ and $0.9\,\mathrm{mm}$, they are able to undergo a transition to a subharmonic bouncing. At the transition, the drops take various phases relatively to the forcing frequency. The mutual distance between two drops depends on whether they bounce in phase or with opposite phases. The aggregate thus becomes disordered before reorganizing in a more complex crystalline structure with two typical lengths that will be discussed elsewhere.

Conclusion. – In our experiment each bouncing drop is a mobile wave source. If isolated, it is either motionless or can move at a constant velocity by breaking of symmetry. When several wave emitters are present simultaneously on the surface they interact and form bound states and organized clusters. Here we have shown that these systems, when formed of uneven droplets, are spontaneously mobile by reaction to the waves they emit outwards. Such a mean of propulsion by reaction to the emission of surface waves was one of the mechanisms

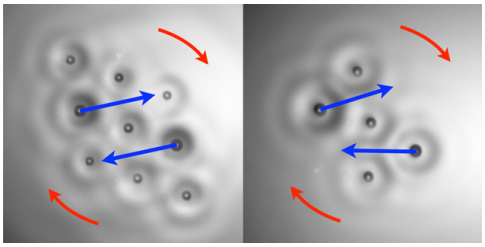

Fig. 5: (Top view) Two crystalline aggregates made of simple bouncers. In order to make the cluster asymmetric, all droplets are identical except two which have a larger diameter. In the two cases, the cluster rotates and the rotating period is around 90 s. The straight arrows represent the propulsion in reaction to the emission of surface waves.

proposed for the motion of water striders [15], even if more recent works [12] have shown that in this case the emission of vortices is the dominant effect. In our experiment, as the reaction depends on the frequency and the amplitude of the waves, bound states of uneven-size droplets present reversals in their motions when one of the drops undergoes subharmonic period doubling. For aggregates of uneven-size droplets, the asymmetry leads to spontaneous translation or rotation.

* * *

We are grateful to S. Protière, S. Bohn, A. Boudaoud, M. Rossi, N. Vandewalle and S. Dorbolo for stimulating discussions. Exchanges between laboratories have been financially helped by the COST action P21 and by the ANR 06-BLAN-0297-03.

REFERENCES

[1] Julicher F., Adjari A. and Prost J., *Rev. Mod. Phys.*, **69** (1997) 1269.
[2] Julicher F. and Prost J., *Phys. Rev. Lett.*, **75** (1995) 2618.
[3] Linke H. *et al.*, *Phys. Rev. Lett.*, **96** (2006) 154502.
[4] Kudrolli A., Lumay G., Volfson D. and Tsimring L. S., *Phys. Rev. Lett.*, **100** (2007) 058001.
[5] Badoual M., Julicher F. and Prost J., *Proc. Natl. Acad. Sci. U.S.A.*, **99** (2002) 6696.
[6] Couder Y., Protiere S., Fort E. and Boudaoud A., *Nature*, **437** (2005) 208.
[7] Protiere S., Boudaoud A. and Couder Y., *J. Fluid Mech.*, **554** (2006) 85.
[8] Terwagne D., Vandewalle N. and Dorbolo S., *Phys. Rev. E*, **76** (2007) 056311.
[9] Gilet T., Vandewalle N. and Dorbolo S., *Phys. Rev. E*, **76** (2007) 035302(R).
[10] Couder Y., Fort E., Gautier C. H. and Boudaoud A., *Phys. Rev. Lett.*, **94** (2005) 177801.
[11] Lighthill J., *Waves In Fluids* (Cambridge University Press, Cambridge) 1978, pp. 279–280.
[12] Hu D. L., Chan B. and Bush J. W. M., *Nature*, **424** (2003) 663.
[13] Protiere S., Couder Y., Fort E. and Boudaoud A., *J. Phys.: Condens. Matter*, **17** (2005) S3529.
[14] Lieber S. I., Hendershott M. C., Pattanaporkratana A. and Maclennan J. E., *Phys. Rev. E*, **75** (2007) 056308.
[15] Sun S. M. and Keller J. B., *Phys. Fluids*, **13** (2001) 2146.

Nonlinearity **24** (2011) R51–R66 doi:10.1088/0951-7715/24/8/R01

INVITED ARTICLE

Tibetan singing bowls

Denis Terwagne[1] **and John W M Bush**[2]

[1] GRASP, Département de Physique, Université de Liège, B-4000 Liège, Belgium
[2] Department of Mathematics, Massachusetts Institute of Technology, 02139 Cambridge, MA, USA

Received 8 April 2010
Published 1 July 2011
Online at stacks.iop.org/Non/24/R51

Recommended by D Lohse

Abstract
We present the results of an experimental investigation of the acoustics and fluid dynamics of Tibetan singing bowls. Their acoustic behaviour is rationalized in terms of the related dynamics of standing bells and wine glasses. Striking or rubbing a fluid-filled bowl excites wall vibrations, and concomitant waves at the fluid surface. Acoustic excitation of the bowl's natural vibrational modes allows for a controlled study in which the evolution of the surface waves with increasing forcing amplitude is detailed. Particular attention is given to rationalizing the observed criteria for the onset of edge-induced Faraday waves and droplet generation via surface fracture. Our study indicates that drops may be levitated on the fluid surface, induced to bounce on or skip across the vibrating fluid surface.

Mathematics Subject Classification: 74-05, 76-05

S Online supplementary data available from stacks.iop.org/Non/24/R51/mmedia

(Some figures in this article are in colour only in the electronic version)

1. Introduction

Tibetan singing bowls are thought to have originated from Himalayan fire cults of the 5th century BC and have since been used in various religious ceremonies, including shamanic journeying and meditation. The Tibetan singing bowl (see figure 1 and the supplementary data (movie 1) available at stacks.iop.org/Non/24/R51/mmedia) is a type of standing bell played by striking or rubbing its rim with a wooden or leather-wrapped mallet. This excitation causes the sides and rim of the bowl to vibrate and produces a rich sound. Tibetan bowls are hand made and their precise composition is unknown, but generally they are made of a bronze alloy that can include copper, tin, zinc, iron, silver, gold and nickel. When the bowl is filled with water, excitation can cause ripples on the water surface. More vigorous forcing generates progressively more complex surface wave patterns and ultimately the creation of droplets via

Figure 1. Our Tibetan singing bowls: (*a*) Tibet 1, (*b*) Tibet 2, (*c*) Tibet 3 and (*d*) Tibet 4.

wave breaking. We here quantify this evolution, and demonstrate the means by which the Tibetan singing bowl can levitate droplets.

Related phenomena are known to appear in other vessels, including the Chinese singing bowl, on which vibrations are generated by rubbing the vessel's handles with moistened hands. The more familiar vibration of a wine glass is produced by rubbing its rim with a moist finger. The dependence of the glass's vibration frequency on its material properties, geometry and characteristics of the contained fluid was elucidated by French [1] and subsequent investigators [2–5]. The coupling between two singing wine glasses has been investigated by Arane *et al* [6]. Apfel [7] demonstrated experimentally that wine glass vibration generates capillary waves near the walls of a fluid-filled glass. Moreover, he made the connection between these waves and the acoustic whispering gallery modes elucidated by Rayleigh [8]. By studying the deformation and the sound spectrum produced by a single wine glass, Rossing [9] elucidated the mechanism of the glass harmonica [10], an instrument designed by Benjamin Franklin. Joubert *et al* [11] provided a theoretical rationale for observations of standing waves in a singing wine glass. The Tibetan singing bowl has to date received relatively little attention. Inacio *et al* examined experimentally the acoustic response of bowls excited by impact and rubbing [12], and proposed a dynamical formulation of the bowl and presented some numerical simulations [13]. The hydrodynamics of a fluid-filled Tibetan bowl will be the focus of our investigation.

In 1831, Faraday [14] demonstrated that when a horizontal fluid layer is vibrated vertically, its interface remains flat until a critical acceleration is exceeded. Above this threshold, a field of waves appears at the interface, parametric standing waves oscillating with half the forcing frequency [15–20]. The form of such Faraday waves depends on the container geometry; however, boundary effects can be minimized by using a large container. The Faraday waves have a wavelength prescribed by the relative importance of surface tension and gravity, being capillary and gravity waves in the short and long wavelength limits, respectively. As the forcing acceleration is increased, progressively more complex wave patterns arise, and the interfacial dynamics become chaotic [19–21]. Ultimately, large amplitude forcing leads to surface fracture and the ejection of droplets from the fluid bath. A recent study on the breaking of Faraday waves in a vertically shaken bath has been performed in both the capillary and gravity wave limits by Puthenveettil and Hopfinger [22]. Goodridge *et al* [23] studied the drop ejection threshold of capillary waves in a glycerine–water solution for frequencies up to 100 Hz.

Faraday [14] reported that such parametric waves can also be emitted by a vertical plate plunged into a liquid bath and shaken horizontally: along both sides of the plate, waves aligned perpendicular to the plate oscillate at half the forcing frequency. These so-called cross waves, or edge-induced Faraday waves, are typically produced by a wave

maker, and have received considerable attention [24–28]. Hsieh [29] examined theoretically wave generation in a vibrating circular elastic vessel, specifically the axisymmetric capillary waves and circumferential crispations that appear in an inviscid fluid subject to radial wall displacement. These studies have demonstrated that the excitation of the cross waves is due to a parametric resonance. The complexity of this problem lies in the nonlinear interactions between the motion of the oscillating rim and the resulting wave field.

Droplets ejected on the liquid surface by breaking Faraday waves may bounce, skid and roll before coalescing. A number of recent studies have examined droplets bouncing on a vertically vibrating liquid bath below the Faraday threshold [30–32]. The air film between the drop and the liquid surface is squeezed and regenerated at each successive bounce, its sustenance precluding coalescence and enabling droplet levitation. A similar effect arises on a soap film, a system more readily characterized theoretically [35]. The bouncing periodicity depends on the size of the drop and the vertical forcing acceleration of the bath [33, 34]. Couder *et al* [30] have shown that, through the waves emitted at previous bounces, some droplets can walk horizontally across the liquid surface. Several factors are needed to sustain a so-called 'walker' [36]. First, the drop must bounce at half the forcing frequency, so that it resonates with the resulting Faraday wave field. Second, the bath must be close to the Faraday instability threshold so that Faraday waves of large amplitude and spatial extent can be excited by the drop impacts. The droplet bounces on the slope of the wave emitted at the previous bounce and so receives an impulsive force in a specific direction, along which it walks with a constant speed. Such walkers have both wave and particle components, and have been shown to exhibit quantum-like dynamical behaviour previously thought to be peculiar to the microscopic realm [37–40]. Might such modern physics arise in our ancient bowls?

The paper is divided into two main parts. In section 2, we examine the acoustics of the Tibetan singing bowls. We begin in section 2.1 by reviewing the related dynamics and theoretical description of the wine glass [1]. In section 2.2, our bowls are presented and their deformation spectra analysed. Then, by adapting the theoretical description of the vibrating wine glass, we infer the Young's modulus of the alloy comprising our bowls. In section 3, we examine the dynamics of flows generated within liquid-filled vibrating bowls. A review of Faraday waves and droplet ejection on a vertically shaken bath is presented in section 3.1. In section 3.2, our experimental technique is detailed. In section 3.3, we analyse the surface waves generated on the liquid bath, and their relation to Faraday waves. In section 3.4, we examine the limit of large amplitude forcing, in which droplets are ejected by breaking Faraday waves. Comparisons are made with experiments performed on a vertically shaken liquid bath. Droplet levitation is considered in section 3.5, where particular attention is given to developing criteria for droplet bouncing and exploring the possibility of walking droplets. A summary of our results is presented in section 4.

2. Acoustics

2.1. Background

Both the wine glass and the Tibetan bowl can be excited by either tapping or rubbing its rim. We denote by (n, m) the vibrational mode with n complete nodal meridians and m nodal parallels. Tapping excites a number of vibrational modes [10], while rubbing excites primarily the (2,0) fundamental mode (see figure 2(*b*)). Entirely flexural motion implies radial and tangential displacements proportional to $n \sin n\theta$ and $\cos n\theta$, respectively, θ being the azimuthal coordinate [41]. For the (2,0) mode the maximum tangential motion is necessarily half the maximum normal motion.

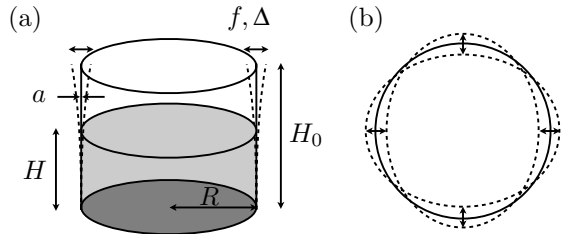

Figure 2. (*a*) Schematic illustration of a vibrating vessel filled with liquid. Relevant parameters are the height H_0 and the radius R of the vessel, the thickness of the rim a, the liquid level H, the frequency f and the amplitude Δ of the oscillating rim. (*b*) Top view of a vibrating vessel in its fundamental mode (2,0), characterized by its 4 nodes and 4 antinodes.

A leather mallet can excite bowl vibrations via a stick-slip process, as does a finger moving on a wine glass. The moving mallet forces the rim to follow the mallet during the stick phase; during the slip phase, the bowl rim relaxes to its equilibrium position. This rubbing results in a sound composed of a fundamental frequency plus a number of harmonics. While the mallet is in contact with the bowl, one of the nodes follows the point of contact [11], imparting angular momentum to the bound liquid.

To simplify the acoustic analysis, one can approximate the glass or bowl by a cylindrical shell with a rigid base and an open top (figure 2(*a*)). The system can then be described in terms of 7 physical variables, the radius R, height H_0, thickness a, Young's modulus Y and density ρ_s of the cylindrical shell, and the frequency f and amplitude Δ of its oscillating rim. The system can thus be described in terms of 4 independent dimensionless groups, which we take to be R/H, Δ/a, Δ/R and a Cauchy number $Ca = \rho_s f^2 \Delta^2 / Y$ that indicates the relative magnitudes of the inertial and the elastic forces experienced by the vibrating rim.

The sound is emitted by bending waves that deform the rim transversely as they propagate. The speed V_b of bending waves on a two-dimensional plate of thickness a is given by [42]

$$V_b = \left(\frac{\pi V_L f a}{\sqrt{3}} \right)^{1/2}, \tag{1}$$

where V_L is the longitudinal wave speed in the solid (approximately $5200\,\mathrm{m\,s^{-1}}$ in glass). In order for the bending wave to traverse the perimeter in an integer multiple of the period, we require

$$\frac{1}{f} \propto \frac{2\pi R}{V_b}. \tag{2}$$

Thus, since $V_b \sim \sqrt{fa}$, we have $f \propto a/R^2$: the frequency increases with rim thickness, but decreases with radius.

A more complete theoretical analysis of the wine glass acoustics [1] can be applied to our Tibetan bowls. An ideal cylinder fixed at the bottom is considered (figure 2(*a*)), its wall vibrating with largest amplitude at its free edge or rim. The rim's kinetic energy and elastic energy of bending in the mode (2,0) are calculated by assuming that the radial position is proportional to $\cos 2\theta$, with θ being the azimuthal coordinate. By considering conservation of total energy (kinetic plus elastic bending energy), an expression for the frequency of this mode can be deduced:

$$f_0 = \frac{1}{2\pi} \left(\frac{3Y}{5\rho_s} \right)^{1/2} \frac{a}{R^2} \left[1 + \frac{4}{3} \left(\frac{R}{H_0} \right)^4 \right]^{1/2}. \tag{3}$$

Table 1. Physical properties of the four Tibetan bowls used in our study.

Bowl name	Tibet 1	Tibet 2	Tibet 3	Tibet 4
Symbol	•	○	⊠	◇
$f_{(2,0)}$ (empty) (Hz)	236	187	347	428
Radius R (cm)	7.5	8.9	6	5.9
Thickness a (cm)	0.34	0.38	0.31	0.37
Mass (kg)	0.690	0.814	0.306	0.312
Volume (cm^3)	76	97	35	33
Density ($kg\,m^{-3}$)	9079	8366	8754	9372

When the bowl is partially filled with liquid to a depth H (figure 2(a)), the frequency decreases. French [1] captured this effect by considering the kinetic energy of the liquid near the rim, and so deduced the frequency of the fundamental mode:

$$\left(\frac{f_0}{f_H}\right)^2 \sim 1 + \frac{\alpha}{5}\frac{\rho_l R}{\rho_s a}\left(\frac{H}{H_0}\right)^4, \tag{4}$$

where ρ_l is the liquid density and $\alpha \sim 1.25$ is a constant indicating the coupling efficiency between the rim and fluid displacements. Similarly, frequencies of higher modes can be calculated by considering a radial position proportional to $\cos n\theta$ and with m nodal parallels [1]:

$$f_{(n,m)} = \frac{1}{12\pi}\left(\frac{3Y}{\rho_s}\right)^{1/2}\frac{a}{R^2}\left[\frac{(n^2-1)^2 + (mR/H_0)^4}{1+1/n^2}\right]^{1/2}. \tag{5}$$

2.2. Tibetan bowls

Four different antique bowls of different sizes have been studied (figure 1). They are referred to as Tibet 1, 2, 3 and 4 and their physical characteristics are reported in table 1.

When a bowl is struck or rubbed, the sound emitted by the resulting bowl vibrations is recorded with a microphone and a fast Fourier transform performed on the signal. Different peaks clearly appear in the frequency spectrum, corresponding to the bowl's different vibrational modes. Figure 3(a) indicates the frequency spectrum generated by striking the empty bowl Tibet 4. When the bowl is rubbed with a leather-wrapped mallet, the lowest mode is excited along with its harmonics, an effect known as a mode 'lock in' [43]. The frequency spectrum of Tibet 4 when rubbed by a leather mallet is presented in figure 3(b). Due to the bowl asymmetry, two peaks separated by several Hz arise and a beating mode is heard. This split is highlighted in a magnification of the first peak $f_{(2,0)}$ in the inset of the figure. The deformation shapes are the same with both frequencies but there is horizontal angular shift observed to be $\pi/4$ between them for the fundamental modes $(2, 0)$ and $\pi/2n$ for other $(n, 0)$ modes. Finally, we note that, owing to the relative squatness of the bowls and the associated high energetic penalty of modes with $m \neq 0$, only modes $(n, 0)$ were excited; henceforth, such modes are denoted simply by n.

We can also find a relation between the different mode frequencies. Since the speed of the bending wave is proportional to the square root of the frequency, $v \propto \sqrt{f}$ and since $\lambda = v/f$, we expect $\lambda \propto 1/\sqrt{fa}$. For the mode n, we thus have $2\pi R = n\lambda_n$. The frequency of this mode n should thus be proportional to

$$f \propto \frac{n^2 a}{R^2}. \tag{6}$$

In figure 4(a), resonant frequencies of the 4 bowls are plotted as a function of their corresponding mode n and a power 2 curve is fit onto each curve. In figure 4(b), we collapse

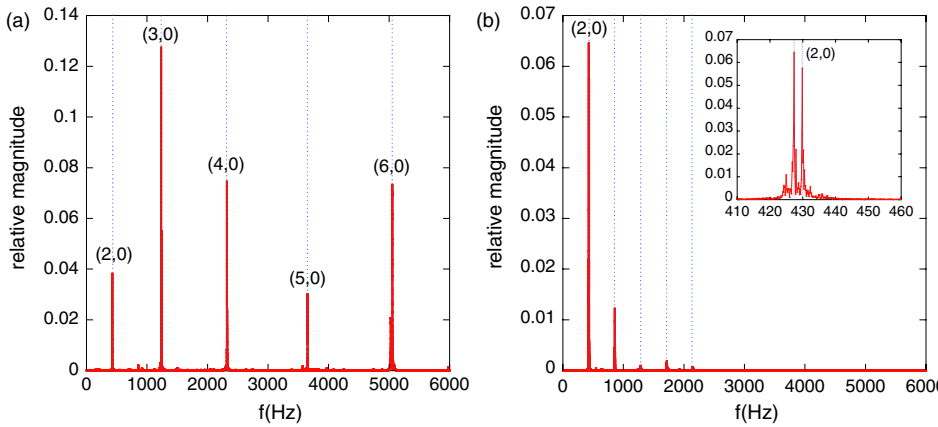

Figure 3. (*a*) Frequencies excited in the bowl Tibet 4 when struck with a wooden mallet. The different peaks correspond to the natural resonant frequencies of the bowl, and the associated deformation modes (n, m) are indicated. (*b*) Excited frequencies of the bowl Tibet 4 when rubbed with a leather mallet. The first peak corresponds to the deformation mode (2,0) and subsequent peaks to the harmonics induced by mode lock-in. In the inset, a magnification of the first peak provides evidence of its splitting due to the asymmetry of the bowl.

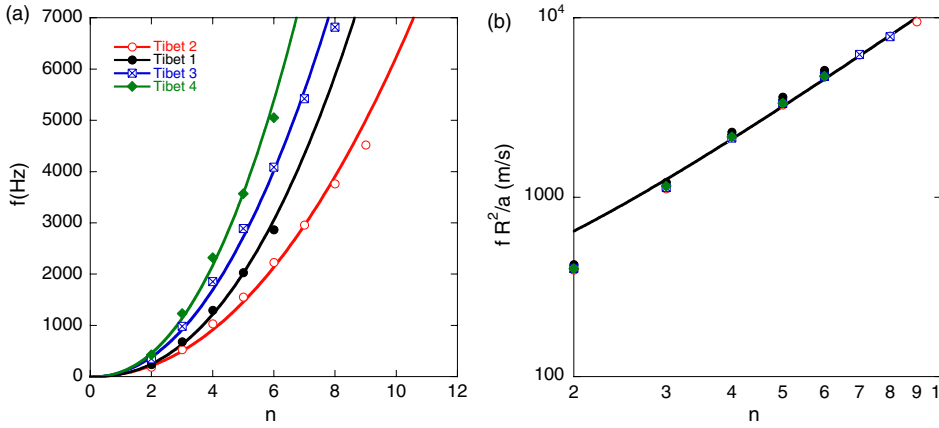

Figure 4. (*a*) Measurements of the resonant frequencies of the different deformation modes n for the 4 different Tibetan bowls. (*b*) Characteristic speed $f R^2/a$ as a function of deformation mode n for the 4 different bowls. Data are fit by a power 2 curve indicating that $f_n \propto n^2 a/R^2$, consistent with equation (6).

all these curves onto a line by plotting the characteristic speed $f R^2/a$ as a function of the mode n, thus validating the proposed scaling (6).

It is readily observed that the resonant frequencies decrease when liquid is poured into a vessel. In the inset in figure 5(*a*), we report the measurements of the fundamental frequency of the bowl Tibet 1 as a function of the dimensionless liquid height H/H_0. In figure 5(*a*), we report $(f_0/f_H)^2$ as a function of $(H/H_0)^4$. According to (4), the slope of this curve gives the ratio $\frac{\alpha}{5}\frac{\rho_l R}{\rho_s a}$. In figure 5(*b*), we present the dependence of $(1 + 1/n^2)(R^2/a)^2 f^2$ on $(n^2 - 1)^2$ for the deformation modes $n = 2$ through 6 of the bowls Tibet 1, 2, 3 and 4. According to (5),

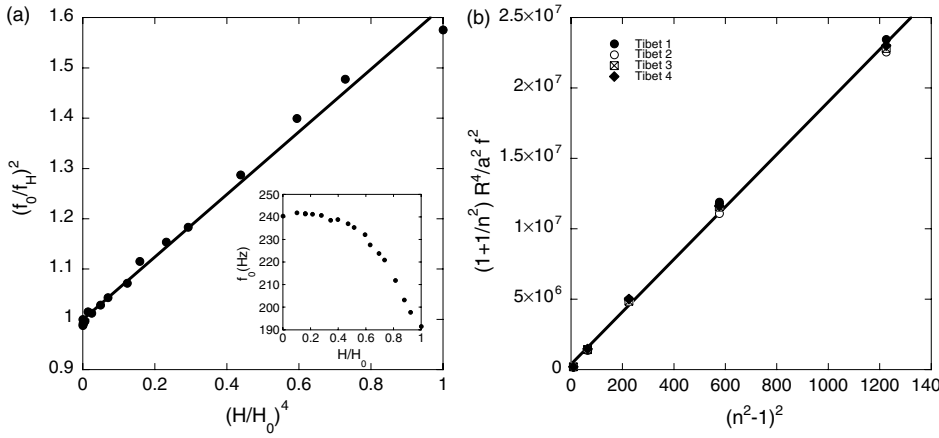

Figure 5. (*a*) The fundamental frequency of Tibet 1's mode (2,0) as a function of the water height H/H_0. According to equation (4), the slope is equal to $\frac{\alpha}{5}\frac{\rho_l R}{\rho_s a}$. (*b*) The dependence of the resonant frequencies f of all the bowls on the deformation mode n may be used to infer the ratio Y/ρ_s. According to (5), the slope of the line shown is $\frac{1}{48\pi^2}\frac{Y}{\rho_s}$, from which we infer $Y/\rho_s = 8.65 \times 10^6\,\mathrm{Pa\,m^3\,kg^{-1}}$.

the slope should be equal to $\frac{1}{48\pi^2}\frac{Y}{\rho_s}$. For each value of the abscissa there are 4 measurements corresponding to the 4 Tibetan bowls. Data points from the different Tibetan bowls overlie each other, especially at low n, indicating that all bowls have the same value of ratio Y/ρ_s, and so are likely made of the same material. A linear fit gives $Y/\rho_s = 8.65 \times 10^6\,\mathrm{Pa\,m^3\,kg^{-1}}$.

We can simply estimate the density for each Tibetan bowl by measuring its mass and volume. Masses are measured by a weight scale with an error of 2 g while bowl volumes are deduced by fluid displacement during submersion. The error made on the volume with this method is estimated to be no more than 5%. All such density measurements are reported in table 1. Taking the mean value of the densities, equal to $8893\,\mathrm{kg\,m^{-3}}$, we calculate a Young modulus $Y = 77 \pm 6\%$ GPa. This value is in the Young's modulus range of glasses and lower than typical brass, copper or bronze alloys for which $Y > 100$ GPa.

3. Fluid dynamics

3.1. Faraday waves

Consider an inviscid fluid of density ρ and surface tension σ in a horizontal layer of uniform depth h in the presence of a gravitational acceleration g. The layer is oscillated vertically in a sinusoidal fashion at a forcing frequency $f_0 = \omega_0/2\pi$, amplitude Δ and acceleration $\Gamma g = \Delta\omega^2$. Above a critical forcing acceleration, standing Faraday waves appear on the surface. The associated surface deformation $a(x, y, t)$ can be expressed in terms of the container's eigenmodes $S_m(x, y)$ as

$$a(x, y, t) = \sum_m a_m(t) S_m(x, y), \tag{7}$$

with $a_m(t)$ being the oscillating amplitude of the eigenmode m. Benjamin and Ursell [16] demonstrate that the coefficients $a_m(t)$ satisfy

$$\ddot{a}_m + \omega_m^2(1 - 2\gamma\cos\omega_0 t)a_m = 0, \tag{8}$$

where

$$\omega_m^2 = \left(g k_m + \frac{\sigma}{\rho} k_m^3 \right) \tanh\left(k_m h\right) \tag{9}$$

represents the classic gravity-capillary wave dispersion relation,

$$\gamma = \frac{\Gamma}{2(1 + Bo^{-1})} \tag{10}$$

is the dimensionless forcing acceleration, and $Bo = \frac{\rho g}{\sigma k^2}$ is the Bond number. $k_m = 2\pi/\lambda_m$ is the wave number of the mode m, and λ_m is the corresponding wavelength.

In the absence of forcing, $\Gamma = 0$, (8) describes a simple harmonic oscillation with frequency prescribed by (9) corresponding to the free surface vibrations of the liquid. When $\Gamma > 0$, (8) describes a parametric oscillator as the forcing term depends on time. The resulting Faraday waves can be either capillary or gravity waves according to the magnitude of Bo; specifically, the former and latter arise in the respective limits $Bo \ll 1$ and $Bo \gg 1$. Equation (8) is known as the Mathieu equation and cannot be solved analytically since one of the terms is time dependent. However, as the forcing is periodic, Floquet theory can be applied to show that an inviscid fluid layer is always unstable to Faraday waves with a frequency ω_F that is half the forcing frequency $\omega_0 = 2\omega_F$ [16]. In the deep water ($kh \gg 1$), capillary wave ($Bo \ll 1$) limit, we can infer from (9) a Faraday wavelength:

$$\lambda_F = (2\pi)^{1/3} (\sigma/\rho)^{1/3} (f_0/2)^{-2/3}. \tag{11}$$

To incorporate the influence of the fluid viscosity, one can add to (8) a phenomenological dissipation term proportional to the velocity [18]:

$$\ddot{a}_m + 2\beta \dot{a}_m + \omega_m^2 (1 - 2\gamma \cos \omega_0 t) a_m = 0, \tag{12}$$

where β is the dissipation rate. This dissipation term leads to an acceleration threshold for the Faraday instability. Assuming capillary waves in an unbounded and infinite depth liquid, the critical acceleration needed to induce parametric instability is given by

$$\Gamma_F \propto \frac{1}{g} (\rho/\sigma)^{1/3} \nu \omega_0^{5/3}, \tag{13}$$

where ν is the kinematic viscosity of the fluid [19, 44].

As the forcing amplitude is further increased, the Faraday wave amplitude increases progressively until the waves become chaotic. Ultimately, the waves break and droplets are ejected from the surface. Since drops will be ejected by the breaking of Faraday waves, we expect their diameter to scale as

$$d_m \sim \lambda_F \sim (\sigma/\rho)^{1/3} f_0^{-2/3} \tag{14}$$

in the capillary wave limit. Droplet ejection arises when the destabilizing inertial driving force $m\Gamma g$ (with $m \sim \rho \lambda_F^3$) exceeds the stabilizing surface tension force $\pi \lambda_F \sigma$. This implies, via (14), a threshold acceleration that scales as

$$\Gamma_d \sim 1/g (\sigma/\rho)^{1/3} f_0^{4/3}. \tag{15}$$

The range of validity of these scalings will be investigated in our experimental study.

3.2. Experimental technique

The experimental setup used for studying the surface waves generated within the Tibetan bowls is presented in figure 6. A loudspeaker is set in front of the bowl, its signal received from

Figure 6. Experimental setup. The bowl deformation is excited by a loudspeaker emitting sound at a frequency corresponding to a particular vibrational mode of the bowl. The deformation of the bowl is measured by an accelerometer glued to the bowl's outer wall at the height of the liquid surface.

a signal function generator then amplified. When the applied signal frequency is close to one of the bowl's resonant frequencies, it oscillates in the corresponding deformation mode. Conveniently, with this method, we can select a single deformation mode. Recall that by striking or rubbing the bowls, we excited several modes (figure 3): moreover, rubbing induced a rotational motion that followed the mallet. We can now examine the vibration-induced flows in a controlled fashion.

In order to extend the range of natural frequencies, we consider Tibetan bowls, wine glasses and soda cans (with their tops removed), whose resonant frequencies span a broad range from 50 to 750 Hz. For each, we can vary the resonant frequency by filling it with liquid. The sound emitted by the loudspeaker was not powerful enough to induce significant oscillations of the soda can rim, a problem we eliminated by directly connecting the vibrating membrane of the loudspeaker to the rim of the soda can with a rigid rod.

We measure the acceleration of the rim at an antinode by gluing a lightweight accelerometer (PCB-Piezotronics, 352C65) on the bowl's rim at the level of the liquid surface. In the following, we characterize the sinusoidal rim oscillation by the dimensionless acceleration Γ defined as the maximal acceleration of the rim normalized by the gravitational acceleration $\Gamma = \Delta\omega^2/g$. For wine glasses, the accelerometer cannot be used since it dramatically alters the resonant frequency. We thus used a light weight strain gauge, whose effect on the resonance frequency is negligible.

The strain gauge system provides a measurement of the local extension length of the rim at an antinode. The length variation of the strain gauge is deduced by measuring its electrical resistance with a Wheatstone bridge. To deduce the acceleration of the radial rim movement, we deduce a relation between the longitudinal extension ϵ and the radial amplitude of the rim Δ. Then, the acceleration Γ can be readily deduced. The validity of this indirect method was tested on Tibet 1. An accelerometer was glued next to a strain gauge at an antinode of the bowl Tibet 1. From the strain gauge measurement, we deduced an acceleration that we compared with the direct measurement from the accelerometer. These two independent measurements match well for a wide range of accelerations.

French [1] gives a relation for the convex change of length δl of a curved segment of thickness a as a function of the initial mean radius of curvature R and the deformed radius of curvature r_c: $\delta_l = l_0 \frac{a}{2}(\frac{1}{r_c} - \frac{1}{R})$ where l_0 is the initial segment length. Since the deformation is small, we can approximate: $\frac{1}{r_c} \sim \frac{1}{R} + \frac{3x}{R^2}$ where x is the radial displacement of the wall [1]. The strain gauge gives the measurement of the convex longitudinal extension of the rim $\epsilon = \delta l / l_0$. We can thus deduce the maximal radial amplitude of the rim deformation [1]: $x_m = \frac{2}{3}\frac{R^2}{a}\epsilon$.

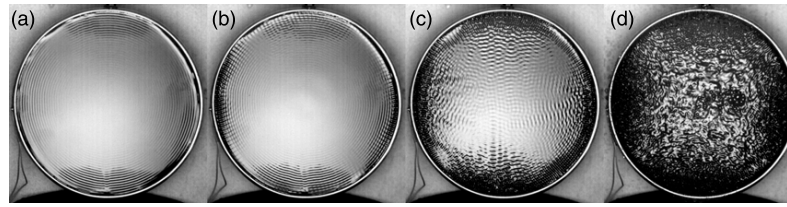

Figure 7. Evolution of the surface waves in Tibet 1 bowl filled with water and excited with a frequency $f = 188$ Hz corresponding to its fundamental mode (2,0). The amplitude of deformation is increasing from left to right: (*a*) $\Gamma = 1.8$, (*b*) $\Gamma = 2.8$, (*c*) $\Gamma = 6.2$, (*d*) $\Gamma = 16.2$.

3.3. Surface waves

Two different liquids were used in our experiment, pure water with density $\rho_w = 1000\,\mathrm{kg\,m^{-3}}$, viscosity $\nu = 1$ cSt and surface tension $\sigma = 72\,\mathrm{mN\,m^{-1}}$, and Dow Corning silicone oil with $\rho_o = 820\,\mathrm{kg\,m^{-3}}$, $\nu = 1$ cSt and $\sigma = 17.4\,\mathrm{mN\,m^{-1}}$. The fluid depth and resulting natural deformation frequencies of the bowl were varied. Specific deformation modes of the bowls were excited acoustically. We proceed by reporting the form of the flow induced, specifically, the evolution of the free surface with increasing rim forcing.

In figure 7 (and supplementary data movie 2 available at stacks.iop.org/Non/24/R51/mmedia), we present snapshots of the bowl Tibet 1 resonating in its fundamental deformation mode with different Γ when it is completely filled with water. The loudspeaker produces a sinusoidal sound at a frequency $f_0 = 188$ Hz that corresponds to the mode (2,0) with four associated nodes and antinodes. The vibration of the water surface is forced by the horizontal oscillation of the rim. When the amplitude of the rim oscillation is small, axisymmetric progressive capillary waves with frequency commensurate with the excitation frequency appear on the liquid surface. Although almost invisible to the naked eye, they can be readily detected by appropriate lighting of the liquid surface (figure 7(*a*)). When Γ is further increased, relatively large amplitude circumferential standing waves appear at the water's edge (figure 7(*b*) and supplementary data movie 3 available at stacks.iop.org/Non/24/R51/mmedia). These standing ripples, aligned perpendicular to the bowl's edge, are spaced by approximately a Faraday wavelength λ_F, as defined in (11). Moreover, their frequency is half that of the axial waves, indicating that these waves correspond to classic cross waves or, equivalently, edge-induced Faraday waves [14]. More complicated wave modes appear at higher excitation amplitude (figure 7(*c*)). At sufficiently high Γ, the Faraday waves break, and water droplets are ejected from the edge of the vessel (figure 7(*d*) and supplementary data movie 4 available at stacks.iop.org/Non/24/R51/mmedia), specifically from the antinodes of the oscillating wall. The ejected droplets may bounce, slide, and roll on the water surface before eventually coalescing.

One of our bowls (Tibet 2) resonates readily in both modes (2,0) and (3,0). When completely filled with water, the resonant frequencies of its (2,0) and (3,0) modes are $f = 144$ Hz and $f = 524$ Hz, respectively. In figure 8, we observe the progression of the surface waves with increasing amplitude for each of these modes. Note that for the mode (3,0), since the frequency is higher, the wavelengths are shorter. Moreover, the sound amplitude needed to produce surface waves is necessarily higher for mode (3,0) than (2,0).

The transition from axisymmetric capillary waves to Faraday waves arises at a critical acceleration Γ_F readily measured by the accelerometer. This threshold was measured as a function of the forcing frequency, the latter having been tuned to excite the fundamental

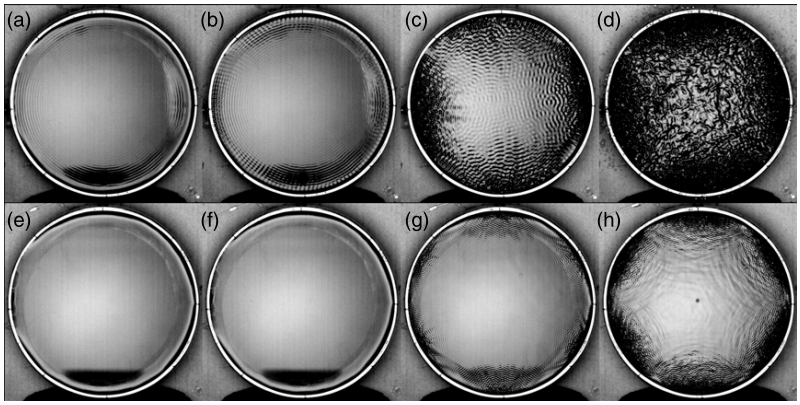

Figure 8. Evolution of the surface waves in Tibet 2 bowl filled with water. (*a*)–(*d*) Mode (2,0) is excited with a frequency $f = 144$ Hz. (*e*)–(*h*) Mode (3,0) is excited with $f = 524$ Hz. The amplitude of deformation is increasing from left to right. For the deformation mode $n = 2$, (*a*) $\Gamma = 1.0$, (*b*) $\Gamma = 1.7$, (*c*) $\Gamma = 5.0$, (*d*) $\Gamma = 12.7$. For the deformation mode $n = 3$, (*e*) $\Gamma = 5.7$, (*f*) $\Gamma = 7.7$, (*g*) $\Gamma = 15.1$, (*h*) $\Gamma = 33.8$.

deformation modes of the bowls with different liquid levels. We also measured this acceleration threshold for the deformation mode (3,0) of the bowl Tibet 2. Higher frequencies were explored with three different wine glasses filled to different levels using the strain gauge system. All the measurements with silicone oil of viscosity 1 cSt are presented in figure 9 (lower curve). Consistent with (13), the data suggest a dependence $\Gamma_F \propto f^{5/3}$. In figure 10(*a*), we report our measurements of Γ_F as a function of frequency for both silicone oil and distilled water. Each data set is fit by a 5/3 power law. Prefactors of 3.5×10^{-4} for water and 1.7×10^{-4} for 1 cSt silicone oil were inferred.

3.4. Surface fracture

When the Faraday waves become sufficiently large, they break, leading to droplet ejection. A second critical acceleration can thus be measured, Γ_d, above which droplets are ejected from the surface. The droplet ejection starts with very few droplets ejected, then the ejection rate increases with forcing amplitude. Our criterion for onset is that at least two droplets are ejected in a 15 s time interval. The dependence of Γ_d on f is presented in figure 9 (upper curve) for bowls and wine glasses filled with different levels of 1 cSt silicone oil. The drop ejection threshold scales as $\Gamma_d \propto f^{4/3}$, which is consistent with the scaling presented in (15).

In figure 10(*b*), our measurements of the dependence of Γ_d on f are reported for bowls filled with different levels of either 1 cSt silicone oil or water. The two Γ_d curves collapse when we use the scaling law (15) expected to apply for vertical forcing. Specifically, we find

$$\Gamma_d \sim 0.23(\sigma/\rho)^{1/3} f^{4/3}. \tag{16}$$

The droplet ejection acceleration threshold is thus in accord with measurements of Goodridge *et al* [23] and Puthenveettil and Hopfinger [22], even though our forcing is horizontal rather than vertical. Moreover, our prefactor is consistent with the results of both, who reported values between 0.2 and 0.3.

The diameter of the ejected droplets was measured for several forcing frequencies. The Tibetan bowls were fully filled with liquid, either 1 cSt silicone oil or pure water. Resonant deformation modes were then excited by the loudspeaker emitting sinusoidal signals at the

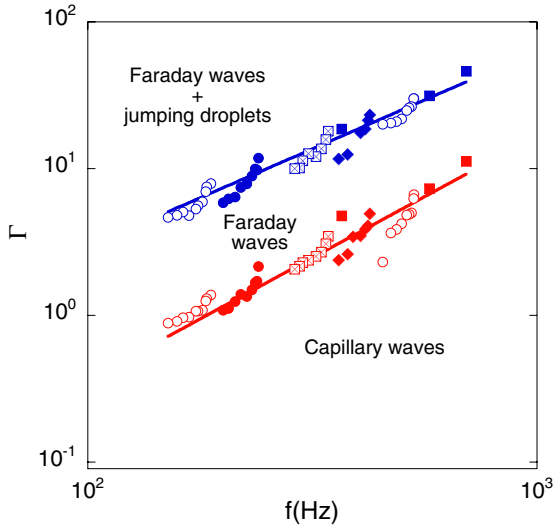

Figure 9. Phase diagram indicating the critical acceleration $\Gamma_F = \Delta\omega^2/g$ above which axial capillary waves give way to Faraday waves, and Γ_d above which the Faraday waves break. The ●, ○, ⊠ and ♦ symbols correspond, respectively, to the measurements made with the bowls Tibet 1, 2, 3 4 and the ■ to wine glasses filled with different levels of 1 cSt silicone oil. The first acceleration threshold (lower curve) scales as $\Gamma_F \propto f^{5/3}$ and the second (upper curve) as $\Gamma_d \propto f^{4/3}$.

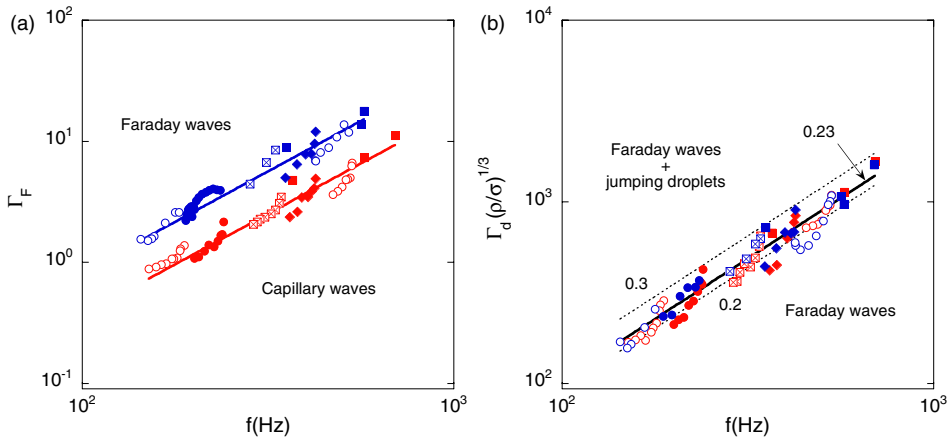

Figure 10. Dependence of acceleration thresholds on the frequency f for our vessels filled with different levels of pure water (blue symbols) and silicone oil of viscosity $\nu = 1$ cSt (red symbols). The ●, ○, ⊠ and ♦ symbols correspond, respectively, to the measurements made with the bowls Tibet 1, 2, 3 4 and the ■ to wine glasses. (*a*) Each data set of Faraday threshold measurements, Γ_F, is fit by a 5/3 power law consistent with (13). (*b*) The droplet ejection threshold, Γ_d, is consistent with the scaling (15).

appropriate resonant frequency. The level of sound was adjusted so that the acceleration of the rim at the antinodes of the bowl were just above the threshold for droplet ejection, Γ_d. A high speed video camera (Phantom) was used to record the ejected droplets, from which drop size measurements were taken. We used a liquid-filled glass in order to extend the frequency range to 720 Hz. Soda cans have very thin walls, and very low resonant frequencies. We were thus

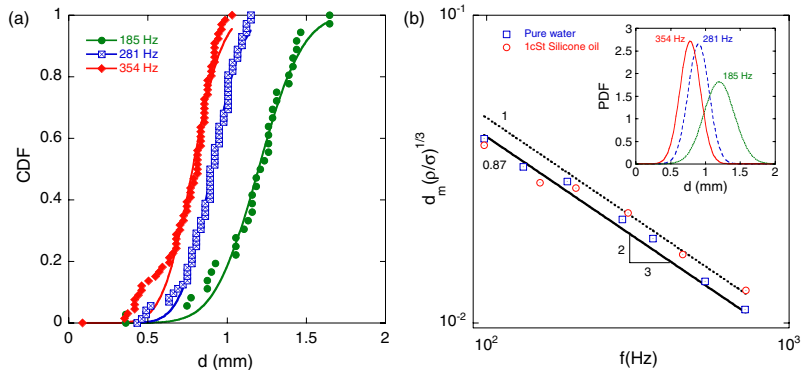

Figure 11. (*a*) Three cumulative distribution functions of ejected droplet sizes for the bowls Tibet 1, 3 and 4, fully filled with pure water and resonating in their fundamental deformation modes (2,0). The lines are the curves fit by an equation of a cumulative distribution function for the Gaussian distribution. (*b*) Mean size of the ejected droplets as a function of the frequency of the oscillating vessel, either a Tibetan bowl, wine glass or soda can. The two leftmost data points are from the measurements made with the soda cans, the two rightmost from the wine glass. Error bars are the size of our symbols. The black curve indicates a power law dependence with slope −2/3 and prefactor 0.87. The dotted line has the same slope, but a prefactor of 1. Inset: the corresponding Gaussian functions inferred from the cumulative distribution functions.

able to measure droplet sizes for the two liquids at a frequency of 98 Hz. Three cumulative distributions of ejected droplet sizes are presented in figure 11(*a*) for the bowls Tibet 1, 3 and 4 resonating in their fundamental deformation modes (2,0). Assuming that these distributions are Gaussian, appropriate fits to the cumulative distribution functions yield the parameters of the Gaussian distribution functions plotted in the inset of figure 11(*b*). The dependencies of the mean droplet size on the forcing frequency for the two liquids are presented in figure 11(*b*). Equation (14) adequately collapses our data, provided we choose a prefactor of 0.87. By way of comparison, Puthenveettil found 0.92 for their experiments with water, and 1.01 with Perfluoro-compound FC-72 liquid. Donnelly *et al* [45] found a prefactor of 0.98 from his measurements of aerosol water droplets.

3.5. Bouncing droplets

With a more viscous fluid (e.g. 10 cSt silicone oil), the waves are less pronounced, and the fluid is more strongly coupled to the vibrating sidewalls; specifically, more of the surface oscillates up and down near the wall's antinode. When a droplet of the same liquid is deposited on the surface, it may bounce, levitated by the underlying wave field. Such sustained levitation was not observed in the Tibetan singing bowl with liquid viscosities lower than 10 cSt.

In figure 12(*a*), we present a still image of a drop of diameter 0.5 mm bouncing on the liquid surface inside the bowl (Tibet 1) resonating at a frequency of $f_0 = 188$ Hz. The drop has been made by dipping then extracting a syringe needle, on the tip of which a capillary bridge forms and breaks, leaving a drop that bounces near the oscillating rim. A movie of the bouncing was recorded (see supplementary data movie 5 available at stacks.iop.org/Non/24/R51/mmedia), then vertical slices of each image through the droplet centreline juxtaposed. We can thus construct an image illustrating the dynamics of the droplet (figure 12(*b*)). In this case, the drop experiences two bounces of slightly different amplitude while the liquid surface (and the rim) oscillates twice. When a smaller droplet (of diameter 0.35 mm) is placed on the

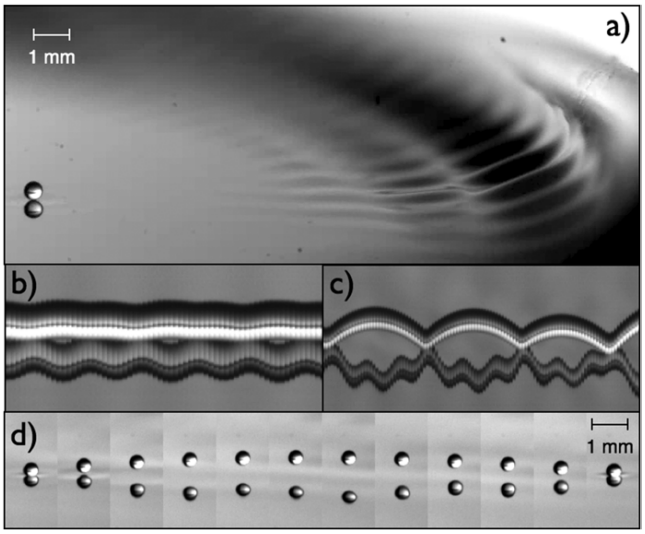

Figure 12. (*a*) Still image of a droplet of 0.5 mm diameter bouncing on a surface oscillating at 188 Hz, the frequency of the rim. Both droplet and bath are 10 cSt silicon oil. Spatio-temporal diagrams indicate the vertical trajectory of droplets of diameter (*b*) 0.5 mm and (*c*) 0.35 mm. Time elapses from left to right and the drop's reflection are apparent. (*d*) A single bounce of a droplet of diameter 0.35 mm is illustrated by an image sequence. Images are spaced by 1 ms.

oscillating surface, the bouncing motion can be more complex. In figure 12(*c*), we see that the droplet bounces only once during three oscillations of the surface. Figure 12(*d*) illustrates the corresponding trajectory. We note that the bouncing motion of sufficiently small drops can become chaotic.

We sought to sustain walking droplets in our system. Once the horizontal forcing amplitude Γ is just above the Faraday wave threshold Γ_F, circumferential Faraday waves are sustained at the edge of the vessel. Then, when Γ is increased, Faraday waves propagate progressively towards the centre of the vessel, their amplitude damped by viscosity. Beyond these waves, the liquid surface was quiescent unless perturbed by a bouncing droplet, in which case it could sustain a field of Faraday waves. This phenomenon was observed in the bowl Tibet 2 almost fully filled with 10 cSt silicone oil ($f_0 = 140$ Hz). Just beyond the Faraday waves, a bouncing droplet of diameter 500 μm was made such that its bouncing frequency corresponded to the Faraday wave frequency, that is, half the frequency of the vibrating rim. Such droplets were unable to excite sufficiently large Faraday waves to enable them to walk. We note that the usual range of walker diameters is between 650 and 850 μm [33, 34]: their mass is thus 4 times larger than that of our drops.

4. Conclusion

We have presented the results of an experimental investigation of the Tibetan singing bowl, its acoustics and hydrodynamics. Its acoustical properties are similar to those of a wine glass, but its relatively low vibration frequency makes it a more efficient generator of edge-induced Faraday waves and droplet generation via surface fracture.

Our observations of the bowl acoustics have been rationalized by adapting French's [1] theory of the singing wine glass. This model allowed us to characterize the bowl acoustics

and infer the Young modulus of the alloy constituting our antique bowls. The value we found, $Y = 77 \pm 6\%$ GPa, is in the range of glass, somewhat smaller than typical brass, copper or bronze alloys. This low value of Y and associated low resonant frequency is a critical component in the hydrodynamic behaviour of singing bowls: bowls with high fundamental frequencies are, like the wine glass, relatively inefficient generators of droplets.

Particular attention has been given to the Faraday waves produced when a critical acceleration of the horizontal rim oscillation is exceeded. These have been shown to be due to a destabilization of the axial capillary waves similar to those observed and studied theoretically [29, 24]. The acceleration threshold for droplet ejection has also been investigated and rationalized by simple scaling arguments. Droplet size was shown to be proportional to the Faraday wavelength, and our measurements were consistent with those on a vertically shaken liquid surface [22, 23, 45].

We have demonstrated that, following their creation via surface fracture, droplets may skip across or roll along the surface of fluid contained within a singing bowl. Moreover, careful choice of fluid properties and droplet position introduces the possibility of stable bouncing states reminiscent of those on a vertically driven free surface [30]. However, stable walking droplets and their concomitant quantum behaviour were not observed. Nevertheless, in developing hydrodynamic analogues of quantum systems, the edge-forcing examined here may be valuable in presenting a lateral gradient in proximity to Faraday threshold.

Acknowledgments

The authors thank Rosie Warburton for bringing this problem to our attention, and for supplying the bowls for our study. We are grateful to Jim Bales (of MIT's Edgerton Center), Barbara Hughey and Stéphane Dorbolo for assistance and fruitful discussions. Denis Terwagne thanks the University of Liège and the GRASP for financial support. This research was supported by the National Science Foundation through grant CBET-0966452.

References

[1] French A 1983 In vino veritas—a study of wineglass acoustics *Am. J. Phys.* **51** 688
[2] Chen K, Wang C, Lu C and Chen Y 2005 Variations on a theme by a singing wineglass *Europhys. Lett.* **70** 334
[3] Chen Y-Y 2005 Why does water change the pitch of a singing wineglass the way it does? *Am. J. Phys.* **73** 1045
[4] Jundt G, Radu A, Fort E, Duda J, Vach H and Fletcher N 2006 Vibrational modes of partly filled wine glasses *J. Acoust. Soc. Am.* **119** 3793
[5] Courtois M, Guirao B and Fort E 2008 Tuning the pitch of a wine glass by playing with the liquid inside *Eur. J. Phys.* **29** 303
[6] Arane T, Musalem A and Fridman M 2009 Coupling between two singing wineglasses *Am. J. Phys.* **77** 1066
[7] Apfel R 1985 Whispering waves in a wineglass *Am. J. Phys.* **53** 1070
[8] Rayleigh L 1945 *Theory of Sound* (Cambridge: Cambridge University Press)
[9] Rossing T 1990 Wine glasses, bell modes and lord Rayleigh *Phys. Teach.* **28** 582
[10] Rossing T 1993 Acoustics of the glass harmonica *J. Acoust. Soc. Am.* **95** 1106
[11] Joubert S V, Fay T H and Voges E L 2007 A storm in a wineglass *Am. J. Phys.* **75** 647
[12] Inacio O, Henrique L and Antunes J 2006 The dynamics of tibetan singing bowls *Acta Acust. United Acust.* **92** 637–53
[13] Inacio O, Henrique L and Antunes J 2004 The physics of tibetan singing bowls (2004) *Rev. Acúst.* **35** 33–9
[14] Faraday M 1831 On a peculiar class of acoustical figures; and on certain forms assumed by groups of particles upon vibrating elastic surfaces *Phil. Trans. R. Soc. Lond.* **121** 299–340
[15] Rayleigh L 1883 On the crispations of fluid resting upon a vibrating support *Phil. Mag.* **16** 50
[16] Benjamin T B and Ursell F 1954 The stability of the place free surface of a liquid in vertical periodic motion *Proc. R. Soc. Lond.* A **255** 505
[17] Miles J and Henderson D 1990 Parametrically forced surface-waves *Annu. Rev. Fluid Mech.* **22** 143

[18] Kumar K and Tuckerman L S 1994 Parametric instability of the interface between two fluids *J. Fluid Mech.* **279** 49
[19] Edwards W and Fauve S 1994 Patterns and quasi-patterns in the faraday experiment *J. Fluid Mech.* **278** 123
[20] Kudrolli A and Gollub J 1996 Patterns and spatiotemporal chaos in parametrically forced surface waves: A systematic survey at large aspect ratio *Physica* D **97** 133
[21] Chen P and Vinals J 1997 Pattern selection in faraday waves *Phys. Rev. Lett.* **79** 2670
[22] Puthenveettil B A and Hopfinger E J 2009 Evolution and breaking of parametrically forced capillary waves in a circular cylinder *J. Fluid Mech.* **633** 355
[23] Goodridge C, Shi W T, Hentschel H and Lathrop D 1997 Viscous effects in droplet-ejecting capillary waves *Phys. Rev.* E **56** 472
[24] Garrett C 1970 On cross-waves *J. Fluid Mech.* **41** 837
[25] Barnard B J S and Pritchard W G 1972 Cross-waves: II. Experiments *J. Fluid Mech.* **55** 245
[26] Mahony J J 1972 Cross-waves: I. Theory *J. Fluid Mech.* **55** 229
[27] Miles J and Becker J 1988 Parametrically excited, standing cross-waves *J. Fluid Mech.* **186** 119
[28] Becker J and Miles J 1991 Standing radial cross-waves *J. Fluid Mech.* **222** 471
[29] Hsieh D 2000 Theory of water waves in an elastic vessel *Acta. Mech. Sin.* **16** 97
[30] Couder Y, Fort E, Gautier C-H and Boudaoud A 2005 From bouncing to floating: noncoalescence of drops on a fluid bath *Phys. Rev. Lett.* **94** 177801
[31] Gilet T, Terwagne D, Vandewalle N and Dorbolo S 2008 Dynamics of a bouncing droplet onto a vertically vibrated interface *Phys. Rev. Lett.* **100** 167802
[32] Dorbolo S, Terwagne D, Vandewalle N and Gilet T 2008 Resonant and rolling droplet *New J. Phys.* **10** 113021
[33] Protiere S, Couder Y, Fort E and Boudaoud A 2005 The self-organization of capillary wave sources *J. Phys. Condens. Matter* **17** S3529
[34] Eddi A, Terwagne D, Fort E and Couder Y 2008 Wave propelled ratchets and drifting rafts *Eur. Phys. Lett.* **82** 44001
[35] Gilet T and Bush J W M 2009 The fluid trampoline: droplets bouncing on a soap film *J. Fluid Mech.* **625** 167
[36] Eddi A, Sultan E, Moukhtar J, Fort E, Rossi M and Couder Y 2011 Information stored in faraday waves: the origin of a path memory *J. Fluid Mech.* **674** 433–63
[37] Couder Y and Fort E 2006 Single-particle diffraction and interference at a macroscopic scale *Phys. Rev. Lett.* **97** 154101
[38] Eddi A, Fort E, Moisy F and Couder Y 2009 Unpredictable tunneling of a classical wave-particle association *Phys. Rev. Lett.* **102** 240401
[39] Fort E, Eddi A, Boudaoud A, Moukhtar J and Couder Y 2010 Path-memory induced quantization of classical orbits *Proc. Natl Acad. Sci.* **107** 17515
[40] Bush J W M 2010 Quantum mechanics writ large *Proc. Natl Acad. Sci.* **107** 17455
[41] Perrin R, Charcley T, Banut H and Rossing T D 1985 Chladni's law and the modern English church bell *J. Sound Vib.* **102** 11
[42] Kinsler L, Frey A, Coppens A and Sanders J 1982 Fundamentals of acoustics 3rd edn (New York: Wiley)
[43] Akay A 2002 Acoustics of friction *J. Acoust. Soc. Am.* **111** 1525
[44] Douady S 1990 Experimental study of the faraday instability *J. Fluid Mech.* **221** 383
[45] Donnelly T, Hogan J, Mugler A, Schommer N, Schubmehl M, Bernoff A and Forrest B 2004 An experimental study of micron-scale droplet aerosols produced via ultrasonic atomization *Phys. Fluids* **16** 2843

Bibliography

[1] Y. Couder, S. Protiere, E. Fort and A. Boudaoud, *Walking and orbiting droplets*, Nature **437**, 208 (2005).

[2] Y. Couder and E. Fort, *Single-particle diffraction and interference at a macroscopic scale*, Phys. Rev. Lett. **97**, 154101 (2006).

[3] A. Eddi, E. Fort, F. Moisy and Y. Couder, *Unpredictable tunneling of a classical wave-particle association*, Phys. Rev. Lett. **102**, 240401 (2009).

[4] A. Eddi, E. Sultan, J. Moukhtar, E. Fort, M. Rossi and Y. Couder, *Information stored in faraday waves: the origin of a path memory*, J. Fluid Mech. **674**, 433 (2011).

[5] E. Fort, A. Eddi, A. Boudaoud, J. Moukhtar and Y. Couder, *Path-memory induced quantization of classical orbits*, Proc. Natl. Acad. Sci. **107**, 17515 (2010).

[6] J. W. M. Bush, *Quantum mechanics writ large*, Proc. Natl. Acad. Sci. **107**, 17455 (2010).

[7] A. Eddi, D. Terwagne, E. Fort and Y. Couder, *Wave propelled ratchets and drifting rafts*, Europhys. Lett. **82**, 44001 (2008).

[8] D. Terwagne and J. W. Bush, *Tibetan singing bowls*, Nonlinearity **24**, R51 (2011).

[9] L. Landau and E. Lifchitz, Course of Theoretical Physics : Fluid mechanics, volume 6 (Addison-Wesley, 1959).

[10] O. Reynolds, *On the iloading of drops on the surface of water depending only on the purity of the surface*, Proc. Proc. Manchester Lit. Phil. Soc. **21** (1881).

[11] F. Blanchette and T. Bigioni, *Partial coalescence of drops at liquid interfaces*, Nat. Phys. **2**, 254 (2006).

[12] T. Gilet, K. Mulleners, J. Lecomte, N. Vandewalle and S. Dorbolo, *Critical parameters for the partial coalescence of a droplet*, Phys. Rev. E **75**, 036303 (2007).

[13] O. Reynolds, *On the theory of lubrication and its application to mr. beauchamp tower's experiments, including an experimental determination of the viscosity of olive oil*, Philos. Trans. R. Soc. London **177**, 79 (1886).

[14] P. Dell'Aversana, F. Montiand *et al.*, *Marangoni flows and coalescence phenomena in microgravity*, Adv. Space. Res. **16**, 95 (1995).

[15] Y. Amarouchene, G. Cristobal and H. Kellay, *Noncoalescing drops*, Phys. Rev. Lett. **87**, 206104 (2001).

[16] W. Ristenpart, J. Bird, A. Belmonte, F. Dollar and H. Stone, *Non-coalescence of oppositely charged drops*, Nature **461**, 377 (2009).

[17] P. Brunet and J. Snoeijer, *Star-drops formed by periodic excitation and on an air cushion–a short review*, Eur. Phys. J. ST. **192**, 207 (2011).

[18] A. Yarin, M. Pfaffenlehner and C. Tropea, *On the acoustic levitation of droplets*, J. Fluid Mech. **356**, 65 (1998).

[19] K. Sreenivas, P. De and J. Arakeri, *Levitation of a drop over a film flow*, J. Fluid Mech. **380**, 297 (1999).

[20] J. Leidenfrost, De aquae communis nonnullis qualitatibus tractatus (Duisburg, 1756).

[21] A. Biance, C. Clanet and D. Quéré, *Leidenfrost drops*, Phys. Fluids **15**, 1632 (2003).

[22] J. Walker, *Drops of liquid can be made to float on the liquid. what enables them to do so*, Sci. Am. **238**, 123 (1978).

[23] Y. Couder, E. Fort, C. Gautier and A. Boudaoud, *From bouncing to floating: Noncoalescence of drops on a fluid bath*, Phys. Rev. Lett. **94**, 177801 (2005).

[24] T. Gilet, N. Vandewalle and S. Dorbolo, *Controlling the partial coalescence of a droplet on a vertically vibrated bath*, Phys. Rev. E **76**, 035302 (2007).

[25] S. Protiere, Y. Couder, E. Fort and A. Boudaoud, *The self-organization of capillary wave sources*, J. Phys-condens. Mat. **17**, S3529 (2005).

[26] T. Gilet and J. Bush, *The fluid trampoline : droplets bouncing on a soap film*, J. Fluid Mech. **625**, 167 (2009).

[27] N. Vandewalle, D. Terwagne, K. Mulleners, T. Gilet and S. Dorbolo, *Dancing droplets onto liquid surfaces*, Phys. Fluids **18**, 091106 (2006).

[28] S. Lieber, M. Hendershott, A. Pattanaporkratana and J. Maclennan, *Self-organization of bouncing oil drops: Two-dimensional lattices and spinning clusters*, Phys. Rev. E **75**, 056308 (2007).

[29] A. Eddi, A. Decelle, E. Fort and Y. Couder, *Archimedean lattices in the bound states of wave interacting particles*, Europhys. Lett. **87**, 56002 (2009).

[30] A. Eddi, A. Boudaoud and Y. Couder, *Oscillating instability in bouncing droplet crystals*, Europhys. Lett. **94**, 20004 (2011).

[31] M. Faraday, *On a peculiar class of acoustical figures; and on certain forms assumed by groups of particles upon vibrating elastic surfaces*, Philos. Trans. R. Soc. London **121** (1831).

[32] L. Rayleigh, *On the crispations of fluid resting upon a vibrating support.*, Philos. Mag. **16**, 50 (1883).

[33] T. Benjamin and F. Ursell, *The stability of the place free surface of a liquid in vertical periodic motion*, Proc. R. Soc. Lond. A **255**, 505 (1954).

[34] J. Miles and D. Henderson, *Parametrically forced surface-waves*, Annu. Rev. Fluid Mech. **22**, 143 (1990).

[35] K. Kumar and L. S. Tuckerman, *Parametric instability of the interface between two fluids*, J. Fluid Mech. **279**, 49 (1994).

[36] W. Edwards and S. Fauve, *Patterns and quasi-patterns in the faraday experiment*, J. Fluid Mech. **278**, 123 (1994).

[37] A. Kudrolli and J. Gollub, *Patterns and spatiotemporal chaos in parametrically forced surface waves: A systematic survey at large aspect ratio*, Physica D **97**, 133 (1996).

[38] P. Chen and J. Vinals, *Pattern selection in faraday waves*, Phys. Rev. Lett. **79**, 2670 (1997).

[39] C. Goodridge, W. T. Shi, H. Hentschel and D. Lathrop, *Viscous effects in droplet-ejecting capillary waves*, Phys. Rev. E **56**, 472 (1997).

[40] B. A. Puthenveettil and E. J. Hopfinger, *Evolution and breaking of parametrically forced capillary waves in a circular cylinder*, J. Fluid Mech. **633**, 355 (2009).

[41] S. Douady, *Experimental study of the faraday instability*, J. Fluid Mech. **221**, 383 (1990).

[42] S. Sun and J. Keller, *Capillary-gravity wave drag*, Phys. Fluids **13**, 2146 (2001).

[43] D. Hu, B. Chan and J. Bush, *The hydrodynamics of water strider locomotion*, Nature **424**, 663 (2003).

[44] S. Protiere, A. Boudaoud and Y. Couder, *Particle-wave association on a fluid interface*, J. Fluid Mech. **554**, 85 (2006).

[45] L. de Broglie, Ondes et mouvements (Gauthier-Villars, 1926).

[46] D. Bohm, *A suggested interpretation of the quantum theory in terms of*, Phys. Rev. **85**, 166 (1952).

[47] S. Dorbolo, D. Terwagne, N. Vandewalle and T. Gilet, *Resonant and rolling droplets*, New J. Phys. **10**, 113021 (2008).

[48] T. Gilet, D. Terwagne, N. Vandewalle and S. Dorbolo, *Dynamics of a bouncing droplet onto a vertically vibrated interface*, Phys. Rev. Lett. **100**, 167802 (2008).

[49] N. Tufillaro, T. Abbott and J. Reilly, An experimental approach to nonlinear dynamics and chaos (Addison-Wesley, 1992).

[50] S. Protiere, S. Bohn and Y. Couder, *Exotic orbits of two interacting wave sources*, Phys. Rev. E **78**, 036204 (2008).

[51] S. Protière and Y. Couder, *Orbital motion of bouncing drops*, Phys. Fluids **18**, 091114 (2006).

[52] D. Terwagne, N. Vandewalle and S. Dorbolo, *Lifetime of a bouncing droplet*, Phys. Rev. E **76**, 056311 (2007).

[53] D. Terwagne, T. Gilet, N. Vandewalle and S. Dorbolo, *Metastable bouncing droplets*, Phys. Fluids **21**, 054103 (2009).

[54] D. Terwagne, T. Gilet, N. Vandewalle and S. Dorbolo, *From a bouncing compound drop to a double emulsion*, Langmuir **26**, 11680 (2010).

[55] D. Terwagne, T. Gilet, N. Vandewalle and S. Dorbolo, *Double emulsion in a compound droplet*, Coll. Surf. A : Physicochem. Eng. Aspect **365**, 178 (2010).

[56] L. Rayleigh, *On the capillary phenomena of jets*, Proc. Roy. Soc. London **29**, 71 (1879).

[57] M. Rein, *Phenomena of liquid drop impact on solid and liquid surfaces*, Fluid. Dyn. Res. **12**, 61 (1993).

[58] S. Courty, G. Lagubeau and T. Tixier, *Oscillating droplets by decomposition on the spherical harmonics basis*, Phys. Rev. E **73**, 045301 (2006).

[59] X. Noblin, A. Buguin and F. Brochard-Wyart, *Vibrated sessile drops: transition between pinned and mobile contact line oscillations*, Eur. Phys. J. E **14**, 395 (2004).

[60] S. Dorbolo, H. Caps and N. Vandewalle, *Fluid instabilities in the birth and death of antibubbles*, New. J. Phys. **5**, 161 (2003).

[61] S. Dorbolo, E. Reyssat, N. Vandewalle and D. Quéré, *Aging of an antibubble*, Europhys. Lett. **69**, 966 (2005).

[62] A. Edris and B. Bergnståhl, *Encapsulation of orange oil in a spray dried double emulsion*, Food **45**, 133 (2001).

[63] C. Laugel, A. Baillet, M. P. Y. Piemi, J.-P. Marty and D. Ferrier, *Oil-water-oil multiple emulsions for prolonged delivery of hydrocortisone after topical application: Comparison with simple emulsions*, Int. J. Pharm. **160**, 109 (1998).

[64] A. Benichou, A. Aserin and N. Garti, *O/w/o double emulsions stabilized with wpi–polysaccharide conjugates*, Polym. Adv. Technol. **13**, 1019 (2002).

[65] M.-F. Ficheux, L. Bonakdar, F. Leal-Calderon and J. Bibette, *Some stability criteria for double emulsions*, Langmuir **14**, 2702 (1998).

[66] M. Lee, S. Oh, S. Moon and S. Bae, *Preparation of silica particles encapsulating retinol using o/w/o multiple emulsions*, J. Colloid. Interf. Sci. **240**, 83 (2001).

[67] I. Loscertales, A. Barrero, I. Guerrero, R. Cortijo, M. Marquez and A. Ganan-Calvo, *Micro/nano encapsutation via electrified coaxial liquid jets*, Science **295**, 1695 (2002).

[68] S. Chiu and T. Lin, *Experiment on the dynamics of a compound drop impinging on a hot surface*, Phys. Fluids **17**, 122103 (2005).

[69] R.-H. Chen, S.-L. Chiu and T.-H. Lin, *Resident time of a compound drop impinging on a hot surface*, Appl. Therm. Eng. **27**, 2079 (2007).

[70] B. Prunet-Foch, F. Legay, M. Vignes-Adler and C. Delmotte, *Impacting emulsion drop on a steel plate: Influence of the solid substrate*, J. Coll. Interf. Sci. **199**, 151 (1998).

[71] S. Okushima, T. Nisisako, T. Torii and T. Higuchi, *Controlled production of monodisperse double emulsions by two-step droplet breakup in microfluidic devices*, Langmuir **20**, 9905 (2004).

[72] C. Goubault, K. Pays, D. Olea, P. Gorria, J. Bibette, V. Schmitt and F. Leal-Calderon, *Shear rupturing of complex fluids: Application to the preparation of quasi-monodisperse water-in-oil-in-water double emulsions*, Langmuir **17**, 5184 (2001).

[73] S. Anna, N. Bontoux and H. Stone, *Formation of dispersions using "flow focusing" in microchannels*, Appl. Phys. Lett. **82**, 364 (2003).

[74] A. Utada, E. Lorenceau, D. Link, P. Kaplan, H. Stone and D. Weitz, *Monodisperse double emulsions generated from a microcapillary device*, Science **308**, 537 (2005).

[75] T. Gilet, D. Terwagne and N. Vandewalle, *Digital microfluidics on a wire*, Appl. Phys. Lett. **95**, 014106 (2009).

[76] D. Bartolo, C. Josserand and D. Bonn, *Singular jets and bubbles in drop impact*, Phys. Rev. Lett. **96**, 124501 (2006).

[77] M. C. Vargas, D. A. Huerta and V. Sosa, *Chaos control: The problem of a bouncing ball revisited*, Am. J. Phys. **77**, 857 (2009).

[78] J.-C. Geminard and C. Laroche, *Energy of a single bead bouncing on a vibrating plate: Experiments and numerical simulations*, Phys. Rev. E **68**, 031305 (2003).

[79] N. B. Tufillaro and A. M. Albano, *Chaotic dynamics of a bouncing ball*, Am. J. Phys. **54**, 1 (1986).

[80] J.-M. Luck and A. Mehta, *Bouncing ball with a finite restitution - chattering, locking, and chaos*, Phys. Rev. E **48**, 3988 (1993).

[81] D. Terwagne, T. Gilet, N. Vandewalle and S. Dorbolo, *From bouncing to boxing*, Chaos **18**, 041104 (2008).

[82] T. Gilet, N. Vandewalle and S. Dorbolo, *Completely inelastic ball*, Phys. Rev. E (2009).

[83] K. Okumura, F. Chevy, D. Richard, D. Quéré and C. Clanet, *Water spring: A model for bouncing drops*, Europhys. Lett. **62**, 237 (2003).

[84] D. Richard and D. Quéré, *Bouncing water drops*, Europhys. Lett. **50**, 769 (2000).

[85] L. Mahadevan and Y. Pomeau, *Rolling droplets*, Phys. Fluids **11**, 2449 (1999).

[86] C. Clanet, C. Béguin, D. Richard and D. Quéré, *Maximal deformation of an impacting drop*, J. Fluid Mech. **517**, 199 (2004).

[87] A. Biance, F. Chevy, C. Clanet, G. Lagubeau and D. Quéré, *On the elasticity of an inertial liquid shock*, J. Fluid Mech. **554**, 47 (2006).

[88] D. Richard, C. Clanet and D. Quéré, *Contact time of a bouncing drop*, Nature **417**, 811 (2002).

[89] T. Gilet and J. Bush, *Chaotic bouncing of a droplet on a soap film*, Phys. Rev. Lett. **102**, 014501 (2009).

[90] B. Eichwald, M. Argentina, X. Noblin and F. Celestini, *Dynamics of a ball bouncing on a vibrated elastic membrane*, Phys. Rev. E **82**, 016203 (2010).

[91] A. Stocco, W. Drenckhan, D. Langevin and B. Binks, *Particle-stabilised foams: an interfactial study*, Soft Matter **5**, 2215 (2009).

[92] J. Glasheen and T. McMahon, *Vertical water entry of disks at low froude numbers*, Phys. Fluids **8**, 2078 (1996).

[93] D. Lee and H. Kim, *Impact of a superhydrophobic sphere onto water*, Langmuir **24**, 142 (2008).

[94] J. Bush and D. Hu, *Walking on water: biolocomotion at the interface*, Annu. Rev. Fluid Mech. **38**, 339 (2006).

[95] E. Klaseboer, J. P. Chevaillier, C. Gourdon and O. Masbernat, *Film drainage between colliding drops at constant approach velocity: Experiments and modeling*, J. Colloid. Interf. Sci. **229**, 274 (2000).

[96] A. Zdravkov, G. Peters and H. Meijer, *Film drainage and interfacial instabilities in polymeric systems with diffuse interfaces*, J. Colloid. Interf. Sci. **296**, 86 (2006).

[97] P. Marmottant and E. Villermaux, *Fragmentation of stretched liquid ligaments*, Phys. Fluids **16**, 2732 (2004).

[98] A. Eddi, Marcheurs, Dualité onde-particule et Mémoire de chemin, Ph.D. thesis, Université Paris VII (2010).

[99] P. Cundall and O. Strack, *A discrete numerical model for granular assemblies*, Geotechnique **29**, 47 (1979).

[100] F. Ludewig, Contribution aux approches numériques de la densification d'assemblées granulaires, Ph.D. thesis, Université de Liège (2006).

[101] N. Taberlet, Ecoulements gravitaires de matériaux granulaires, Ph.D. thesis, Université de Rennes 1 (2005).